CHALMERS
UNIVERSITY OF TECHNOLOGY

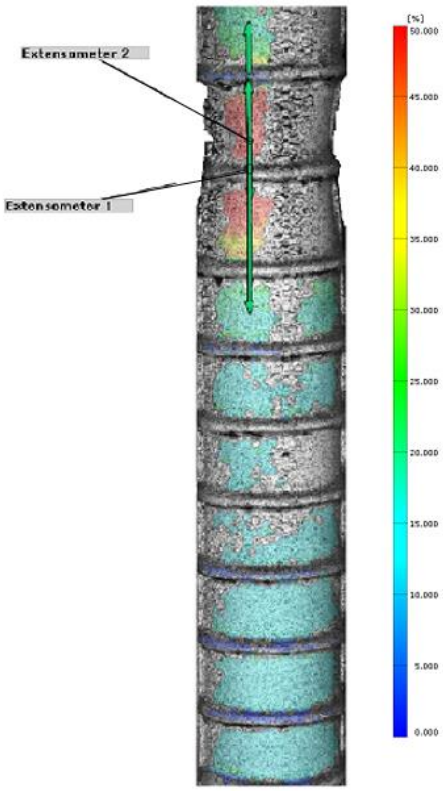

Mechanical properties of naturally corroded steel bars:

Experimental study

Master of Science Thesis in the Master's Programme Structural Engineering and Building Technology

AMEL CATO
MATIUR RAHMAN RAJU

Department of Architecture and Civil Engineering
Division of Structural Engineering
Concrete Structures
CHALMERS UNIVERSITY OF TECHNOLOGY
Master's Thesis ACEX30-18-53
Gothenburg, Sweden 2018

MASTER'S THESIS ACEX30-18-53

Mechanical properties of naturally corroded steel bars:

Experimental study

Master of Science Thesis in the Master's Programme Structural Engineering and Building Technology

AMEL CATO
MATIUR RAHMAN RAJU

CHALMERS
UNIVERSITY OF TECHNOLOGY

Department of Architecture and Civil Engineering
Division of Structural Engineering
Concrete Structures
CHALMERS UNIVERSITY OF TECHNOLOGY
Göteborg, Sweden 2018

Mechanical properties of naturally corroded steel bars:
Experimental study

Master of Science Thesis in the Master's Programme Structural Engineering and Building Technology

AMEL CATO
MATIUR RAHMAN RAJU

Examensarbete ACEX30-18-53
Institutionen för arkitektur och samhällsbyggnadsteknik
Chalmers tekniska högskola, 2018

Department of Architecture and Civil Engineering
Division of Structural Engineering
Concrete Structures
Chalmers University of Technology
SE-412 96 Göteborg
Sweden
Telephone: + 46 (0)31-772 1000

Cover:
Digital Image Correlation (DIC) results for one of the tested reinforcing steel bars with digital extensometers.

Department of Architecture and Civil Engineering
Göteborg, Sweden, 2018

Mechanical properties of naturally corroded steel bars:
Experimental study

Master of Science Thesis in the Master's Programme Structural Engineering and Building Technology

AMEL CATO
MATIUR RAHMAN RAJU

Department of Architecture and Civil Engineering
Division of Structural Engineering
Concrete Structures
Chalmers University of Technology

ABSTRACT

In reinforced concrete structures, corrosion of steel reinforcement is still considered to be one of the main reasons of deterioration, causing high costs for repairing and replacing critical corroded elements in reinforced concrete structures. This has directed to a rising demand and need for a better understanding of the structural effects of corrosion. Pitting and generalized corrosion are the two main corrosion mechanisms for reinforcing steel. Pitting corrosion is characterized by local corrosion and generalised corrosion can be seen as several local pits uniformly distributed along the bar. Those cause effects on the apparent mechanical properties, consequently the overall steel bar behavior is modified, causing a performance reduction.

The aim of this study is to obtain actual mechanical properties of uncorroded reinforcing bars and to describe apparent mechanical properties of corroded reinforcing bars in different ways, hence to increase the level of knowledge about the local effects produced by corrosion on the steel bar. This knowledge will lead to better understanding of structural behavior for corroded steel reinforced concrete structures in serviceability and ultimate limit states, which will provide a better understanding of the degradation and evaluation of existing materials and structures where reinforcing steel are used.

To investigate the mechanical behavior of corroded and uncorroded reinforcing steel, an experimental program was carried out; monotonic tensile tests on steel bars measured by Digital Image Correlation (DIC) technique were conducted by using different bar diameters and lengths for uncorroded and corroded specimens. The corrosion levels were measured by using different methods such as gravimetric (weight loss) and 3D scanning techniques. Further, postprocessing was performed by using the software: GOM® Correlate Professional 2017 in combination with MATLAB® and Microsoft® Excel, which enabled results such as force, displacements, engineering- and true stress-strain.

The combined analyzed results from the performed tests indicated general reduction for all the evaluated parameters, i.e. elongation, yield load, ultimate load, fracture strain, ultimate strain, yield strength, ultimate strength and modulus of elasticity, which presented a significant drop with the increase of corrosion levels.

Key words: Steel reinforcement, Digital Image Correlation (DIC), tensile test, engineering stress-strain, true stress-strain, mechanical properties of reinforcement, generalized corrosion, pitting corrosion, corroded rebars, uncorroded rebars, average cross-section, critical cross-section.

Contents

Preface

This study covers 30 credits and was performed at the Chalmers University of Technology at the Department of Architecture and Civil Engineering in the period between January 2018 and June 2018. All specimen preparations and tension tests have been carried out in the laboratory of the Department of Structural Engineering at the Chalmers University of Technology.

We would like to express our most sincere gratitude and appreciation to our supervisor and examiner, Ignasi Fernandez for the support, specifically through hours of meetings where he would help with useful advice, expert knowledge, and guideline throughout this study. We would also like to thank Sebastian Almfeldt who helped us with the setup of the DIC equipment. Finally, special thanks to our opponents, Dijana Miteva and Hassan Husain for their continuous feedback.

Göteborg June 2018

Amel Cato

Matiur Rahman Raju

Notations

Roman upper-case letters

A	stands for area of the tested specimen
A_o	stands for the original cross-sectional area of the specimen
$A_{act.}$	stands for the actual (uncorroded) area of the tested specimen.
$A_{avg.}$	stands for the average corroded area of the tested specimen
$A_{ccs.}$	stands for the critical cross-sectional area of the tested specimen
A_{real}	stands the cross-sectional area within the failure zone of the specimen.
C	stands for the actual corroded specimen weight
DIC	stands for the Digital Image Correlation
E	stands for the modulus of elasticity
L_o	stands for the initial length of the specimen
P	stands for the force measured by the universal testing machine

Roman lower-case letters

ff	stands for the fracture strength
f_y	stands for the yield load of the specimen
f_u	stands for the maximum load on the specimen
r	stands for the measured (actual) radius of the uncorroded reinforcing steel bar.
r_{real}	stands for is the real radius of the reinforcing steel bar varying for every load stage.

Greek upper-case letters

ΔL	stands for the elongation in the direction of applied force

Greek lower-case letters

σ	stands for the stress
$\sigma_{avg.}$	stands for the average corroded stress
$\sigma_{ccs.}$	stands for the critical cross section stress
σ_E	stands for the engineering stress
σ_f	stands for the fracture stress
$\sigma_{act.}$	stands for is the actual stress
σ_T	stands for the true stress
σ_u	stands for the ultimate stress
σ_y	stands for the yield stress
ε_E	stands for the engineering strain

Special characters

$n.C$ stands for the average weight of non-corroded reference specimen
$avg.cor.lev$ stands for the average corrosion level.

1 Introduction

1.1 Background

Despite the used technology at the leading edge and substantial innovations in construction practice and design, corrosion of steel bars in reinforced concrete structures is still considered to be one of the main reasons of deterioration which causes high costs due to repairing and replacing critical corroded elements in reinforced concrete structures (Fernandez, Bairán and Marí, 2016; Tahershamsi et al., 2017). This has directed to a rising demand and need for a better understanding of the structural effects of corrosion.

Corrosion of reinforcing steel can be divided into two subcategories: Pitting corrosion and generalised corrosion. Pitting corrosion is characterized by the formation of localized pits along the steel bar when generalised corrosion can be seen as several local pits distributed along the bar. The common outcome for the two subcategories are increases in volume of corrosion products and by so causing surrounding concrete cover to expand and crack. Furthermore, when a reinforcing steel bar is affected by pitting corrosion and subjected to tension, local effects at the cross section due stress concentration and local bending are unveiled. In addition, multi-axial stress behavior is also observed due to the presence of those pits. Hence, due to those mentioned effects, the apparent mechanical properties that states the overall steel bar behavior are affected, producing a performance reduction (Fernandez, Bairán and Marí, 2015, 2016). This leads to a major concern to the structural behavior in serviceability and ultimate limit states, which needs to be investigated.

1.2 Aim and objectives

The aim of this study is to obtain actual mechanical properties of uncorroded reinforcing bars and to describe apparent mechanical properties of corroded reinforcing bars in different ways, hence to increase the level of knowledge about the local effects above mentioned. This knowledge will lead to better understanding of structural behavior for corroded steel reinforced concrete structures in serviceability and ultimate limit states. To find such properties Digital Image Correlation (DIC) technology will be used experimentally in tensile tests for naturally corroded specimens to obtain strain values in a detailed way. Based on these results the different relations stress-strain for corroded and uncorroded reinforcement bars will be determined. To accomplish the aim of the study several objectives are defined:

- To develop and improve methods of cleaning and preparing corroded reinforcement steel bars extracted from different sources.

- To learn and develop methods for testing steel reinforcement bars under tensile loads.
- To acquire knowledge and independency on using data acquisition method such as Digital Image Correlation (DIC) system.
- To investigate the obtaining of true and engineering stress-strain curves and its variation due to corrosion.
- To study the impact of corrosion and corrosion type in the measured mechanical properties.

1.3 Scope and Limitations

Some considerations related to the test specimen, equipment, method of preparing the test specimen, software used in the study and analyzing the results which needs to have into consideration for the understanding of the obtained results are described below:

- The chosen cleaning method was sandblasting, other methods e.g. mechanical wire bristle brushing, chemical cleaning which can provide different results were not used.
- The length of the specimens was fixed to 300 and 400 mm.
- Test specimens with 10mm and 16mm diameters were used in this study.
- For the 10mm specimen, the only skewed type was tested.
- Only naturally corroded test specimens were used, artificially corroded were not considered.
- The used optical 3D scanning method to measure the corrosion level for the natural corroded specimens could only detect the subsurface corrosions.
- Only successfully tested specimens were used in the results, the corrupted test results were dismissed.
- All postprocessing of the tested raw data was performed by the software GOM® Correlate Professional 2017, the limit in the extensometer length was 1mm.
- The true stress-strain section is limited to present a method to postprocess the result to successfully obtain such relations for uncorroded bars.
- Correlations between corrosion and the attained mechanical properties are limited to the engineering part, i.e. force versus displacement, force versus engineering strain and engineering stress-strain curve.

1.4 Outline of the thesis

The outline of this thesis is organized in following chapters:

- Chapter 1: Introduction
- Chapter 2: Theoretical background
- Chapter 3: Experimental study
- Chapter 4: Method of postprocessing
- Chapter 5: Experimental results
- Chapter 6: Result analysis and discussion
- Chapter 7: Conclusion
- Chapter 8: Further research
- Chapter 9: References

The report consists of 9 chapters. *Introduction* consists of background, aim and objective, scope and limitations and finally outline of the thesis. *Theoretical background* presents the needed literature to understand the corrosion impacts on the mechanical behavior of reinforcing steel. *Experimental study* introduces the test specimens, equipment and testing methods used in this work. Further in *method of postprocessing*, the software and tools used to postprocess the raw data are presented. *Experimental results* contain the results, where in the *result analysis and discussion* correlation between corrosion and reduction of mechanical properties for corroded reinforcing bars are discussed. *Conclusion* summarizes the study and results. In *further research*, suggestions for further studies are to be found. Lastly, the *references* used in the study are presented.

2 Theoretical background

This chapter reviews the existing literature relevant to understand the mechanical properties of steel bars and the effect of general and pitting corrosion on steel bars.

In reinforced concrete structures, the most frequent cause of deterioration is reinforcement corrosion which occurs in different ways (Llano Trueba, 2015). As a basis on previous research works the most relevant mechanisms of deterioration are carbonation and chloride ingress for reinforced concrete structures world-wide (Division, 2002; Apostolopoulos, Demis and Papadakis, 2013; François, Khan and Dang, 2013; Llano Trueba, 2015; Lau and Lasa, 2016). Furthermore, (Mutsoyoshi, 2001) as reported by (Division, 2002) also concluded that the main causes of deterioration of reinforced concrete bridges in Japan are carbonation and chloride ingress (see *Figure 2.1*). To predict the behavior of the reinforced concrete structures, the study of corrosion effect in the mechanical properties of reinforcing steel bars is essential.

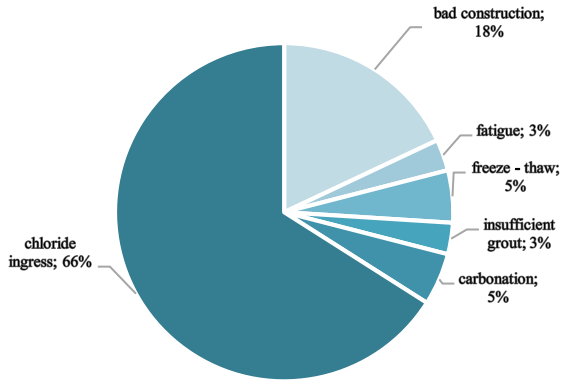

Figure 2.1: The main causes of deterioration of reinforced concrete bridges in Japan. (Mutsoyoshi, 2001), (Division, 2002).

2.1 Corrosion of reinforcement steel in concrete structures

Unprotected steel, when subjected to the elements of nature, will eventually corrode due to different chemical, electrochemical and physical reactions (Burström, 2007). This will cause loss of cross-sectional area, due to the formation of corrosion products which are highly expansive; this will continue until some protective masseurs are taken to protect the steel.

Concrete provides several corrosion protection systems for the reinforcing steels. Concrete cover creates a physical barrier by operating as buffer zone with relative impermeable and dense structure between the aggressive environment and the reinforcement (U, 2001; Lau and Lasa, 2016).

The thickness of the buffer zone also called cover thickness is regulated by the European building Code (CEN 1992). Furthermore, the chemical corrosion protection is also provided by the concrete, due to its alkaline property. Hydrated concrete in normal state, when not exposed to exterior impacts presents a pH value between 12.5 to 13.5. This provides a favorable environment for the reinforcing steel at which the level of aggressive ions is negligible. Further, a defensive passive film with sub-microscopic dimensions (<10nm) forms around the surface of the steel and by so decreases the rate of corrosion to safe levels, due to the presence of such alkaline environment. The earlier mentioned can be graphically seen in Pourbaix diagram, *Figure 2.2* which explains how prone steel is to corrosion (U, 2001; Angst, 2011; Balestra et al., 2016; Lau and Lasa, 2016).

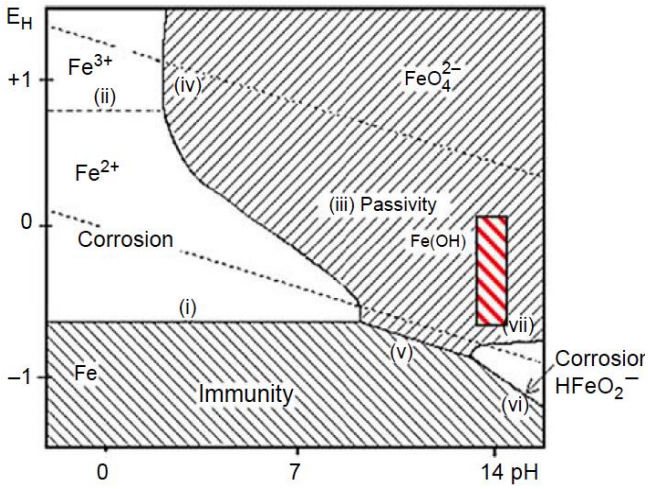

Figure 2.2: Pourbaix diagram, which explains how prone steel is to corrosion, (Fe-H2O at 25°C), (Lau and Lasa, 2016).

However, when external impacts such as de-icing salts, seawater and carbon dioxide from the surrounding environment start to react with the reinforced concrete structures, the corrosion protection of the concrete starts to deteriorate. The alkaline properties start to drop and the pH value decrease causing a more hostile environment for the reinforcing steel. Even the defensive passive film loses its protective function and can be easily penetrated. These described characteristics in the text above are known as carbonation and chloride ingress in concrete (Angst, 2011; Lau and Lasa, 2016).

2.1.1 Carbonation of concrete (generalised corrosion)

Carbonation is a chemical reaction where calcium hydroxide reacts with water and carbon dioxide, by so forms calcium carbonate:

$Ca(OH)_2 + CO_2 \rightarrow CaCO_3 + H_2O$ (Lau and Lasa, 2016).

It is explained as a reversible reaction where the concrete returns to its original state of a lime stone (svenskbetong.se,2018). Another consequence of carbonation is the reduction of pH value, from approximately 13.5 to less than 8.3.

The alkalinity of concrete in practice can be reduced by two potential ways:

1. When reacting with atmospheric (acidic) gases such carbon dioxide or sulphur dioxide.
2. By water (rain water, leached surface water, seawater etc.)

Carbonation depth or also called carbonation front is the advancing depth in concrete where carbonation has occurred. If the carbonation front reaches the reinforcement it will destroy the passive film mentioned in Section 2.1 due to a reduction of pH. Since moisture and oxygen now are accessible it is only a matter of time before corrosion starts. The type of corrosion that carbonation entails is of a general and homogeneous character. This can be translated to evenly distribute surface corrosion. See more how the general corrosion is impacting the mechanical properties of reinforcement steel in Section 2.3.

2.1.2 Chloride ingress in concrete (pitting corrosion)

Chloride, which can be located in various environments, is known to attack the protective passivation film that is formed around the reinforcement steel explained in Section 2.1 (Angst, 2011). The attack on the passivation film is of a localized character. Initiation of the corrosion process is first started when adequate amount of chloride ions reaches the reinforcing steel (Lau and Lasa, 2016). In northern countries such as Canada and the Scandinavian countries the de-icing salts stands for a major source of chloride in conjunction with infrastructural concrete, other governing chloride sources are seawater in marine contexts (Silva, 2013; Lau and Lasa, 2016; Zhu, François and Liu, 2017).

The transportation of chloride through concrete is performed by three different mechanisms:

- Diffusion
- Capillary suction
- Migration

Diffusion occurs as a mechanism of chloride transportation in situations when the concrete is saturated, for instance in submerged environments.

In cases when the concrete is partly dried, the capillary suction becomes leading mechanism of chloride transportation. When dissolved ions in water comes into contact with concrete the capillary suction due to the surface tension gets absorbed in to the concrete (Silva, 2013).

The final way of chloride transportation in concrete is through migration. It occurs through the act of an electrical field where the transportation of ions follows (Silva, 2013).

In summary, when enough chloride ions due to the mechanisms of diffusion, capillary suction or migration reaches the reinforcing steel and its protective film, localized attacks occur on the film and causes localised corrosion on the reinforcing steel. This can be translated to pits, hence the name pitting corrosion (Angst, 2011; Lau and Lasa, 2016). See more how the pitting corrosion is impacting the mechanical properties of reinforcing steel in Section 2.3.

2.2 Natural and artificial corrosion

Corrosion occurs naturally through either carbonation or chloride ingress in concrete as explained in the Section 2.1. The corrosion mechanism can also be artificially produced by different methods in protected laboratorial environments. One of the most widely used artificial methods to accelerate the corrosion is the impressed current method, where electric current is used (El Maaddawy and Soudki, 2003). Most of all studies regarding corrosion of reinforcing steel are performed by using accelerated artificial methods where the governing parameters are controlled. Only a small number of tests in this field are performed by naturally corroded reinforcing steel (Balestra *et al.*, 2016). A comparison is conducted in the text below, between the naturally and artificially corroded reinforcing steel regarding the mechanical properties.

(Papadopoulos *et al.*, 2011) and (Zhang *et al.*, 2012) have respectively performed experiments with naturally corroded reinforcing steel. The results of their work lead to the conclusion that corrosion has a negative impact on the mechanical properties of the reinforcing steel. Further studies such as (Apostolopoulos, Demis and Papadakis, 2013; François, Khan and Dang, 2013) and (Zhu and François, 2014) have used the artificial corroded reinforcing steel method. Their work shows also similar behavior to (Papadopoulos *et al.*, 2011) and (Zhang *et al.*, 2012) in mechanical properties when the corrosion level of the reinforcement steel is increased. The combined trend for mentioned studies shows a reduction in mechanical properties when the corrosion level of the reinforcing steel is increased disregard if naturally or artificial corrosion was used in the experiment (Papadopoulos *et al.*, 2011; Balestra *et al.*, 2016).

2.3 Mechanical properties

2.3.1 Uncorroded steels

For analyzing the mechanical properties of steel bars, the obtained stress-strain curve from steel specimen under tensile loading can describe the major mechanical parameters like modulus of elasticity, yield strength, ultimate tensile strength, fracture strain, and yield strain etc (Faridmehr *et al.*, 2014). Due to increasing tensile loading on specimen the stress-strain curves show the two-deformation region, elastic and plastic deformation region with different mechanical properties (see *Figure 2.3*) (Technology and Structures, 2017).

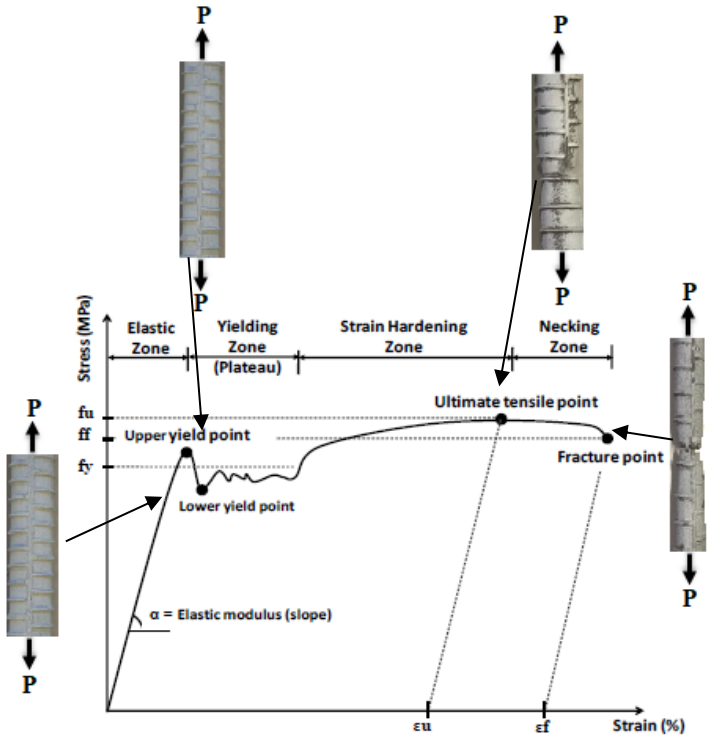

Figure 2.3: Typical stress-strain curve for a steel specimen under tensile loading (Llano Trueba, 2015).

2.3.1.1 Engineering stress-strain relationship

To determine the engineering stress-strain value, a tensile test will be performed. A test specimen is placed on a Universal Testing Machine (UTM) and then, applied the force in the longitudinal direction until failure. Elongation and force values corresponding to displacement until specimen failure are recorded (Faridmehr et al., 2014). During the tensile test all the parameters which are used to determine the stress-strain value are presented in *Figure 2.4*. Engineering stress and strain can be calculated according to equation (2.1) and (2.2) in relation to the initial cross-section and length of the specimen.

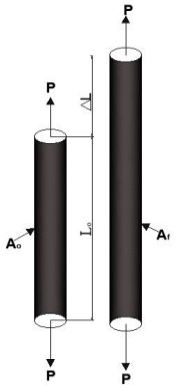

Figure 2.4: Schematic representation of specimen tension test.

$$\sigma_E = \frac{P}{A_o} \tag{2.1}$$

$$\varepsilon_E = \frac{\Delta L}{Lo} \tag{2.2}$$

where:

σ_E is the engineering stress.

ε_E is the engineering strain.

P is the actual force measured by the universal testing machine.

A_o is the original cross-sectional area of the specimen.

L_o is the initial length of the specimen.

ΔL is the elongation in the direction of applied force.

Modulus of elasticity:

In the elastic zone, the engineering stress is proportional to the engineering strain linearly which follow the Hooke' law and the slope of the curve in the elastic zone (see *Figure 2.3*) defined the modulus of elasticity (E) as the ratio between the stress and strain values using below equation (2.3).

$$E = \frac{\sigma_E}{\varepsilon_E} \tag{2.3}$$

Yield strength:

In the stress-strain curve, the yield strength is the stress value which can be obtained from the yielding zone (plateau) where elongation is increasing suddenly without the change of stress level (Faridmehr et al., 2014). The yield strength has an important impact on structural design due to plastic deformation. At the same time yield stress (σ_y) can be calculated using below equation (2.4).

$$\sigma_y = \frac{f_y}{A_o} \tag{2.4}$$

where:

f_y is the yield strength of the specimen.

Ultimate tensile strength:
After yielding, the stress for permanent elongation occurs due to continue loading which specifies the strain hardening zone (Faridmehr *et al.*, 2014). In the stress-strain curve before the necking zone the maximum ultimate stress (σ_u) point recorded for the specimen which indicates the ultimate tensile strength, see equation (2.5).

$$\sigma_u = \frac{f_u}{A_o} \tag{2.5}$$

where:
f_u is the maximum load on the specimen.

Fracture strength:
After the necking the stress decreases until failure where the fracture strength of the specimen can be measured by drawing a straight line at the fracture point in the stress-strain curve (Faridmehr *et al.*, 2014). At the same time fracture stress (σ_f) can be calculated using the equation (2.6).

$$\sigma_f = \frac{ff}{A_o} \tag{2.6}$$

where:
ff is the fracture strength.

2.3.1.2 True stress-strain relationship

As discussed before in section 2.3.1.1, the stress value is calculated with the original fixed cross-sectional area and length of the steel specimen. In the plastic region due to increased tensile load the cross-sectional area and length of the specimen are not same as original geometry. The measured stress value with changing geometry of the steel specimens defined as a true stress using below equation (2.7) (Roylance, 2001).

$$\sigma_T = \frac{P}{A_{real}} \tag{2.7}$$

where:
σ_T is the true stress.
A_{real} is the cross-sectional area within the failure zone of the specimen.
P is the actual force measured by the universal testing machine.

The true strain value in the changing geometry of the steel specimens is correlated to engineering strain. From the above equation (2.2) where total elongation by applied force was used to determine engineering strain. For the true strain sequential elongation (ΔL_1, $\Delta L_{2,\ldots}$ ΔL_n) value are recorded by applied force instead of total elongation (ΔL) and divided each elongation value by the initial length (L_o) of the specimen between corresponding extensometer (Brinson and Brinson, 2015).

To measure the total true strain value of the specimen the calculated sequential strain value needed to be added collectively in the following equation (2.8),

$$\varepsilon_T = \sum\left(\frac{\Delta L1}{Lo} + \frac{\Delta L2}{Lo} + \cdots + \frac{\Delta Ln}{Lo}\right) \quad (2.8)$$

where

ε_T is the true strain.

L_o is the initial length of the specimen.

$\Delta L_1, \Delta L_{2....} \Delta L_n$ is the sequential elongation in the direction of applied force.

To obtain the true stress-strain value in the necking region, the average local axial strain and radius difference can be measured by optical systems (Morka and Niezgoda, 2012). From this it is possible to develop the true stress-strain curve for comparison with engineering stress-strain curve to further measure the real mechanical behavior after reduction of the cross section and changing length (*see Figure 2.5)*.

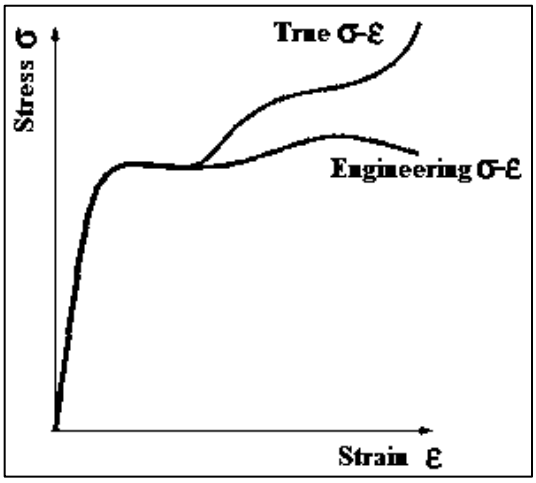

Figure 2.5: Schematic representation for engineering stress-strain and true stress-strain curve (Faridmehr et al., 2014).

2.3.2 Corroded steels

Many researchers such as U, 2001; Du, Clark and Chan, 2005; Apostolopoulos, 2007; Zhang et al., 2012; Apostolopoulos, Demis and Papadakis, 2013; François, Khan and Dang, 2013; Balestra et al., 2016; Tahershamsi et al., 2017; Zhu et al., 2017; Fernandez, Bairán and Marí, 2016; Fernandez, Bairán and Marí, 2015 have already studied the effects for different corrosion types of steel reinforcement and its influence on the mechanical properties. An experimental study of both natural and artificial corroded specimens for tensile test results showed a significant degradation in ultimate strength. Further studies show that naturally corroded rebars have more affecting mechanical results than artificial corroded rebars (Zhang et al., 2012). Due to the generalised and pitting corrosion of steel reinforcement, the cross-section geometry is changing by the loss of the real cross-section diameter of the specimens (Fernandez, Bairán and Marí, 2016). Moreover, pitting corrosion affects a specific part of the bar with non-uniform stress distribution due to the displacement of the center of gravity at the cross-section (Fernandez, Bairán and Marí, 2015; Tahershamsi et al., 2017) and stress concentration due to notch effect. Zhu, François: Liu, (2017), also investigated that reduction of 1% cross-sectional area of the tensile steel reinforcement which leads to 1% loss of flexural yield and 0.84% loss of ultimate loading capacity of the reinforced concrete structures. Apostolopoulos, (2007), experimental results for corroded steel bars which also showed a reduction of ductility, elongation and strain energy density with an exposure time of the specimens.

Fernandez, Bairán and Marí, (2015), performed monotonic tests on bars which ranged corrosion levels between 8% to 22%, and described a decreased ultimate and yield strength where the modulus of elasticity and the measured strain showed higher scattering than the stresses. U, (2001), also tested different bar diameters of corroded steel reinforcement subjected to accelerate corrosion, which indicated that the tensile strength has no significant impact on high levels of corrosion degree using the actual cross-section area. But the corrosion levels beyond 12.6% indicates brittleness of the steel bars and by so decreases the yield strain. Balestra et al., (2016), studied the naturally corroded steel reinforcement effects on both yield and ultimate strength were corrosion degrees considered up to 25%. The same study concludes that yield and ultimate strength values are similar up to 5% of corrosion degree. When the corrosion degree increased up to 12%, the difference between yield and ultimate strengths values were observed in a large limit but the specimens with a corrosion degree about 25% presented the much larger difference between yield and ultimate strengths value due to the pitting damage. François, Khan and Dang, (2013), research work performed on 27-year-old reinforcement corroded steel bars showed that the true yield strength is constant, but the true ultimate strength increased with the increasing of corrosion level. Llano Trueba, (2015), experimental work showed that, ultimate elongation intensely reduced based on the corroded rebars with increased corrosion level up to 20%, but the effective yield and ultimate strengths does not provide enough correlation with increased corrosion level.

Furthermore, in the case for pitting corrosion (Fernandez, Bairán and Marí, 2016) observed that same pit length in corroded specimens with different pit angle apertures and depth with respect to the degree of corrosion level (0-60%) has no significant impact on the tensile steel parameters such as; modulus of elasticity, yield stress and ultimate stress. Apostolopoulos, Demis, and Papadakis, (2013), investigated the effects of chloride-induced corrosion to compare the embedded and bare samples for the same level of mass loss. The analysis results indicate that embedded samples have more strength than bare samples, but at the same time for embedded samples reduce the ductile properties such as; yield strength and uniform elongation. Further, a significant difference in mechanical behavior was observed between pitting depth and area where the pitting depth was the governing factor for failure point. Du, Clark and Chan, (2005), reported that residual capacity is similar for bare and embedded samples with the same corrosion level but due to local corrosion the residual strength decreased more rapidly compared to uncorroded bars when the corrosion level is more than 16%.

This chapter discussed a literature review about the two most leading mechanisms of deterioration; carbonation and chloride ingress which causes corrosion on steel reinforcement in concrete structures. The effects of generalised and local corrosion on corroded steel reinforcement were also mentioned which impact the mechanical properties of corroded bars. The Bayesian network from *Figure 2.6* shows that how corroded rebars impacts on the mechanical properties.

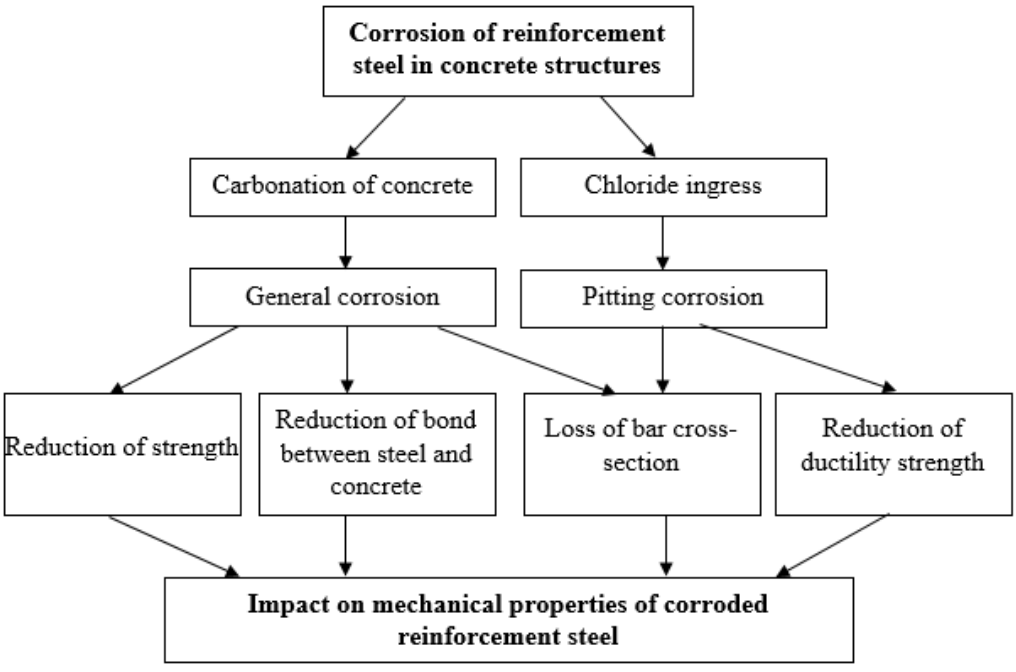

Figure 2.6: Bayesian network for corroded rebar impact on mechanical properties.

3 Experimental study

In this experimental study, monotonic tests on steel bars measured by Digital Image Correlation (DIC) techniques were conducted by using different bar diameters and lengths for uncorroded and corroded specimens, with the underlying purpose to investigate the impact of corrosion on the mechanical properties of the steel reinforcement. The corrosion levels were measured by using different methods in terms of steel geometry and weight, hence possible correlation between corrosion degree and mechanical properties of uncorroded and corroded specimens were defined.
The experimental work for this project was conducted in several steps. First, the collection of corroded and uncorroded reinforcing steel samples followed by cutting the specimens for further stages. Thereafter the bars were cleaned to remove the corrosion products attached on the surface and assess the corrosion damage using both gravimetric and 3D scanning techniques. Finally, test specimens were painted with a stochastic pattern for assessing the mechanical properties by using the Digital Image Correlation (DIC) measuring techniques in combination with monotonic tests. The post-processing method for the different types of specimen are presented in Chapter 4.

3.1 Test specimens

A total of 57 reinforcement test specimens divided in three different set, organized by the source and characteristics of the bars were tested, see *Figure 3.1*. Each group was at the same time divided in two groups to differentiate between corroded and uncorroded specimens. The sub types are:

- Type A1: 16mm naturally corroded, skewed, reinforcing bars.
- Type A2: 16mm uncorroded, skewed reinforcing bars.
- Type B1: 16mm naturally corroded, straight reinforcing bars.
- Type B2: 16mm uncorroded, straight reinforcing bars.
- Type C1: 10mm accelerated naturally corroded, skewed reinforcing bars
- Type C2: 10mm uncorroded, skewed reinforcing bars.

(a)

(b)

(c)

(d)

(e)

Figure 3.1:Images of some specimens from different sources where figures (a) shows the type A1 and B1 naturally corroded 16mm rebars, (b) shows the type C1 accelerated naturally corroded 10mm rebars, (c) shows type A2 uncorroded 16mm rebars, (d) shows type B2 uncorroded 16mm rebars, (e) shows the type C1 accelerated naturally uncorroded 10mm rebars.

Test specimens (type A1, A2, B1 and B2) of diameter 16mm were part of a large experimental study (Gestsdottir and Gudmundsson, 2012; Tahershamsi, 2016), where beams were tested in four-point suspended bending to obtain anchorage failure. This experimental study was conducted at Chalmers University of Technology from the edge beams of the Stallbacka Bridge. This is one of the largest bridge in Sweden with the length of 1400m, a height of 27m and a total width of 14.95m (Arnholm, 2004). The bridge has been localised between Stallbacka industrial area and Överby shopping centre since 1981. After more than 30 years the bridge needed restoration due to cracking of the edge beams. After cracking it can be concluded that de-icing salts caused severe corrosion on the reinforcing steel in form of general and pitting corrosion (Gestsdottir and Gudmundsson, 2012). Another master's study project has been conducted to assess the corrosion behavior with correlations to the critical cross section for different corrosion levels using the specimens (type A1, A2 B1 and B2) (Das, Unpublished). The (type C1 and C2) specimens were obtained from a long-term experiment conducted between the Chalmers University of Technology and Thomas Betong group. This research work was performed by naturally accelerated corrosion technique to induced different damage for corroded steel reinforcement (Berrocal, 2017).

3.2 Preparation of test specimens

For the experiment purpose, rebars were cut by a horizontal band saw machine with ranging lengths of 300 and 400mm. According to Fernandez et al. (Fernandez, Lundgren and Zandi, no date), the most common methods to clean the corrosion products of the rebars are metallic brushing, acid immersion and sandblasting. The comparison results of 3D scanning and gravimetric measurements for different cleaning methods shown that the sandblasting cleaning method has the best agreement irrespective of the actual corrosion level. Consequently, after cutting the rebars in specific lengths, sandblasting cleaning method was used with silica particle to remove all corrosion products from the reinforcing steel in a closed loop system.

After removal of corrosion products from the corroded specimens, the diameter of the rebars was measured by using the Vernier caliper. The explained preparations steps are visualized in *Figure 3.2.*

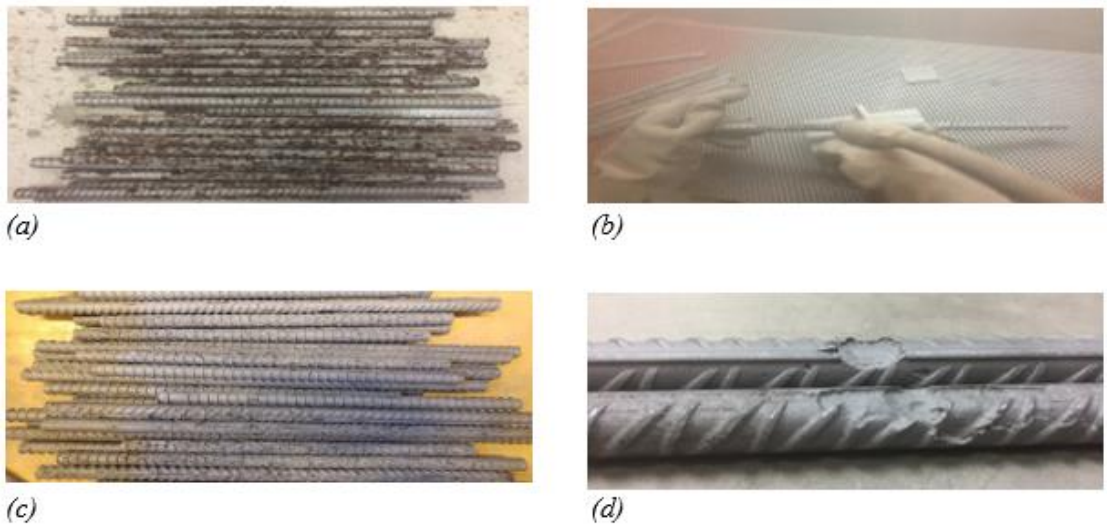

Figure 3.2: (a) Collection of corroded rebars, (b) removal of corrosion products using sandblasting method, (c) cleaned bars by means of sandblasting method, (d) visualised example of pitting corrosion.

3.3 Corrosion level measurements

To be able to draw parallels between the corrosion level and how it is impacting the mechanical properties of the reinforcement steel it is crucial to use accurate and reliable corrosion level measurements. In this study gravimetric measurements and 3D scanning measurements were used to determine the corrosion level. Two measurement methods were conducted to complement each other, increase the trustworthiness and credibility of the results.

3.3.1 Gravimetric measurements

Gravimetric measurement is a method where the calculations are based on weighted corroded and non-corroded steel reinforcement, i.e. weight loss. After the corroded steel reinforcement was prepared as mentioned in the Section 3.2, the specimen was weighted on a digital scale with an accuracy of 0,01 gram.

The corroded weight-values for each specimen were compared with the average weight-value of non-corroded steel reinforcement, which was used as reference when calculating the corrosion degree. This procedure was used because the initial weight of each bar before corrosion was unknown.
When the reference weight of the non-corroded steel reinforcement is established, then the calculation can be performed to check the average corrosion degree by using the equation 3.1. See *Table 3.1* for the calculated corrosion levels for the tested bars.

$$avg.cor.lev = \frac{(n.C. - C.)}{n.C.} \quad (3.1)$$

where:
$avg.cor.lev$ is the average corrosion level.
$n.C$ is the average weight of non-corroded reference specimen.
C is the actual corroded specimen weight.

3.3.2 3D scanning measurements

The 3D scanning is a method that relies on optical measurements. The 3D-scanned results used in this study are a continuation of a previous year research work conducted at Chalmers University of Technology, see *Table 3.1* (Das, unpublished; Berrocal, 2017). For those research works the scanning was performed by using a pair of industrial scaled cameras of five megapixel each, set to film in stereo setting. A maximum accuracy of 2.0 μm was possible to obtain due to the used cameras, which is sufficient in conditions where the corrosion imperfections on the surface of the reinforcing steel needs to be measured. The consequence of the scanning resulted into a fine mesh of surface polygons with triangular shape connected by nodes. For every scanning a number of 2,000,000 to 4,000,000 triangular elements was obtained, creating a high-resolution 3D picture of the scanned specimen detailed enough to gain important information such as: pit distribution, pit depth, pit length and loss of cross-sectional area along the reinforcing steel bar see *Figure 3.3* (Tahershamsi *et al.*, 2017).

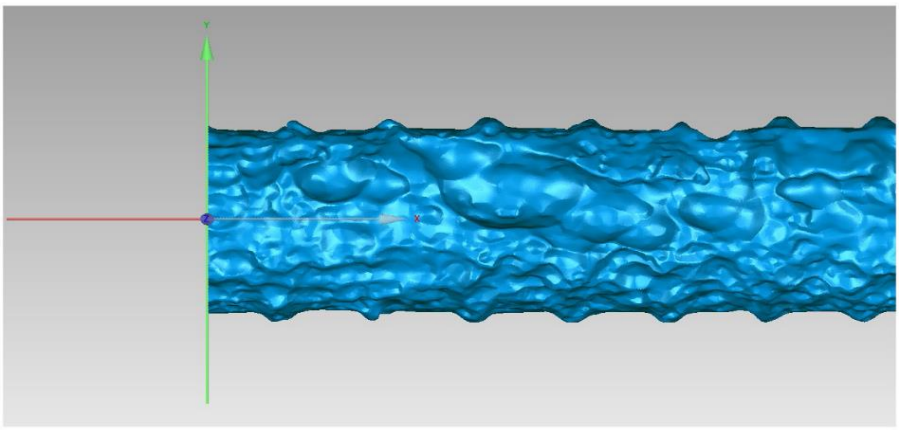

Figure 3.3: 3D scanned surface of the bar (Tahershamsi et al., 2017).

The procedure to establish the corrosion level based on the 3D scanning was conducted in accordance with (Tahershamsi *et al.*, 2017). This can be directed in six steps shown below:

1. The geometry of the scanned reinforcement bar *Figure 3.4 (a)* was converted into a "cloud point mesh" which enabled a possibility to preserve the measured shape.
2. The original Cartesian coordinate system of each node (*X*, *Y*, *Z*) were transformed into a polar coordinate system (θ, r, x), due to the ability of a straight forward approach of calculating the cross-sectional areas, where θ

stands for the angel with respect to the local cross-section y-axis, r was the Euclidian distance of point regarding the normal axis and x stands for the longitudinal coordinate X in the global coordinates, see *Figure 3.4 (b*).

3. The current data from (2.) was interpolated to create a certain mesh-grid defined by (θ′, x′) generating a new interpolated r′ minor to every pair of (θ′, x′) coordinates. These when plotted in a surface plot pictures the penetration of corrosion along the reinforcement bar surface where the different colors are directly linked to the level of penetration see *Figure 3.4 (b).*
4. A function displayed below was used to define the cross-sectional area at x′ where it subsequently was plotted in blue in *Figure 3.4 (d).* The red line in *Figure 3.4 (d)* symbolizes the levelled fit between the plotted blue deviations.

$$A(\mathrm{x}') = \int_{-x}^{x} \frac{\mathrm{r}'(\theta', \mathrm{x}')^{\,2}}{2} * d\theta'$$

5. The reference A_0 was set to be an average non-corroded region of the reinforcement bar.
6. Finally, a levelled fit of the cross-sectional area was regulated by the $A_{0,}$ see *Figure 3.4* (e) and the corrosion level varied along the bar length, see *Figure 3.4* (e).

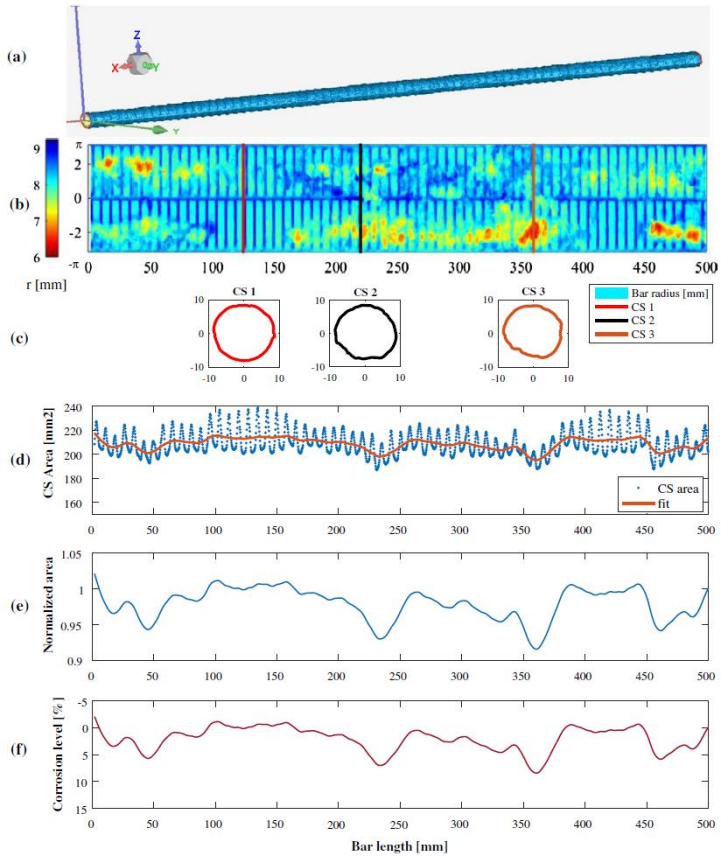

Figure 3.4: Images shows the outline of the procedure to obtain the corrosion degree of the reinforcing bar (Tahershamsi et al., 2017).

3.3.3 Corrosion level comparison and analysed areas

From the two methods earlier discussed, the gravimetric method measured the average corrosion level for the full bar length of each specimen which can be related to generalized corrosion. The 3D scanning assessed the corrosion level in the critical cross-section where the bar failed which in turn is related to pitting corrosion. 3D scan method was also further used to validate the results from the gravimetric method and by so increase the trustworthiness. Both average corrosion levels by weight and by 3D scanning, were compared to each other and described in *Figure 3.5*, where it described a linear trend i.e. similar values. Based on these two methods the cross sectional area of the rebar was reduced in two ways: average (idealized) corroded area along the rebar, founded on the actual, uncorroded radius see equation (3.2 - 3.3) and critical cross-section (CCS) reduced area from 3D scan.

Summarizing, three different areas for the reinforcing steel were used in this work:

- Actual (uncorroded) area.
- Average (idealized) corroded area.
- Critical cross-section (CCS) reduced area.

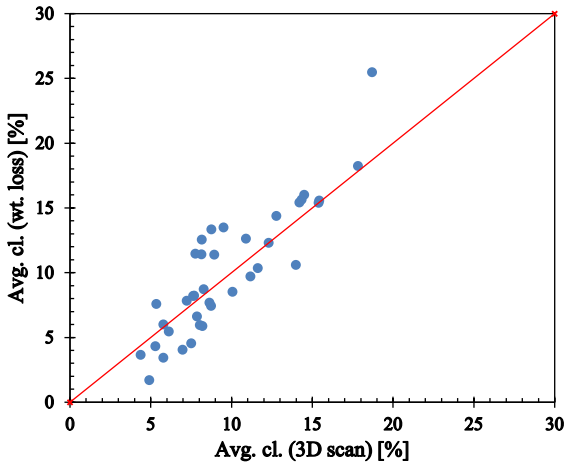

Figure 3.5: Comparison between average gravimetric (wt. loss) and average 3D scan.

$$A_{act.} = \pi r^2 \tag{3.2}$$

where:

$A_{act.}$ is the actual (uncorroded) area of the tested specimen.

r is the measured (actual) radius of the uncorroded reinforcing steel bar.

$$A_{avg.} = A_{act.} \times (1 - avg.cor.lev.) \tag{3.3}$$

where:

$A_{avg.}$ is the average corroded area of the tested specimen.

$avg.cor.lev$ is the average corrosion level.

The actual (uncorroded), average corroded and CCS areas are respectively displayed in *Figure 3.6*. The detailed description of all the acquired parameters is summarized in *Table 3.1*.

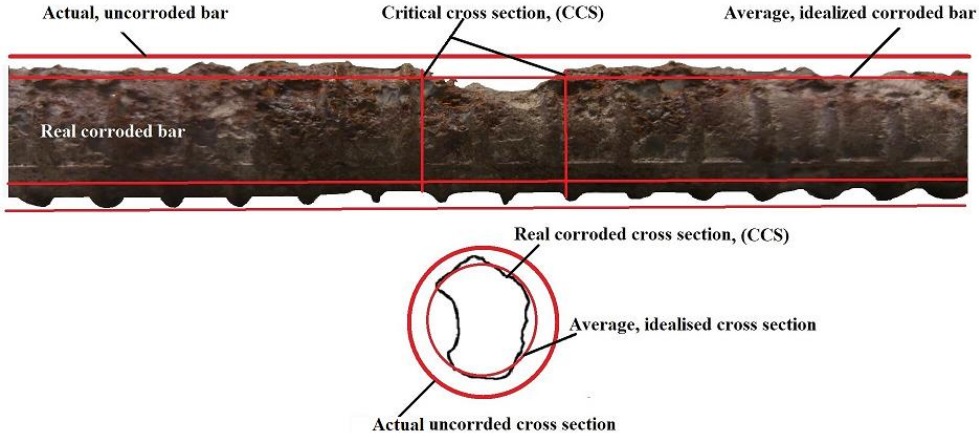

Figure 3.6: Different type of steel reinforcement areas used in this study.

Table 3.1: Specifications of test specimens.

Type of specimen	Specimen number	Bar length [mm]	Actual (uncorroded) diameter [mm]	Average corrosion level (wt. loss) [%]	Average corrosion level (3D scan) [%]	Corrosion at critical cross-section (3D scan) [%]	Actual area [mm^2]	Average (Idealized) area (wt. loss) [mm^2]	Average (Idealized) area (3D scan) [mm^2]	Critical cross-sectional (CCS) area [mm^2]	Type of rib	Corrosion type
Type A1	1	410	16,59	7,5	4,5	13,4	216,05	200	206	187	Skewed	Naturally corroded
	3	400	16,59	8,2	11,4	25,5	216,05	198	191	161	Skewed	
	5	400	16,59	8,7	7,4	12,3	216,05	197	200	189	Skewed	
	6	400	16,59	7,2	7,8	21,4	216,05	200	199	170	Skewed	
	8	415	16,59	7,0	4,0	14,6	216,05	201	207	184	Skewed	
	9	410	16,59	7,7	8,2	19,3	216,05	199	198	174	Skewed	
	10	400	16,59	10,1	8,5	12,9	216,05	194	198	188	Skewed	
	11	410	16,59	8,2	5,9	9,7	216,05	198	203	195	Skewed	
	16	410	16,59	8,6	7,7	16,7	216,05	197	199	180	Skewed	
	17	-	-	-		-	-	-	-	-	-	-
	18	400	16,59	7,8	11,5	20,0	216,05	199	191	173	Skewed	
Type A2	U49	400	16,59	-	-	-	216,05	-	-	-	Skewed	Uncorroded
	U51	400	16,59	-	-	-	216,05	-	-	-	Skewed	
	U53	280	16,59	-	-	-	216,05	-	-	-	Skewed	
	U54	400	16,59	-	-	-	216,05	-	-	-	Skewed	
	U55	400	16,59	-	-	-	216,05	-	-	-	Skewed	
Type B1	2	410	16,41	8,0	5,9	11,2	211,60	195	199	188	Straight	Naturally corroded
	4	400	16,41	9,5	13,5	30,6	211,39	191	183	147	Straight	
	7	400	16,41	14,0	10,6	17,8	211,39	182	189	174	Straight	
	12	400	16,41	8,7	13,3	26,9	211,39	193	183	155	Straight	

Table 3.1: Specifications of test specimens (continued).

Type of specimen	Specimen number	Bar length [mm]	Actual (uncorroded) diameter [mm]	Average corrosion level (wt. loss) [%]	Average corrosion level (3D scan) [%]	Corrosion at critical cross-section (3D scan) [%]	Actual area [mm^2]	Average (Idealized) area (wt. loss) [mm^2]	Average (Idealized) area (3D scan) [mm^2]	Critical cross-sectional (CCS) area [mm^2]	Type of rib	Corrosion type
Type B1	13	410	16,41	5,3	4,3	10,1	211,39	200	202	190	Straight	Naturally corroded
	14	400	16,41	10,9	12,6	20,0	211,39	188	185	169	Straight	
	15	400	16,41	8,9	11,4	16,3	211,39	193	187	177	Straight	
	19	400	16,41	8,2	12,5	24,3	211,39	194	185	160	Straight	
	20	300	16,41	14,5	16,0	27,1	211,39	181	178	154	Straight	
	21	300	16,41	14,2	15,4	19,7	211,39	181	179	170	Straight	
	22	310	16,41	5,8	3,4	7,7	211,39	199	204	195	Straight	
	23	300	16,41	8,3	8,7	16,7	211,39	194	193	176	Straight	
	24	300	16,41	6,1	5,5	17,7	211,39	198	200	174	Straight	
	25	300	16,41	7,6	8,2	14,6	211,39	195	194	181	Straight	
	26	300	16,41	14,3	15,6	25,0	211,39	181	178	158	Straight	
	27	300	16,41	12,8	14,4	18,4	211,39	184	181	173	Straight	
	28	300	16,41	7,9	6,6	13,0	211,39	195	197	184	Straight	
	29	300	16,41	11,6	10,4	19,1	211,39	187	189	171	Straight	
	30	300	16,41	5,8	6,0	13,1	211,39	199	199	184	Straight	
	31	310	16,41	4,9	1,7	6,5	211,39	201	208	198	Straight	
	32	300	16,41	11,2	9,7	21,8	211,39	188	191	165	Straight	
	33	300	16,41	17,8	18,2	30,4	211,39	174	173	147	Straight	
	34	300	16,41	5,4	7,6	14,2	211,39	200	195	181	Straight	
	35	305	16,41	4,4	3,7	10,3	211,39	202	204	190	Straight	

Table 3.1: Specifications of test specimens.

Type of specimen	Specimen number	Bar length [mm]	Actual (uncorroded) diameter [mm]	Average corrosion level (wt. loss) [%]	Average corrosion level (3D scan) [%]	Corrosion at critical cross-section (3D scan) [%]	Actual area [mm^2]	Average (Idealized) area (wt. loss) [mm^2]	Average (Idealized) area (3D scan) [mm^2]	Critical cross-sectional (CCS) area [mm^2]	Type of rib	Corrosion type
Type B1	36	305	16,41	15,4	15,6	20,9	211,39	179	178	167	Straight	Naturally corroded
	37	300	16,41	15,4	15,4	28,5	211,39	179	179	151	Straight	
	38	300	16,41	18,7	25,5	39,0	211,39	172	158	129	Straight	
	39	300	16,41	12,3	12,3	20,6	211,39	185	185	168	Straight	
Type B2	U48	400	16,41	-	-	-	211,39	-	-	-	Straight	Uncorroded
	U50	400	16,41	-	-	-	211,39	-	-	-	Straight	
	U52	295	16,41	-	-	-	211,39	-	-	-	Straight	
	U58	400	16,41	-	-	-	211,39	-	-	-	Straight	
	U59	400	16,41	-	-	-	211,39	-	-	-	Straight	
Type C1	40	400	10,1	0,8	-	15,6	80	78,9	-	67,1	Skewed	Accelerated
	41	405	10,1	1,1	-	-	80	-	-	-	Skewed	naturally corroded
	42	405	10,1	0,6	-	-	80	-	-	-	Skewed	
	43	400	10,1	3,5	-	16,4	80	76,7	-	66,5	Skewed	
	44	400	10,1	1,8	-	16,8	80	78,1	-	66,2	Skewed	
	45	400	10,1	0,6	-	15,1	80	79,0	-	67,5	Skewed	
	46	405	10,1	4,6	-	-	80	-	-	-	Skewed	
	47	400	10,1	2,9	-	-	80	-	-	-	Skewed	
Type C2	U56	400	10,1	-		-	80	-	-	-	Skewed	Uncorroded
	U57	400	10,1	-		-	80	-	-	-	Skewed	

3.4 Assessment of Mechanical Properties

3.4.1 Monotonic test procedure

After assessing the corrosion level of the bars, tensile test to failure were performed on an UTM machine of 250 kN capacity with a loading increment of 0.5 kN/s to evaluate the mechanical properties. The different diameter and length specimens were affixed by two clamps, which transferred the load to the rebars controlled by the hydraulic jack of the UTM machine (see *Figure 3.7*). Between the two clamps, the specimen length was chosen 150/200mm and the remaining length placed in each clamp for uniform stress distribution. The applied load and elongation were recorded by DIC system with a high-speed camera until the specimen failure. Uncorroded specimens with the different length and diameter were also tested to compare the mechanical behavior with corroded bars.

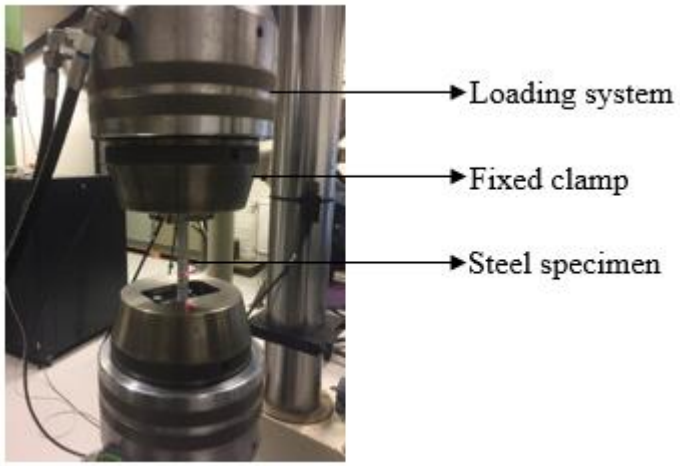

Figure 3.7: Performed tensile test on specimen (MTS machine).

3.4.2 Digital Image Correlation (DIC) measurement system

Digital Image Correlation (DIC) is an optical non-contact 3D measuring system, which enables high qualitative measurements of strains and displacements of a tested item exposed to loading. As a main difference from other traditional measuring equipment, such as strain gauges or extensometers, are the low level of preparations for the specimen, the size of the region where it is possible obtain data from, and the number of measurement points (Jandejsek and Vavrik., 2008). As a main drawback it could be said that the offered accuracy of the system is lower, however, it would be impossible to obtain similar measurements by the use of other existing measuring equipment. Hence is within the scope of this thesis to provide some background on the scope and limitations of such technology when applied to uncorroded and mainly corroded reinforcing steel bars.

The used DIC system in this project was an Aramis® 12M from GOM®. The system consists of two high-resolution cameras with 12 megapixels including a black and white image sensor and 75 mm lenses. Two lights are connected to the cameras support which are in charge of providing the adequate light conditions for reliable measurements. The equipment is, at the same time, connected to a computer responsible of recording the acquired images. The system allows the acquisition of other external data, by connecting it to the optical channels available. The external source of loading was registered which in this project was the tensioning machine explained in the Section 3.4.1. The setup of the DIC system is showed in *Figure 3.8*.

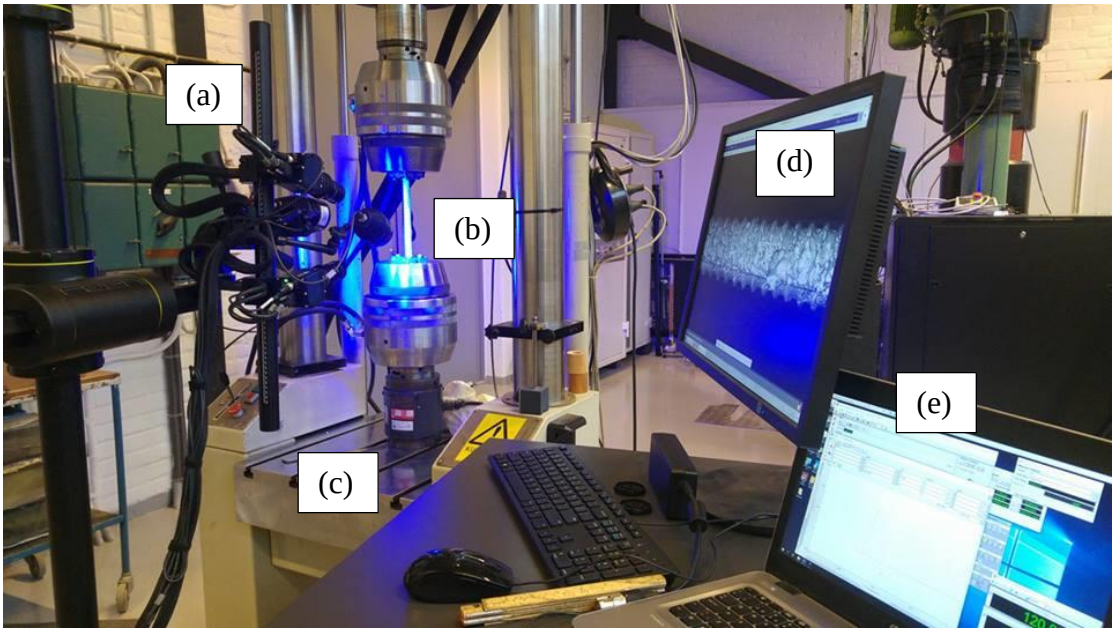

Figure 3.8: Setup of the Digital Image Correlation (DIC) system. (a) double cameras and LED lights, (b) tested specimen, (c) tensile test machine, (d) DIC software, (e) controls for tensile test machine.

The system can monitor different test specimen with different sizes and shapes but needs to be specially calibrated for each case. In this project, the calibration was set up for measuring areas of 100 x 20mm following the manufacturer`s guidelines and standards (Wanat, 2016).

To use the DIC system a stochastic pattern needs to be applied on the specimen. Depending on the size of the specimen different methods to create such pattern are utilized. Due to the size of the specimens used in this project a system of spraying was decided to be used. First, a white dull paint was applied followed by a dull black paint. This created a stochastic pattern (see *Figure 3.9)* that agreed with the manufacturer's recommendations. The DIC system uses this pattern to track the deformation of the specimen, provided by the application of specific loading.

The sequence of images obtained are subsequently compared the reference picture, hence a field of displacements is calculated (Wanat, 2016). The post processing of such measurements allows the obtention of many other relevant parameters.

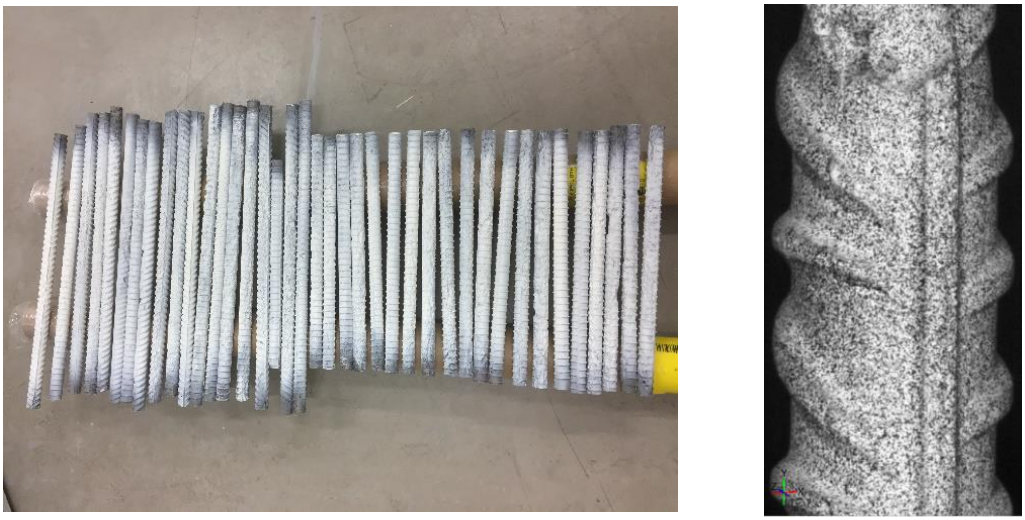

(a) *(b)*

Figure 3.9: (a) Displays the painted reinforcement bars. (b) the bar in zoomed-in setting displaying the stochastic pattern.

4 Method of postprocessing

In this chapter the developed methods for the obtention of the results, force, displacements, strains and stresses are presented.

4.1 Digital Image Correlation (DIC) set-up

The configuration of the DIC equipment for this project allowed an average measuring area of 100 x 20mm, see *Figure 4.1*. Further affected by parameters related to the pits shape, size and corrosion level was the image acquisition rate of the cameras adjusted. This rate varied between 1 to 3 Hz, setting a higher acquisition rate for higher corrosion levels. Collection of raw data measured by DIC equipment from the tension tests is explained in Chapter 3. The post-processing of such data is performed with the software GOM® Correlate Professional 2017 (gom.com, 2018) developed from the same manufacturer who developed the Aramis® 12M system used in this project. This qualifies compatibility between the software and hardware. By using different tools in GOM® Correlate Professional 2017 such as digital extensometers in combination with the measured force, important parameters such as displacement or, strains could be obtained, but also essential data for further postprocessing for obtaining the stress values. The methodology for receiving the needed parameters is presented in further sections.

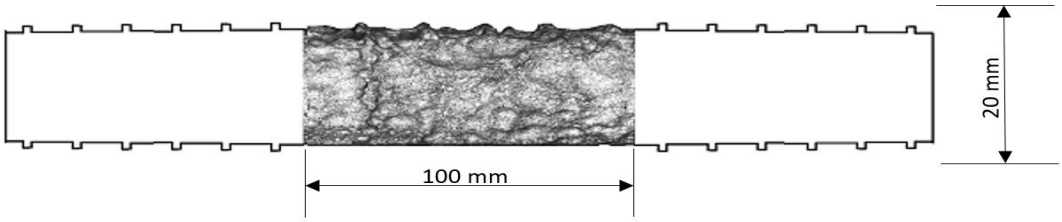

Figure 4.1: Captured area by the cameras in relation to the rest of the specimen.

4.2 Strain and displacement analysis method

As it was mentioned in section 4.1, the GOM® Correlate Professional 2017 software enables the user to obtain strain along the tested specimen. In cases, where the strain and displacement are of interest, a tool in the software named "Extensometer" was used to obtain the requested data. GOM tool works in the same manner when compared to physical extensometers. They operate by, monitoring and measuring the changes in length of the test specimen which is elongated due to the applied tension load, between a specific length. The outcome of the extensometer measurements results in longitudinal or transversal displacement values presented in (mm). To obtain the strains the displacement value is divided by the extensometer length earlier explained in chapter 2.3.1.1 (see equation 2.2). In this study the longitudinal displacements and strains will be considerate.

After establishing the function for GOM extensometer, an analysis of the strain distributions along the measured length was done. The analysis methodology used here was to place several extensometers with a length of 5mm between the ribs of the reinforcing steel bar, see *Figure 4.2*. The specific extensometer length was selected to fit between the ribs, i.e. without interfering with them. The interference with ribs generates a lot of so-called noise, due to discontinuities in the measurements of the DIC system. This can be translated to inaccurate results, which were avoided due to the taken measures.

Figure 4.3 describes clearly two different phases during the testing to failure of the bar: first the whole bar presents a uniform strain distribution in the measured length more or less about the maximum force. Subsequently, the strain starts concentrating in a specific region which corresponded to the necking zone. At the same time the rest of the bars presents some unloading, due to the elastic strain, and the strains at the failure cross-section increases drastically up to 60% of the initial length. The beginning of the necking establishes the maximum force that the bar can take.

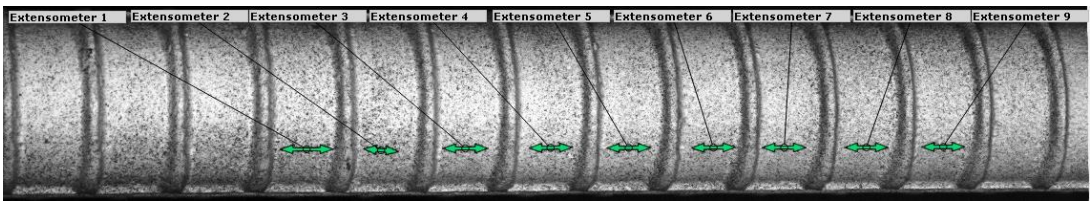

Figure 4.2: The location of extensometers between the ribs of the specimen.

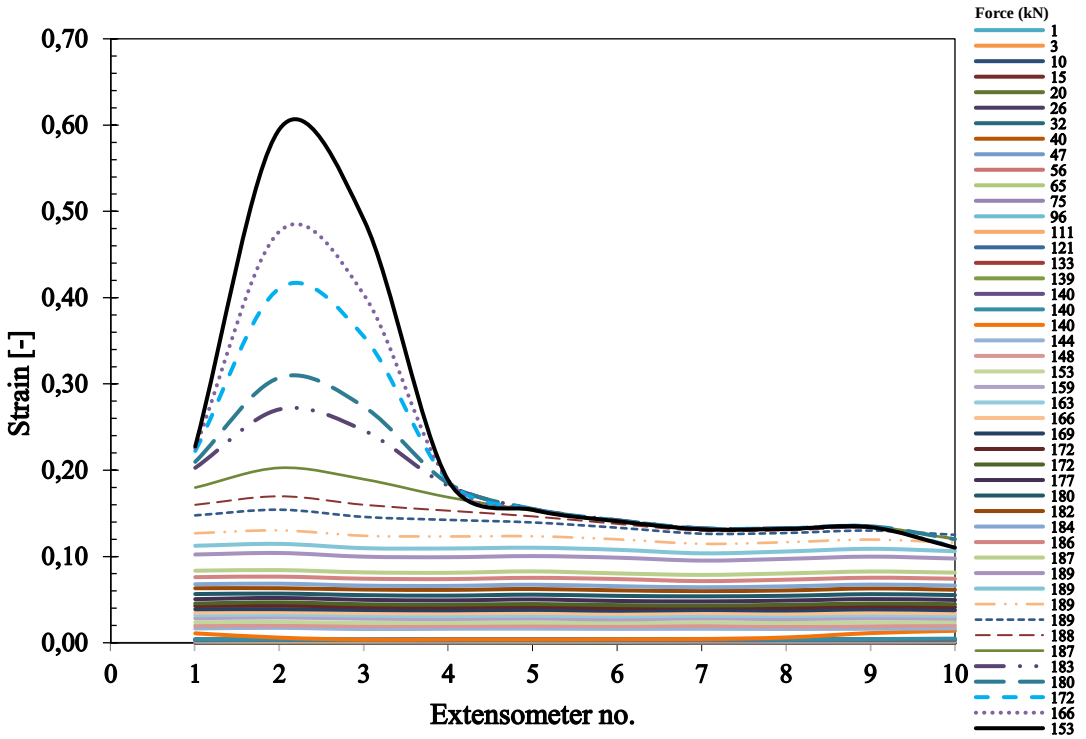

Figure 4.3: Strain distribution along the rebar.

To study the effect of the extensometer characteristics, both the position and the length, in the final observations, two separate analyses were performed, one with the focus put on the impact of the extensometer length and the other putting the focus on the location of the same

In *Figure 4.4*, the description of the different extensometers lengths in the ranges between 1 mm to 40mm is visualized. Corresponding measurement from such extensometers are depicted in *Figure 4.5*. The observed phenomena are that shorter extensometers are giving more exact strain values at the failure zone whereas the longest ones are giving an average strain value between the peak strain and the rest of the bar. This can be explained that longer extensometers are covering a longer length and by so creating an averaged strain value, in comparison to the short extensometers which are smaller and creates a more exact value or close to a true strain value.

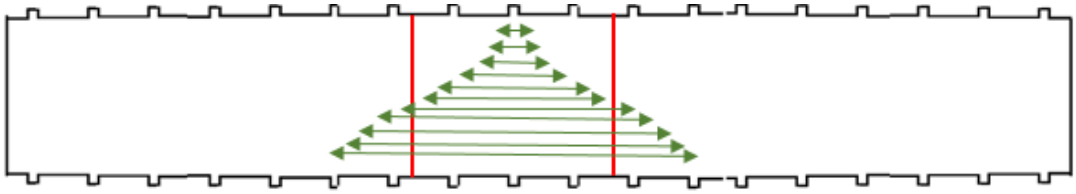

Figure 4.4: Schematic image for extensometer location.

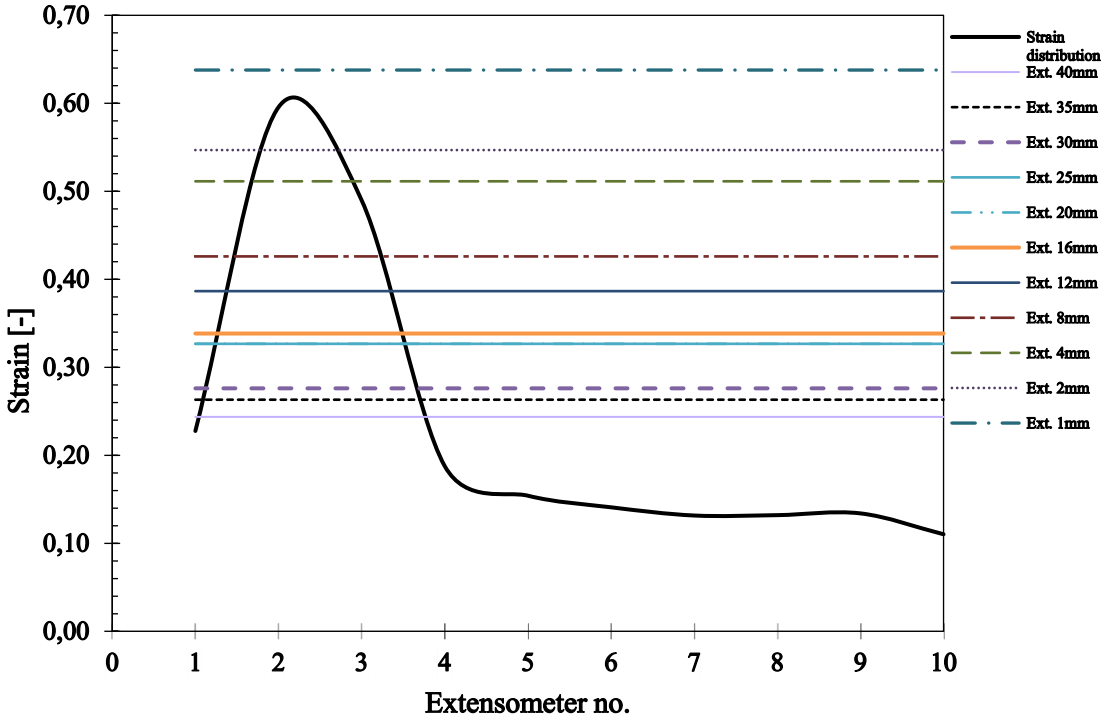

Figure 4.5: Strain level analysis using different extensometer length.

This indicated that the expressed strain when showed the different strain curves of the bar is strongly connected to the measurement length, hence it can have a significant influence on the final results and conclusions.

In this study the failure zone is always included within the extensimeter length, consequently the values after necking represents an average of the strain field between the chosen measurement length.

In *Figure 4.6* extensometers of 25mm length are placed in different locations, 3 within the failure zone (red mark zone in *Figure 4.6*) and 1 outside of failure region to observe the impact of the location on the strain values. As described in *Figure 4.7*, the apparent strain when the extensometer is placed within the failure zone presented no significant variations. However, for the extensometer placed outside the necking region, it was observed in accordance with *Figure 4.3* that after the maximum force at the bar was reached the measured strain decreases elastically with the reduction of the applied load. However, the measurements before the peak load are more or less similar regardless the position of the extensometer. Consequently, if the full curve up to failure is described, then the placed extensometer must be within the failure zone, which is in accordance to the previous results.

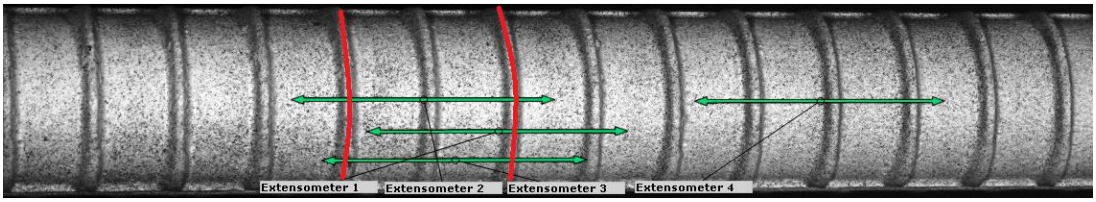

Figure 4.6: Different extensometer location along the bar.

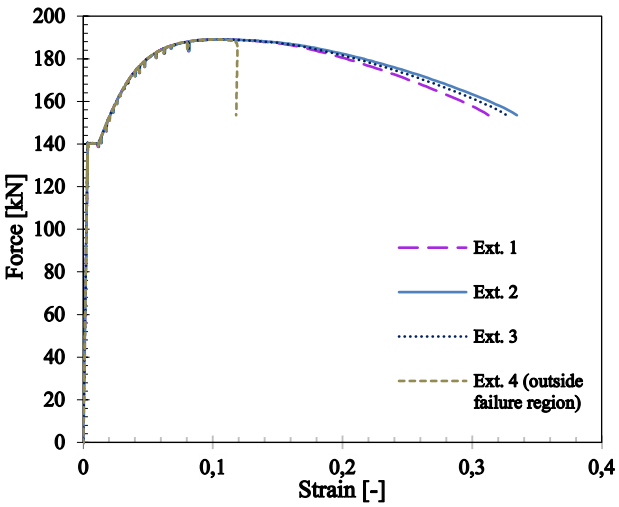

Figure 4.7: Force versus strain behaviour for different extensometer location.

In the following sections it is described how the different measurements in the present work are defined.

4.2.1 Engineering strain and displacement

As it can be seen in *Figure 4.5* the longer extensometers are generating a more averaged strain value. An analysis was performed to obtain a suitable extensometer length needed for the engineering strain. The analysis was conducted by placing 6 different extensometers with different lengths inside the failure zone according to *Figure 4.8*. The outcome of the analysis is presented in the *Figure 4.9*. A similar trend as for the location analysis in *Figure 4.7* was observed, the extensometers are generating same values until peak load. After the peak load the difference between the extensometers starts to increase. A clear formation of the extensometers with the lengths of 20 to 40 mm are visible while the shorter of 15mm is deviating. The conclusion was made that the extensometer length used for the engineering strain and displacement should be between 20 to 40mm and in this study the extensometer of 25mm was selected based on the performed analysis but also on previous works such as (Morka and Niezgoda, 2012).

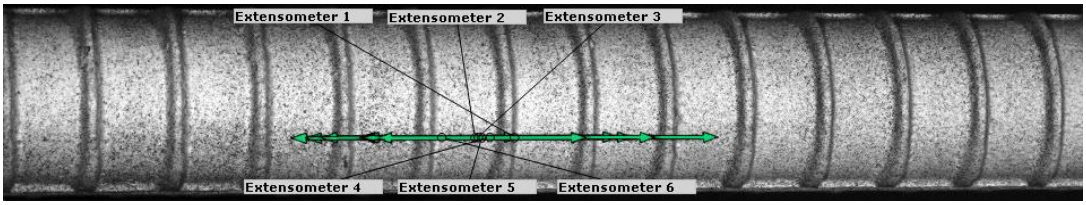

Figure 4.8: Location of different extensometer lengths within failure zone.

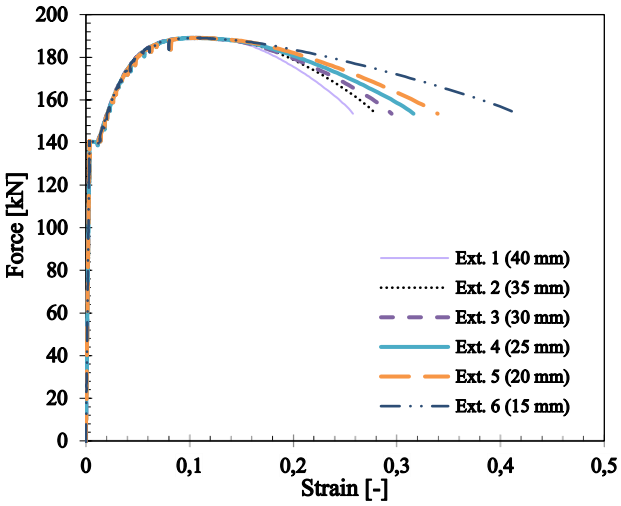

Figure 4.9: Extensometer analysis for the engineering strain showing different extensometer lengths and force versus strain relationships.

4.2.2 True strain

In *Figure 4.5*, the shorter extensometers are closer to the strain peak and by so to the true strain. An additional analysis was performed to see which extensometer length is most suitable for obtaining the true strain. A selection of different lengths that ranges between 1mm up to 20mm were tested. The strain results of such extensometers are displayed in the *Figure 4.10* where the strain value is on the y-axis and the different extensometer lengths on x-axis. A clear trend was noticed throughout the different extensometer lengths where the larger strain value the smaller the extensometer, regardless the magnitude of the applied force. This settle and confirms that small extensometer length is generating strains closer to the true strains. In this study an extensometer length of 1mm was selected due to the explained reasons in the text above. An additional reason for the selection of 1mm length was also the limitation of the used software/hardware where the shortest extensometer length possible giving trustworthy was 1mm.

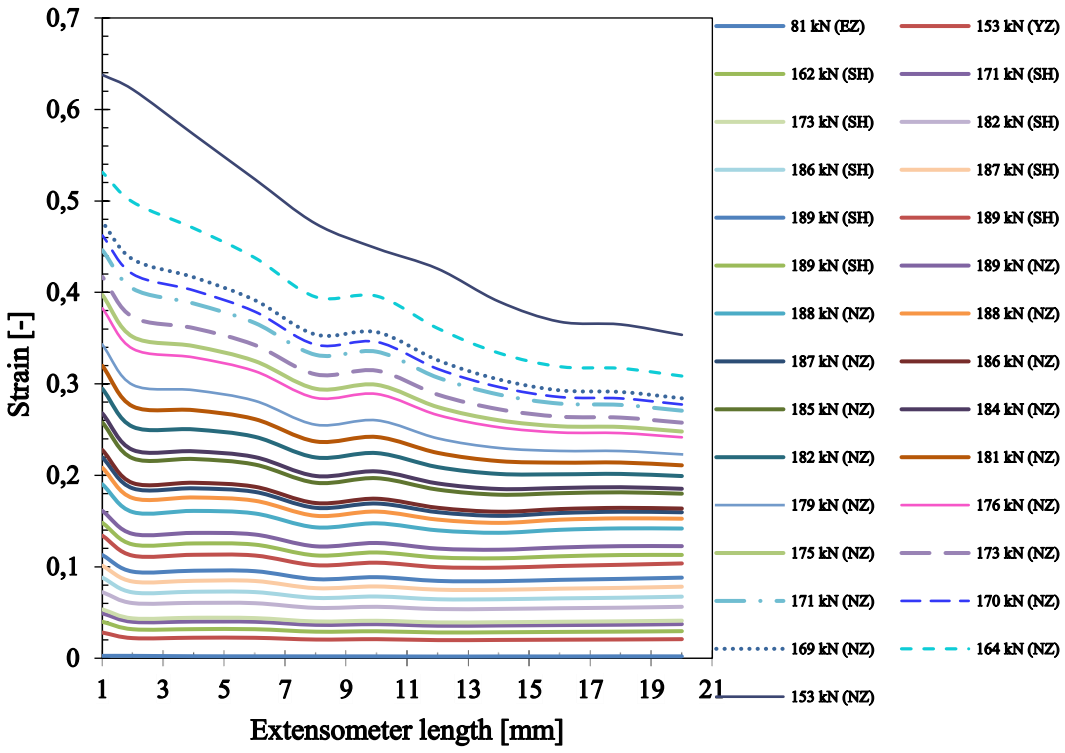

Figure 4.10: Extensometer analysis for true strain at the failure zone using different force pattern where (EZ) is elastic zone, (YZ) is yielding zone, (SH) is strain hardening, (NZ) is necking zone.

4.3 Stress analysis method

For the stress analysis, two parameters are identified as the most relevant, which in addition are used to calculate the corresponding stresses; measured force and area of the tested specimen, see section 2.3.1 The force and area of the tested specimen are used in the equation (4.1), which give the stress value.

Force is directly recorded in GOM Correlate software as an input from the testing machine described in chapter 3.4.1.
In this project two different classifications for the stresses are used, first engineering stresses (section 4.3.1) and second true stress (section 4.3.2).

$$\sigma = \frac{P}{A} \tag{4.1}$$

where:
σ is the stress.
A is area of the tested specimen.
P is the force measured by the universal testing machine.

4.3.1 Engineering stress

In this study three different engineering stresses are defined according to the corresponding areas described in chapter 3.3.3. These areas are defined as: actual (uncorroded), average corroded and critical cross section area. Equation (4.1) can be rewritten by changing the areas as described in equation (4.2), (4.3) and (4.4), respectively

$$\sigma_{act.} = \frac{P}{A_{act.}} \tag{4.2}$$

$$\sigma_{avg.} = \frac{P}{A_{avg.}} \tag{4.3}$$

$$\sigma_{ccs.} = \frac{P}{A_{ccs.}} \tag{4.4}$$

where:
$\sigma_{act.}$ is the actual stress.
$\sigma_{avg.}$ is the average corroded stress.
$\sigma_{ccs.}$ is the critical cross section stress.
$A_{act.}$ is the actual (uncorroded) area of the tested specimen.
$A_{avg.}$ is the average corroded area of the tested specimen.
$A_{ccs.}$ is the critical cross sectional area of the tested specimen.
P is the force measured by the universal testing machine.

In all the cases the calculation for the stresses has performed by assuming the area as an invariant during the test to failure, hence it is defined as a constant value which divided the corresponding load.

4.3.2 True stress

To obtain the true stress same equation presented in 4.3 can be used. However, in this particular case the area it is considered to change due to the applied load. Consequently, two phenomena are accounted in the calculation, first the poison effect, which for tensile stresses reduces the transversal area proportionally to the longitudinal strains. Second the reduction of area at necking is accounted as well so it is possible to obtain the actual stress level at the failure cross-section prior failure, see *Figure 4.11*.

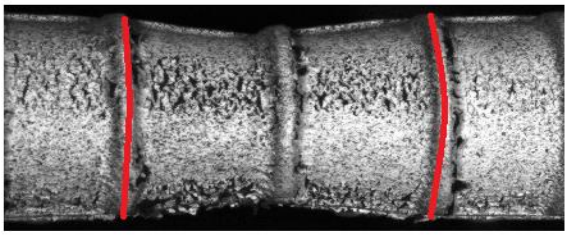

Figure 4.11: Reduced area in the failure zone (red line zone).

To obtain the reduced cross-sectional area for every load stage of the tested bar a method needs to be developed. From GOM® Correlate Professional 2017 single section tool was used. This function allowed to follow the movement of all the measurement points within the section, hence to measure and obtain the x, y, and z-values for each single step with respect to the origin of coordinates. By placing this tool at the failure section, see *Figure 4.12*, the coordinates of such points could be established and linked to the corresponding load stage.

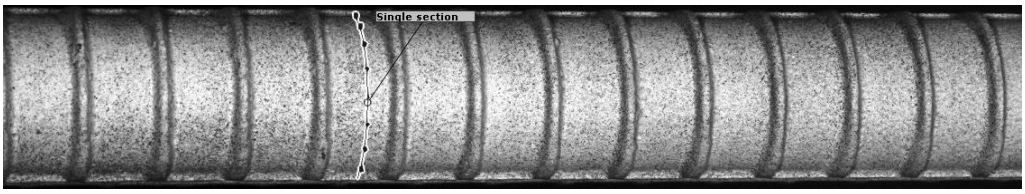

Figure 4.12: Displays the GOM tool: single section placed in the failure zone.

Due to the limited area covered by the cameras only a reduced surface of the reinforcing bar could be monitored, see *Figure 4.13*. This generated only in the best cases just under 50% of the radius shape. Consequently, a need to recreate the rest of the radius aroused. It was solved by a so-called curve fitting using the software MATLAB® where the parts of the reduced radius where fitted with several radius sizes until a best fit match between them was obtained see *Figure 4.14*. To perform such fitting two hypothesis which allowed the development of the code were performed:

- First the area of the bar between ribs was assumed to perfectly fit a circle
- Second the area is assumed to be reduced uniformly in the transversal direction, which means that the cross-section remains circular up to failure.

Finally, when the radius of every load stage was obtained with increased force (see *Figure 4.15*), the actual areas were calculated by using equation (4.5).

Subsequently the same areas were inserted in equation (4.6) where the new true stress could be obtained for the corresponding load level.

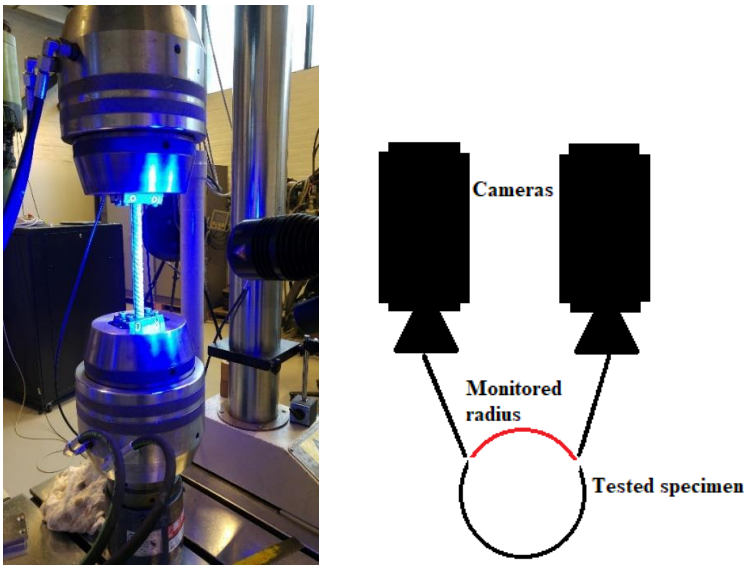

(a) *(b)*

Figure 4.13:(a) Displays the monitored radius with DIC system, (b) show a schematic layout of monitored radius.

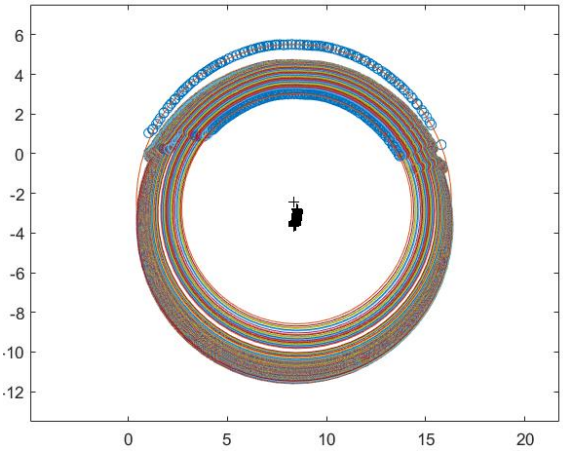

Figure 4.14: Graphical images acquired by MATLAB® displays the curve fitting and reduction of area for the tested specimen.

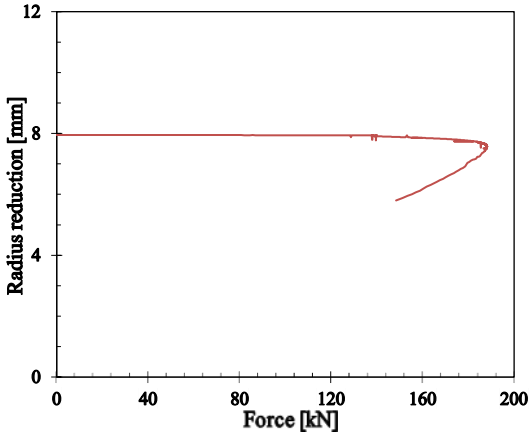

Figure 4.15: Reduction of radius with increased force.

$$A_{real} = \pi r_{real.}{}^2 \tag{4.5}$$

where:
A_{real} is the cross-sectional area within the failure zone of the specimen.
$r_{real.}$ is the real radius of the reinforcing steel bar varying for every load stage.

$$\sigma_T = \frac{P}{A_{real}} \tag{4.6}$$

where:
σ_T is the true stress.
P is the force measured by the universal testing machine.

5 Experimental results

The experimental results diagrams for a few corroded and uncorroded rebars with force versus displacement, force versus engineering strain, stress-strain (engineering and true) relationship are presented in this Chapter 5, while rest of the diagram are gathered in (Appendix A.1, A.2, B.1, B.2, C.1 and C.2).

5.1 Uncorroded rebars

5.1.1 Force versus displacement

Figure 5.1 displays the three different types of uncorroded rebars for force versus displacement behavior. The figures show expected behavior for uncorroded bars. A difference is observed in elastic and plastic range based on the bar diameters with different types of ribbed in steel reinforcement.

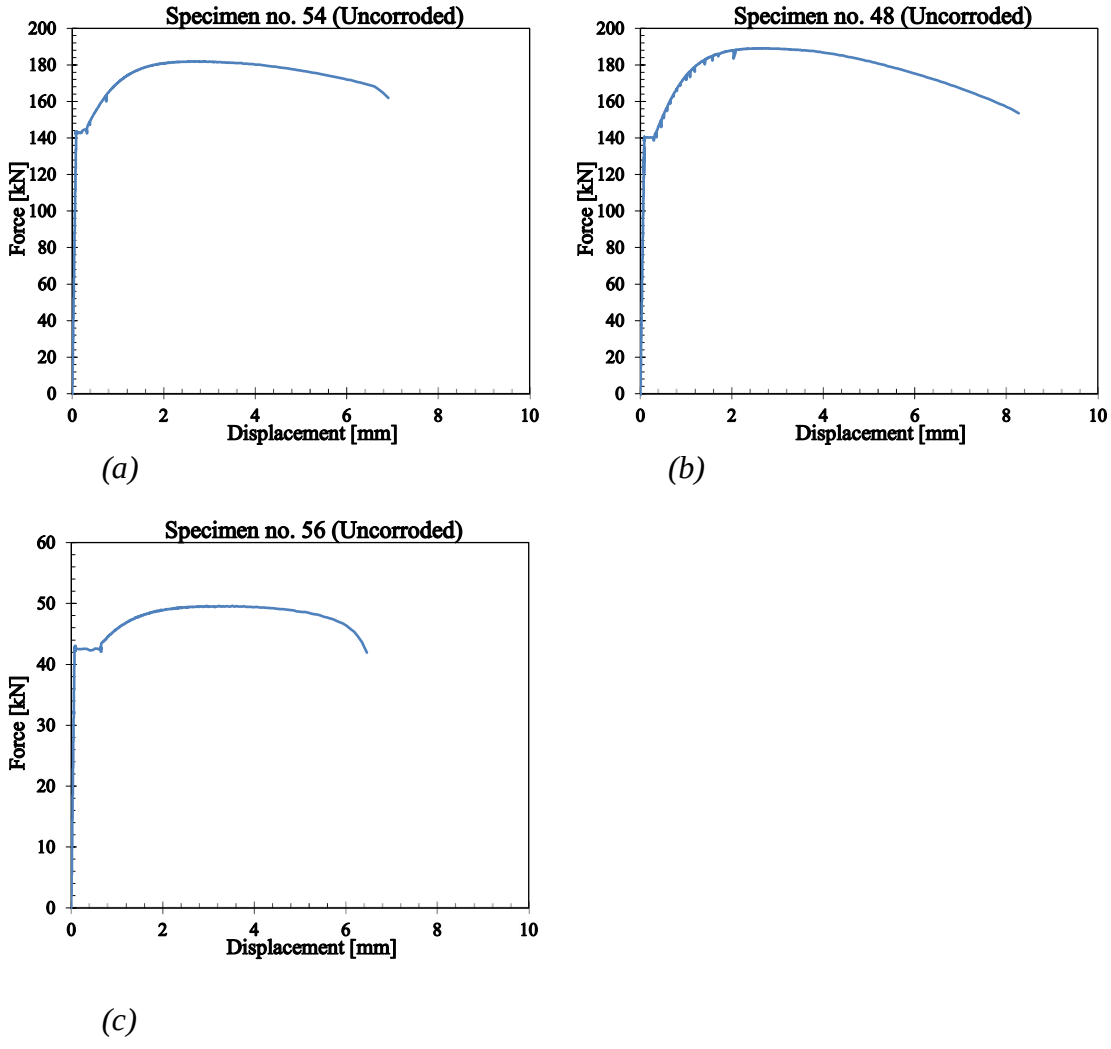

Figure 5.1 : Force versus displacement diagram for different type of uncorroded rebars. (a) Type A2 (16mm, skewed), (b) Type B2 (16mm, straight) and (c) Type C2 (10mm, skewed)

The yielding and ultimate load for a specific type of rebars were determined from the corresponding force-displacement curve. The yielding load was determined by the average value between upper and lower yield load. The upper yield load is the maximum force in the elastic zone and lower yield load (e.g. steel reinforcement yielding) is the minimum force in the force-displacement figures. The ultimate load was determined at the point of the maximum force values from this force-displacement figures. From the same curve permanent elongation for specimens at failure can be determined.

5.1.2 Force versus engineering strain

Figure 5.2 displays the three different types of uncorroded rebars for forces versus engineering strain behavior until failure point. From this figure, the yield and fracture strain was determined which are used to indicate ductility measurement in the specimens. The yield strain occurs in elastic region, where the fracture strain occurs in plastic region.

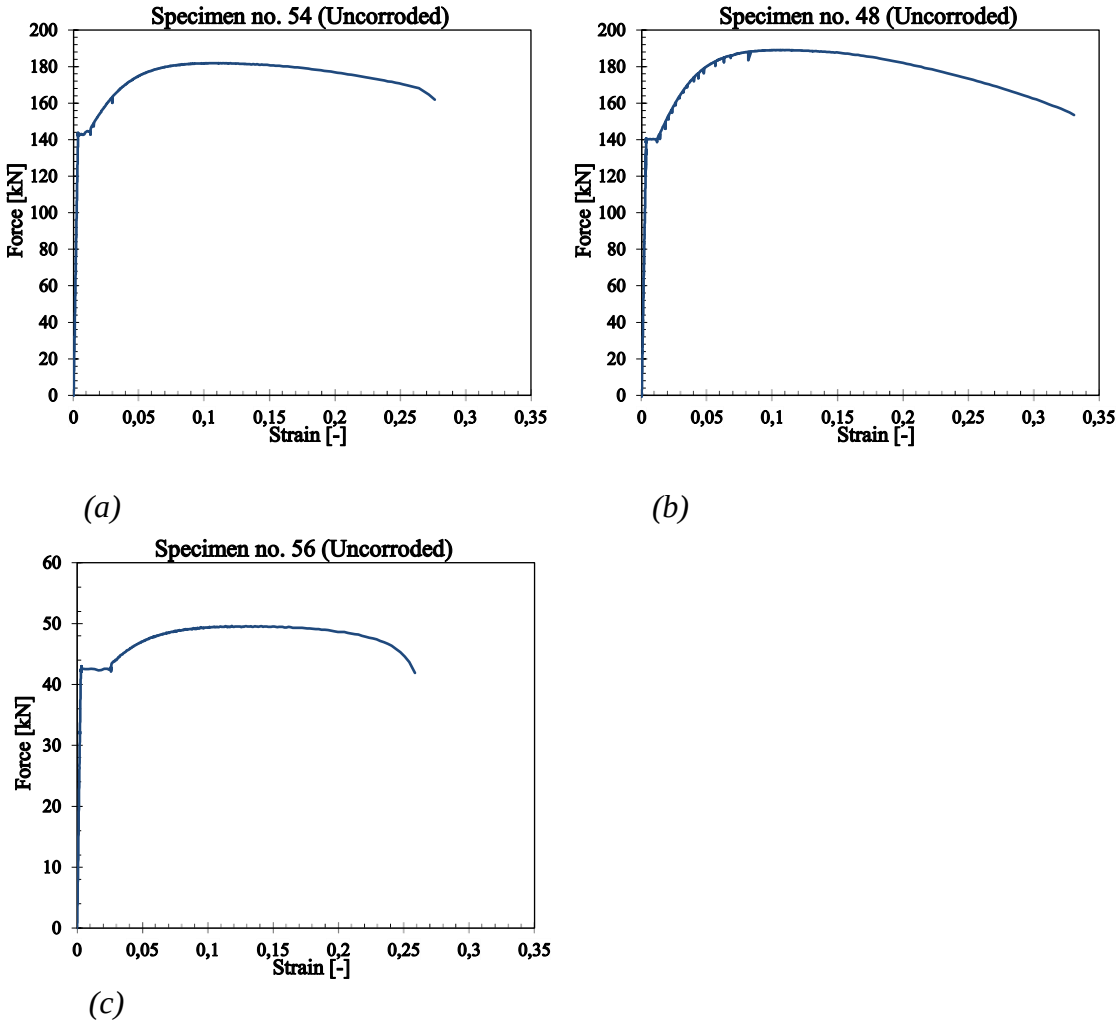

Figure 5.2: Force versus engineering strain diagram for different type of uncorroded rebars. (a) Type A2 (16mm, skewed), (b) Type B2 (16mm, straight) and (c) Type C2 (10mm, skewed)

5.1.3 Engineering stress-strain curve

In *Figure 5.3* the engineering stress-strain curve for the same uncorroded rebars are displayed. The parameters obtained from this stress-strain relation used in this study are described in Chapter 2.3.1.1.

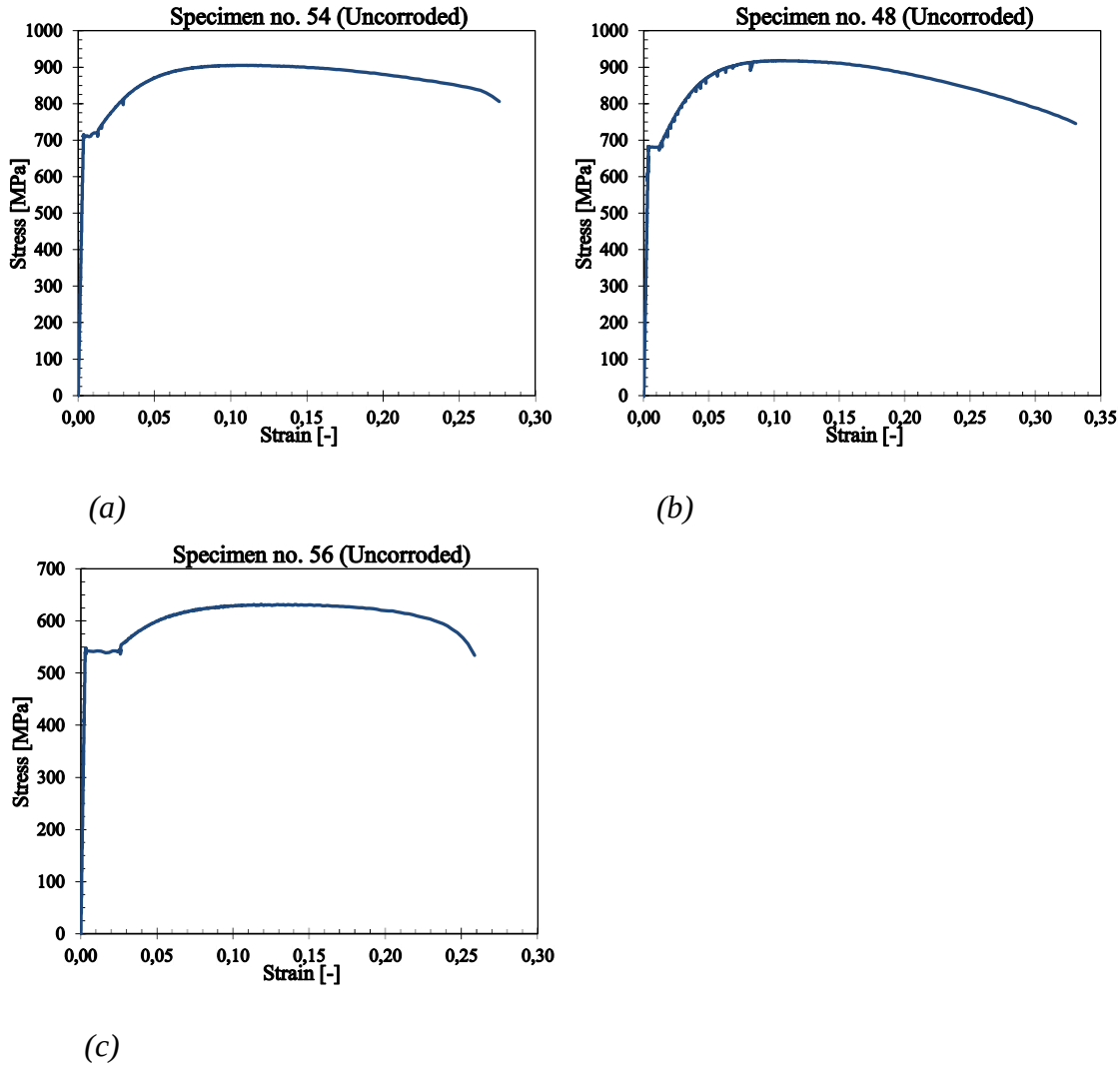

Figure 5.3: Engineering stress-strain behavior results for different type of uncorroded rebars. (a) Type A2 (16mm, skewed), (b) Type B2 (16mm, straight) and (c) Type C2 (10mm, skewed)

In the elastic zone, all the curve from above figure showing a linear trend, the yield point has been defined in the endpoints of linearity. In those engineering stress-strain curve, the slope (α) in the elastic region defined as an elastic modulus (see *Figure 2.3*). The length of the yielded plateau which is a function of the steel grade, for different types of specimens from above figure showing the different length of the yield plateau. From *Figure 5.3* (a) and (b) exhibit the shorter yield plateau than *Figure 5.3* (c), because of high-strength steel (16mm diameter) according to (Llano Trueba, 2015). The yield and ultimate tensile strength from this *Figure 5.3* can be described by using the chapter 2.3.1.1, see equation (2.5) and (2.6).

5.1.4 True stress-strain curve on reduced cross section

The *Figure 5.4* shows the true stress-strain behavior for a uncorroded specimen. The true stress-strain curve is related to engineering stress-strain behavior. As it can be observed the stresses increases dramatically when compared to the engineering ones. That is due to the inclusion of the reduction of area in the computation of the stresses. However, it should be noted that the stresses prior the ultimate strain is reach resembles very much to the engineering stresses, which indicates that the reduction of area purely from the poison effect has a decreased impact on the results in comparison to the necking. In any case, the maximum stress reached by the bar is about 1400 MPa what represents more than 50% of increment to that engineering values.

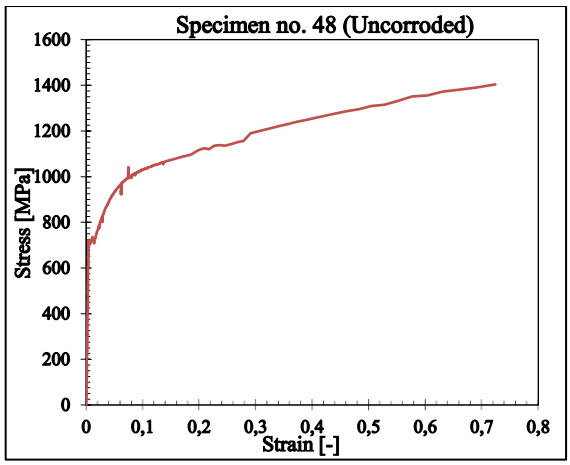

Figure 5.4: Tensile true stress-strain curve for uncorroded rebar.

5.2 Corroded rebars

Same as for the uncorroded bars a representative sample of specimens for each set will be presented in the following sections. The detailed results for all the testes bars are described in the corresponding appendix (Appendix A.1, A.2, B.1, B.2, C.1 and C.2).

5.2.1 Force versus displacement

Figure 5.5 displays the three different types of corroded rebars for force versus displacement behavior until the failure point. Different type of corrosion level was considered for this study e.g. average corrosion level and corrosion level at the critical cross-section. For the corroded bar, the *Figure 5.5* shows the different behavior compare to uncorroded force-displacement curve in *Figure 5.1.*

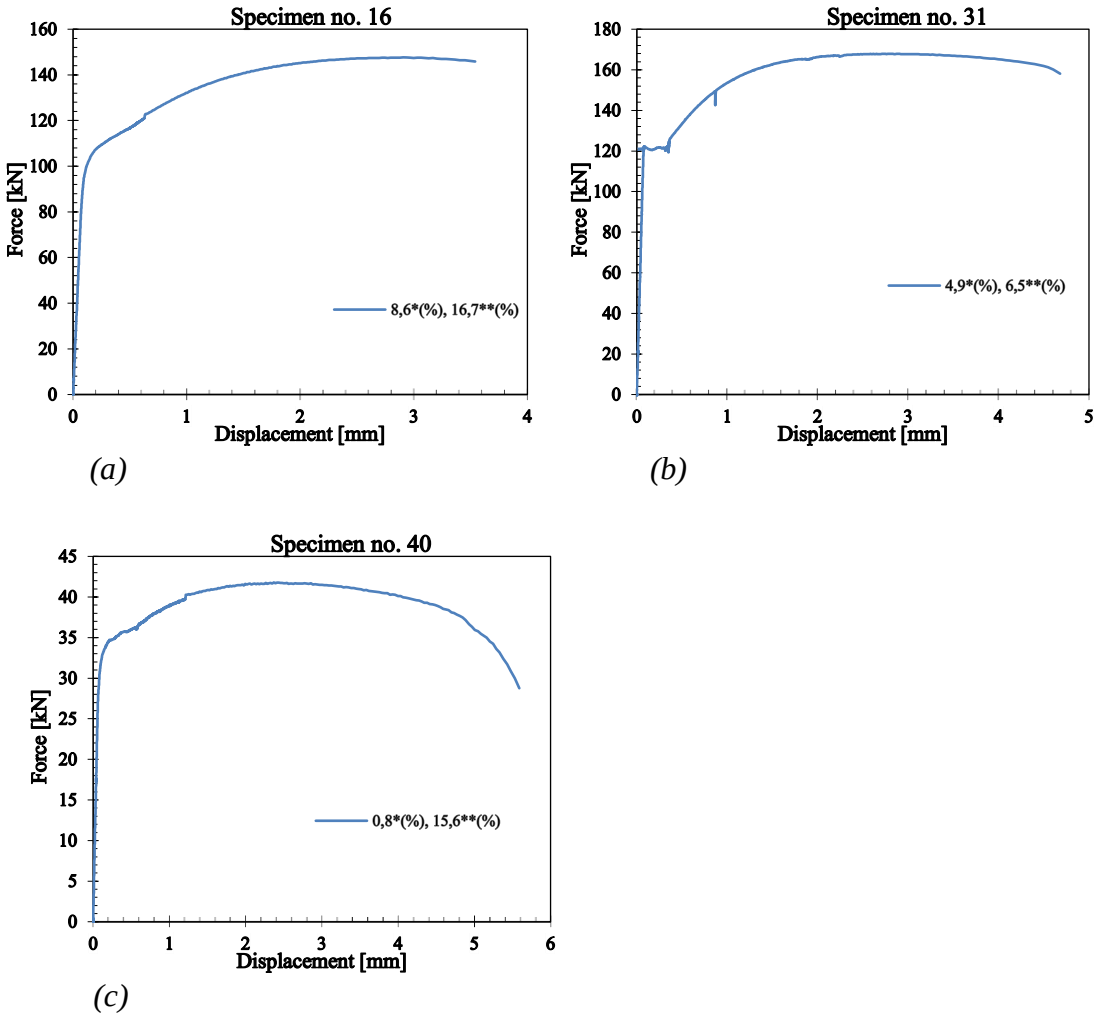

*Figure 5.5: Force versus displacement diagram for different type of corroded rebars. (a) Type A2 (16mm, skewed), (b) Type B2 (16mm, straight) and (c) Type C2 (10mm, skewed). *Average corrosion level. **Corrosion level at critical cross section (CCS).*

As described in section 5.1.1, the yielding load, ultimate load and permanent elongation was determined from this figure for different type of corroded rebars.

5.2.2 Force versus engineering strain

Figure 5.6 displays the three different types of corroded rebars for force versus engineering strain curves. From this figure, the yield and fracture strain was determined for the different type of corroded rebars as described in section 5.1.2.
From this below *Figure 5.6 (a) and (c)* show the similar curve trend for both of this skewed bar, but in *Figure 5.6 (b)* showing yield plateau length for this straight corroded bar.

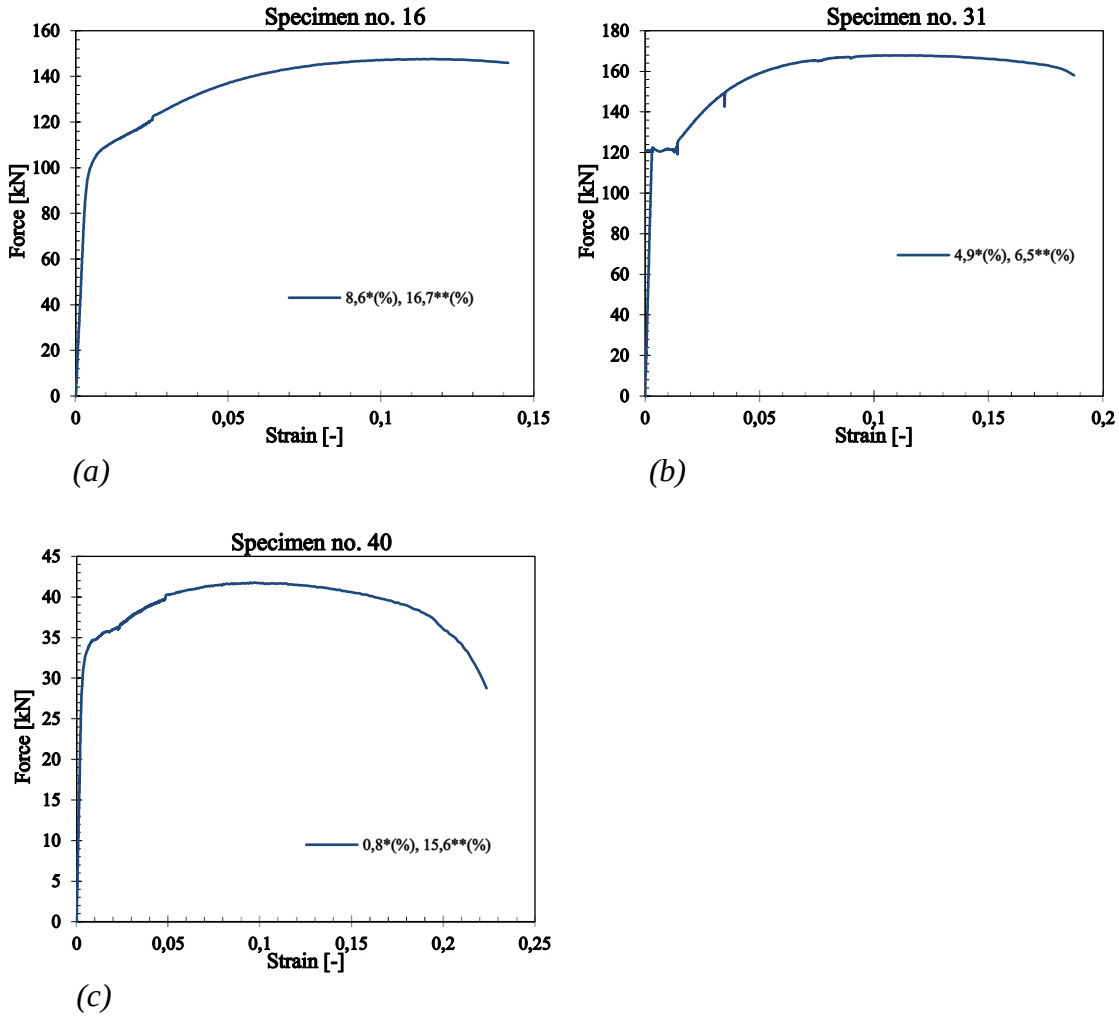

*Figure 5.6: Force versus engineering strain diagram for different type of corroded rebars. (a) Type A2 (16mm, skewed), (b) Type B2 (16mm, straight) and (c) Type C2 (10mm, skewed). *Average corrosion level. **Corrosion level at critical cross section (CCS).*

5.2.3 Engineering stress-strain curve

Figure 5.7 is showing the engineering stress-strain curve for three different types of corroded rebars considered actual cross-section, average cross section and critical cross section (3D scanning). From this below three stress-strain curves the yield strength, ultimate strength and elastic modulus can determine as described in section 5.1.3.

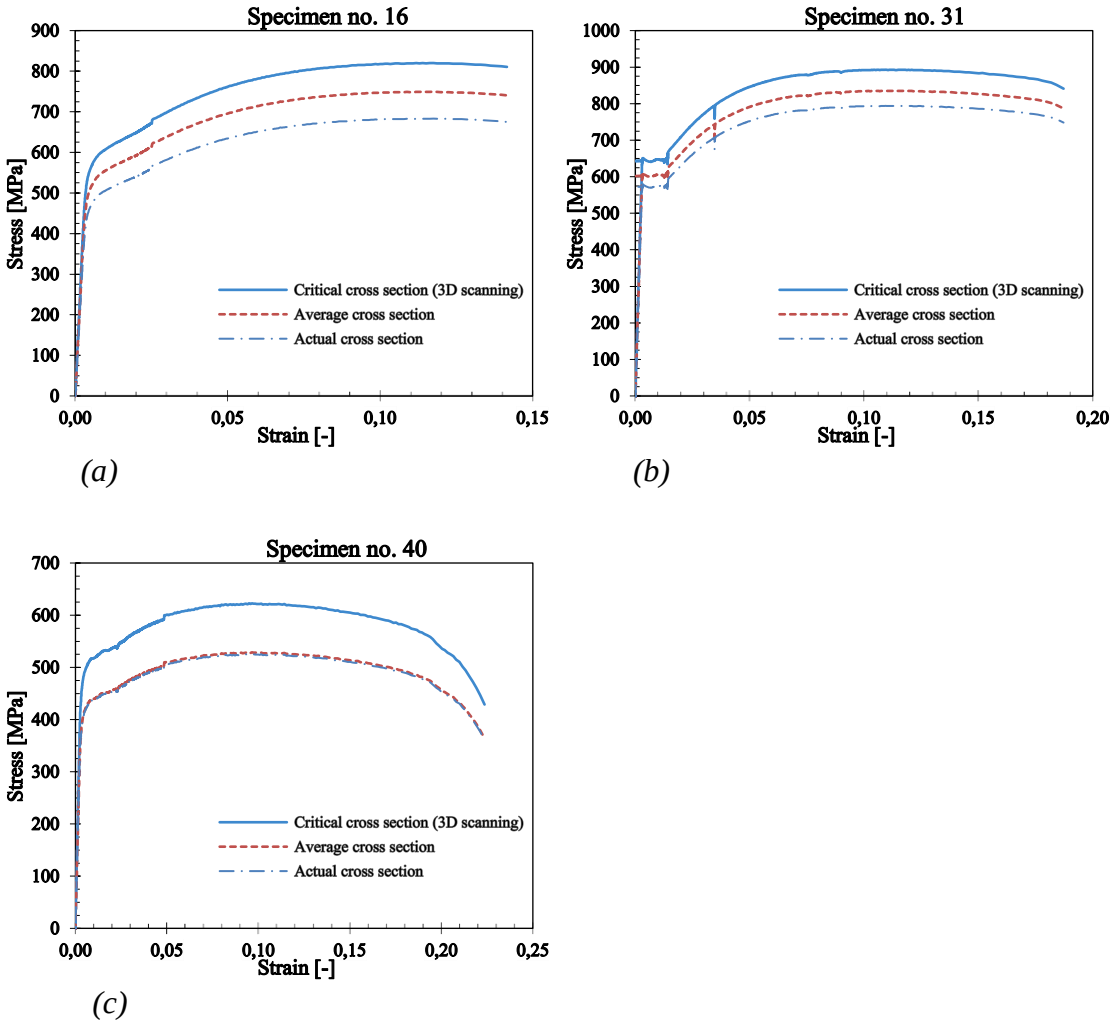

Figure 5.7: Engineering stress-strain behavior results for different type of corroded rebars. (a) Type A2 (16mm, skewed), (b) Type B2 (16mm, straight) and (c) Type C2 (10mm, skewed).

Analyzing the results yielded by the different cross section used in the calculations, the critical cross section curve always returns the highest strength values when compared to other cross sections. Furthermore, different diameter bar with same rib type (type A1 and C1, skewed) shows same trend for all the cross section i.e. critical cross section, average cross section and actual cross section. For B1 (straight bars) a different trend was noticed compared to A1 and C1.

In the upcoming chapter 6, comparison and analysis will be performed between uncorroded and corroded rebars. Furthermore, the effect of mechanical properties at specific corrosion level for average and critical cross section area will be studied and discussed.

6 Results analysis and discussion

In this chapter, the individual results presented from chapter 5 are analyzed and discussed with respect to the influence of corrosion. The main types of graph used in the analysis are the force versus displacement, force versus engineering strain and finally engineering stress-strain. From those curves, different mechanical parameters for the tested rebars were extracted and collected in *Table 1* (appendix D). These parameters are used in the following sections to define the different relations between them and the corrosion levels.

6.1 Force versus displacement

In this section a comparison between the elongation, force at yielding and the ultimate force against the different corrosion levels is presented. *Figure 6.1* depicts how such parameters were obtained for both uncorroded and corroded bars.

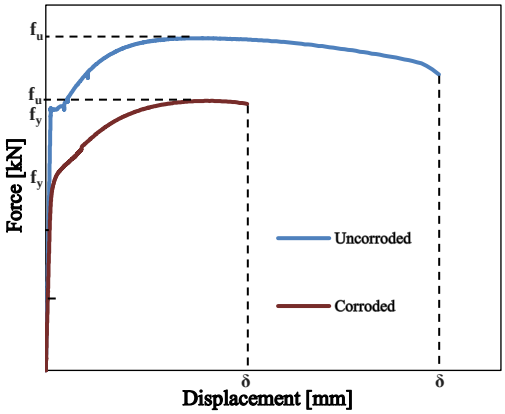

Figure 6.1: Explains how elongation (δ), yield (f_y) and ultimate force (f_u) was obtained for the uncorroded and corroded steel bars.

In the following three different plots where the different types of reinforcing steel are combined on base of their type e.g. A1 and A2 are presented. Further the two corrosion levels previously defined were used, average corrosion level (avg. cl) and corrosion level at critical cross section (cl. CCS), see Figure 6.2.

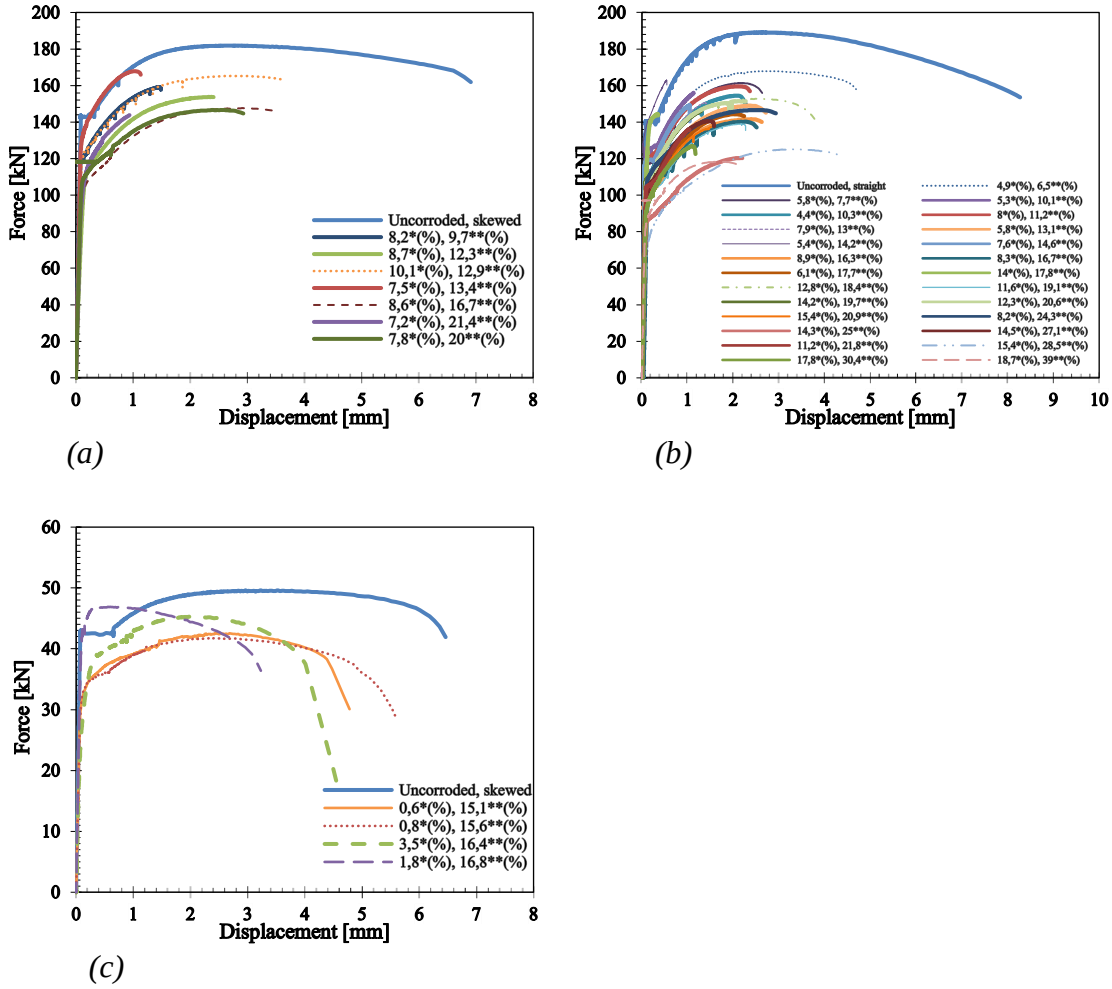

*Figure 6.2: Displays force versus displacement graphs. (a) A1 and A2, 16mm skewed bars, (b) B1 and B2, 16mm straight bars and (c) C1 and C2, 10mm skewed bars. *Average corrosion level. **Corrosion level at critical cross section (CCS).*

By analyzing the combined results in *Figure 6.2* from the performed tests, a trend was observed. When the corrosion level of the reinforcing steel increases the equivalent displacement before failure point decreases. Further, with increasing corrosion levels the load carrying capacity is reduced. Same behavior was observed by (U, 2001). From *Figure 6.2* exact elongation, yield load and ultimate load for all rebar where obtained for further analysis.

6.1.1 Elongation (displacement)

In *Figure 6.3(a)*, the elongation was plotted against the average corrosion. For the bar types: A1, A2, C1, and C2 a linear fit was used, where a polynomic fit was used for B1 and B2. Different types of trendlines were used, this was performed to follow the behavior of the results and to obtain a higher coefficient of determination (R^2) as possible. The coefficient of determination (R^2) is a statistical measure of how close the data are to the fitted regression line.

Despite scattered values, a clear reduction of the elongation due to corrosion are noticed from the fitted trendlines. This behavior has also been observed by several other researchers such as (U, 2001; Fernandez, Bairán and Marí, 2015; Llano Trueba, 2015). Further analysis indicates that the reduction of elongation occurs within three corrosion intervals. For average corrosion level, the intervals were 0-7%, 7-15% and finally 15-20%. The largest reductions were observed in the first interval range, where the reductions are of linear character. This was applied to all types of bars. In the second interval range, the reductions were constant i.e. the elongation is not that affected by the corrosion level. For the third and last interval-range, a reduction of elongation was noticed again. In *Figure 6.3(b)*, the elongation was plotted against the corrosion level at the critical cross section. The obtained results were closer in relation to reality than the average corrosion level used in *Figure 6.3(a)* since the corrosion level at critical cross section was done measuring the corrosion level where the failure occurred (see chapter 3.3.2). By comparing the results within *Figure 6.3*, several similarities were observed. The reduction of elongation occurs also within three corrosion intervals. The only difference was that the corrosion levels are higher because they are closer to reality. For the corrosion level at the critical cross section, the intervals were 0-18%, 18-28% and finally 28-40%. In the first interval-range, the reduction occurs linearly. In the second interval it remains constant and finally, in the last interval-range it starts to decrease again.

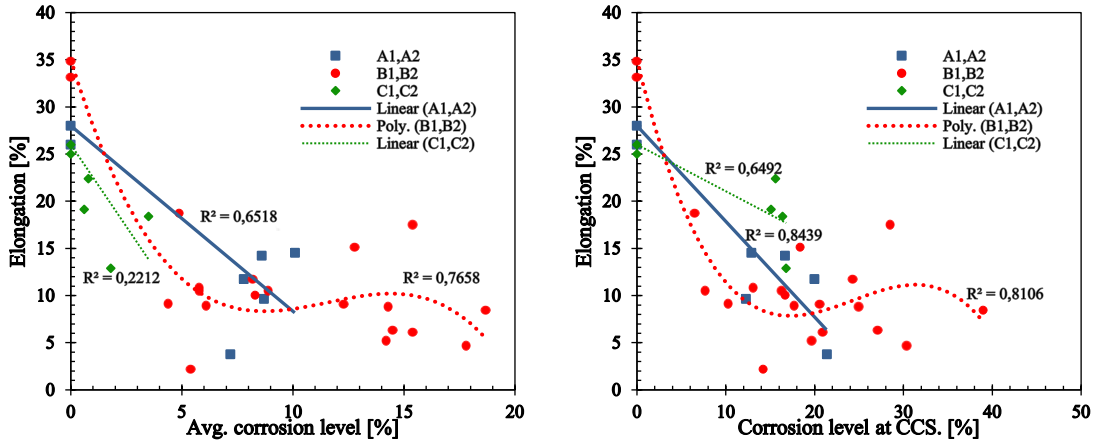

(a) *(b)*

Figure 6.3:(a) Elongation versus average corrosion level, (b) elongation versus corrosion level at critical cross section.

6.1.2 Yield and ultimate load

In this section, an analysis was performed to see how the yield load capacity and ultimate load capacity of the tested reinforcing steel bars were affected by corrosion. *Figure 6.4(a)* and *Figure 6.4(b)* displays the yielding load versus average corrosion and corrosion level at the critical cross section. In general, it could be noticed a linear reduction of the yield load capacity due corrosion for the bar types: A1, A2, B1, B2 regardless corrosion level used to represent the results. The results and the fitted trendlines for C1 and C2 do not provide trustworthy data, this can be explained in the small numbers of tested bars with too similar corrosion levels to each other.

In addition, the type of corrosion observed in such bars differed a lot in comparison to the corrosion described by the other steel bars (from pitting corrosion to more generalized corrosion). Further, same behavior as in section 6.1.1 was observed between the average corrosion level and corrosion level at the critical cross section, where the values are more realistic and accurate than for the averaged one. This can also be seen in coefficient of determination (R^2) which are higher in *Figure 6.4(b)* than for *Figure 6.4(a)*, indicating that the scatter in the measurements is much lower, hence they depict a clear trend. In *Figure 6.5(a)* and *Figure 6.5(b)*, the ultimate load capacity of the tested bars versus average corrosion and corrosion level at the critical cross section is displayed. A linear reduction of the ultimate load was established.

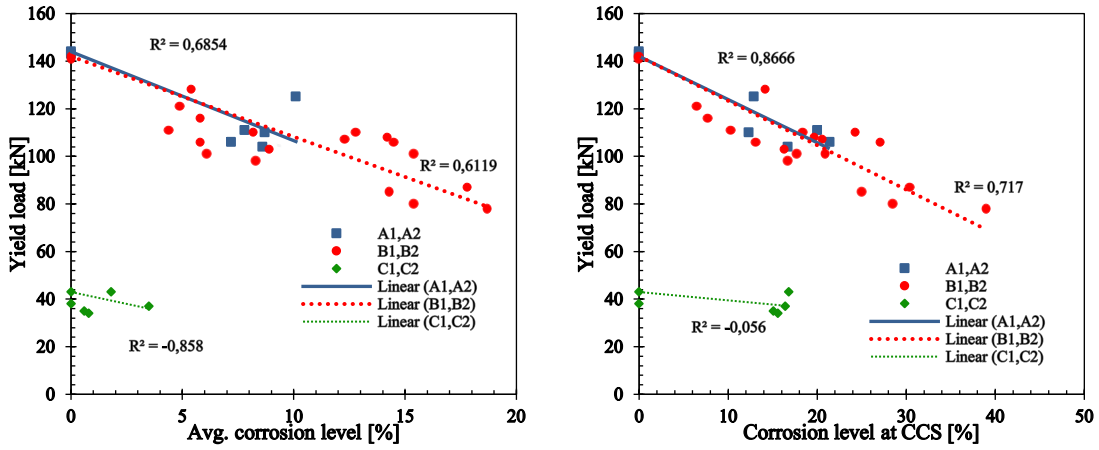

(a) *(b)*

Figure 6.4:(a) Yield load versus average corrosion level, (b) yield load versus corrosion level at critical cross section.

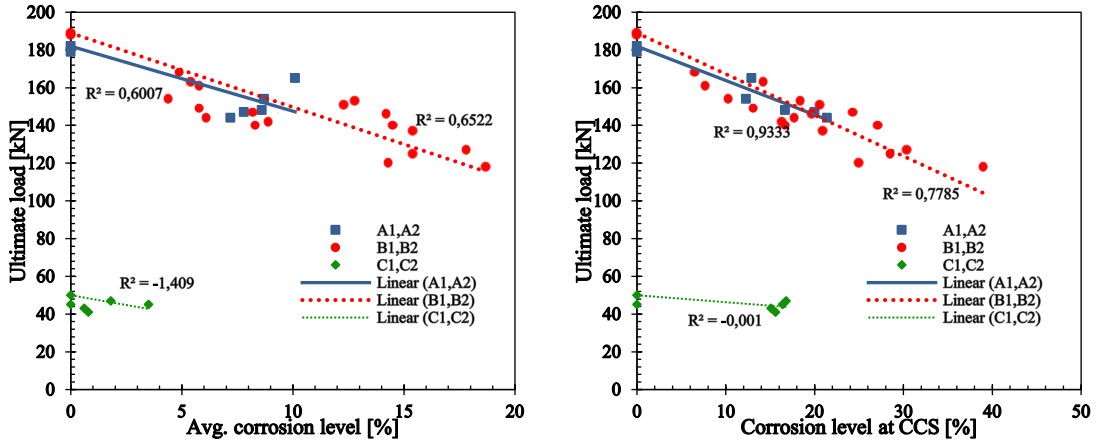

(a) *(b)*

Figure 6.5: (a) Ultimate load versus average corrosion level, (b) ultimate load versus corrosion level at critical cross section.

In *Figure 6.6* theoretical trendlines were plotted, representing the expected reduction of the load by corrosion increase. In *Figure 6.6 (a)* the ultimate load and yielding load were reduced more than expected, were in *Figure 6.6 (b)* the experimental values reduced in a more expected manner. This can be justified by the method of measuring corrosion level at the critical cross section where the failure will occur and by this correspond more to the reality than the average corrosion level.

Additionally, the yielding load and ultimate load for the bar type A1-A2 were compared. 1% of increased average corrosion leads to 5.35 kN loss for the ultimate load capacity and 5.27 kN yield load capacity. For the CCS corrosion same trend was noticed where 1% of corrosion decreased the ultimate load and yield load by 1.82 kN respectively 1.64 kN. Type B1-B2 had a similar behavior to the A1-A2 where the ultimate load also decreased slightly more than yielding load. As mentioned before, the results and the fitted trendlines for C1 and C2 do not provide trustworthy data and hence will not be considerate here.

The conclusion was made that the yield load and ultimate load are reduced more or less the same due to corrosion disregard of corrosion method. This can potentially be explained by the cross sectional loss of area for the reinforcing steel bar where both parameters showed similar sensitivity to the certain phenomena. Furthermore, 1% of corrosion reduces 2.16 mm^2 of the area for the skewed rebars and 2.11 mm^2 for the straight, indicating a strong linearly correlation with the reduced load earlier discussed in the text. Similar correlations had been observed by researchers such (U, 2001) where the load carrying capacity is related to the available area.

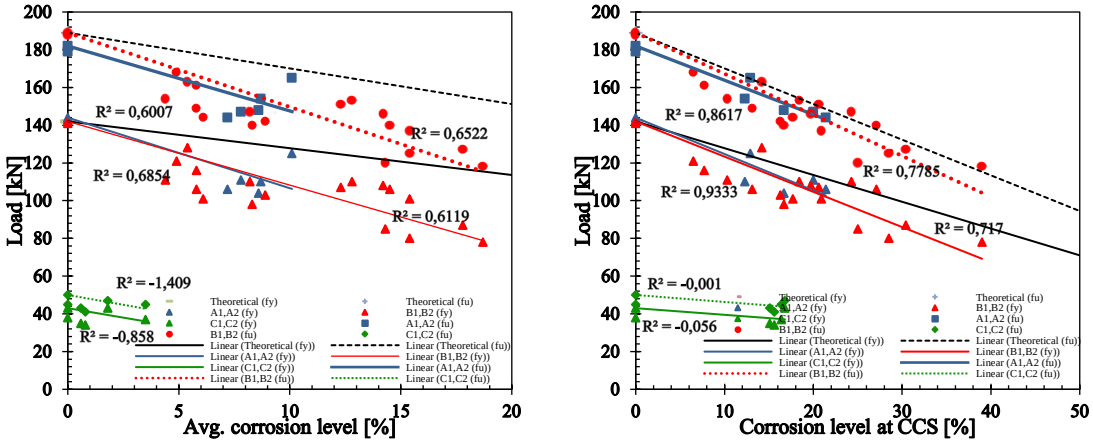

(a) *(b)*

Figure 6.6: (a) Combined ultimate (f_u) and yield load (f_y) versus average corrosion level, (b) combined ultimate (f_u) and yield load (f_y) versus corrosion level at critical cross.

6.2 Force versus engineering strain

In this section the impact on the yield- and fracture strain due to corrosion increase is presented. *Figure 6.7* depicts how such parameters were obtained for both uncorroded and corroded bars.

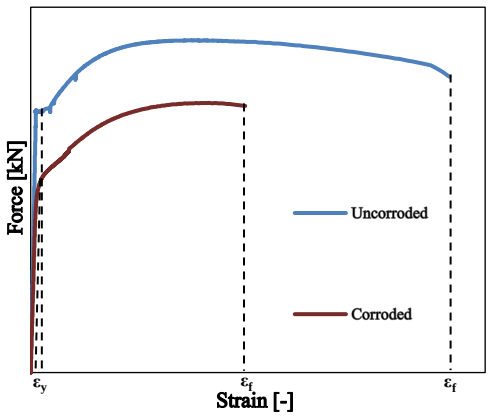

Figure 6.7: Explains how yield strain (ε_y) and fracture (ε_f) was obtained for the uncorroded and corroded steel bars.

The second type of results used for analyzing the measured behavior of the bars for this study was force versus engineering strain. As explained in section 6.1 three different graphs were displayed for every type of bar used in this study i.e. A1 and A2 in one graph. By comparing the different curves in *Figure 6.8*, a reduction in strain with the increase on corrosion level was noticed. Same observation was made by researchers such as (U, 2001; Fernandez, Bairán and Marí, 2015; Llano Trueba, 2015) in their studies. From the same figure, exact values for the yield and fracture strain were extracted for deeper analysis.

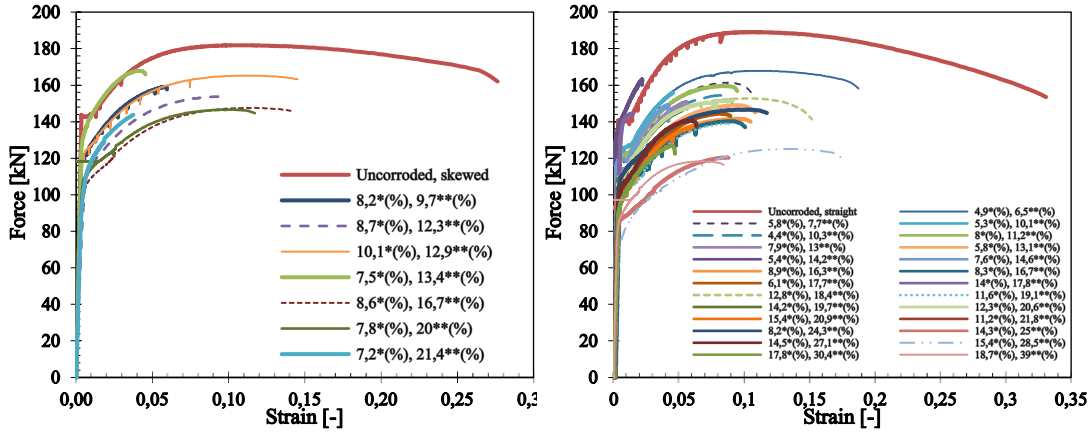

(a) *(b)*

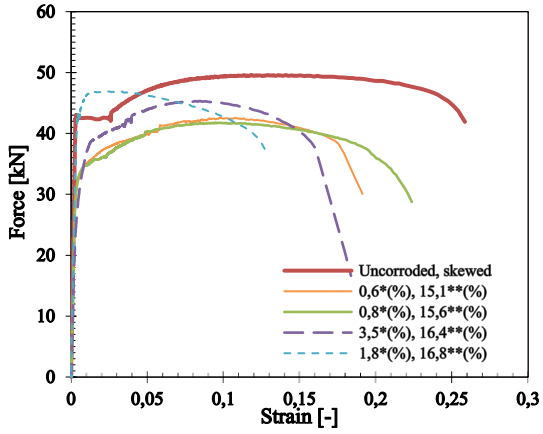

(c)

*Figure 6.8: Displays force versus engineering strain graphs (a) A1 and A2, 16mm skewed bars, (b) B1 and B2, 16mm straight bars and (c) C1 and C2, 10mm skewed bars. *Average corrosion level. **Corrosion level at critical cross section (CCS).*

6.2.1 Yield and fracture strain

In Figure *6.9*, the yield strain was plotted against the average corrosion and corrosion at the critical cross section. Different types of regression lines were used to obtain a high coefficient of determination (R^2) as explained in section 6.1.1. By analyzing the graphs, reduction of the yield strain with increase of corrosion level was noticed. The highest reduction was noticed between the corrosion interval range 0-10%. The results are in agreement with results obtained by (U, 2001). Best correlation was obtained for the type A1-A2 which depicted a R^2-value of 0,81 for the average corrosion and 0,91 for the corrosion level at the critical cross section.

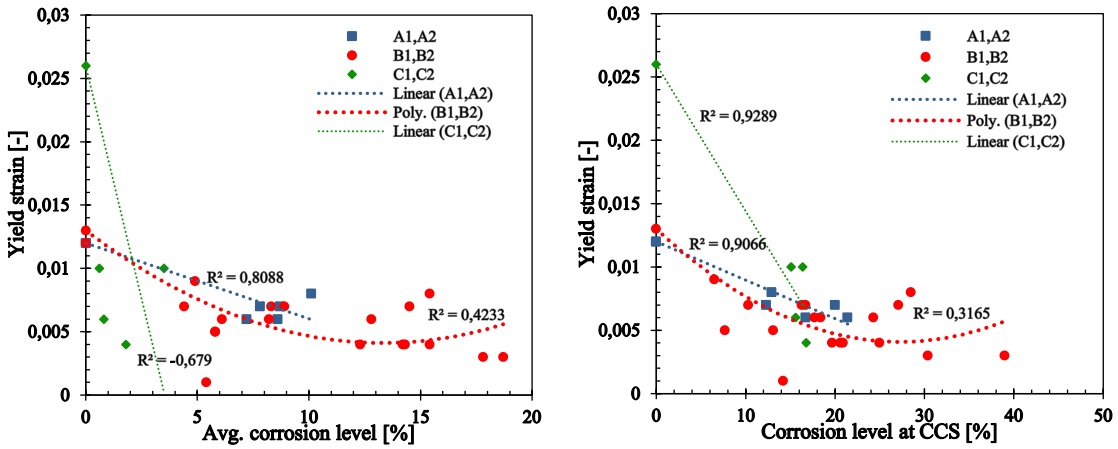

(a) *(b)*

Figure 6.9: (a) Yield engineering strain vs average corrosion level, (b) yield engineering strain vs corrosion level at critical cross section.

In *Figure 6.10(a)*, the fracture strain was plotted versus the average corrosion. By analyzing the results, an important scatter was observed, this behavior is as well reported by many other researchers (U, 2001; Fernandez, Bairán and Marí, 2015; Llano Trueba, 2015). Despite the scattered data, some behaviors can be observed, the reduction of the fracture strain due to corrosion could be noticed from the fitted trendlines. This behavior has also been observed in other studies (U, 2001; Fernandez, Bairán and Marí, 2015; Llano Trueba, 2015). Further analysis indicates that the reduction of elongation occurs within three corrosion intervals. For average corrosion, the intervals were 0-7%, 7-15% and finally 15-20%. The largest reductions were observed in the first interval range, where the reductions are of linear character. This was applied to all types of bars. In the second interval range the reductions are constant i.e. the fracture strain was not affected by the corrosion level. For the third interval-range, a further reduction in fracture strain was noticed.

Similar to *Figure 6.10(a)* with the exception to the corrosion level, *Figure 6.10(b)*, displays fracture strain versus the corrosion level at the critical cross section. The obtained results were closer in relation to reality, as explained in section 6.1.1 than the average corrosion. Comparing the results in *Figure 6.10(b)* with *Figure 6.10(a)*, several similarities were observed. The main differences are the corrosion levels, which are higher, and the coefficients of determination are slightly higher for the critical cross section.

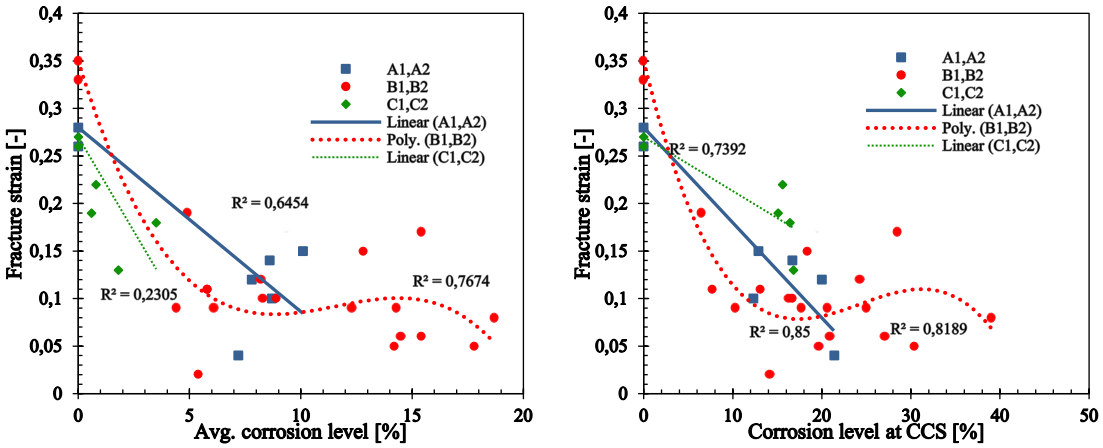

(a) *(b)*

Figure 6.10: (a) Fracture engineering strain vs average corrosion level, (b) Fracture engineering strain vs corrosion level at critical cross section.

When analyzing the behavior for both the yield and fracture strain, a trend of reduction due to increased corrosion level is established. This reduction of the strains can be partially explained due to the increase of brittleness for the reinforcing steel. Brittleness of steel is clearly affected by corrosion, this is observed when comparing uncorroded specimens which show high yielding before reaching the fracture point in contrast to the heavily corroded specimens which showed a decrease of yielding strain (*see Figure 6.9*). Same observations were made by (U, 2001).

Further reasons for the decrease of the strains are the loss of the cross sectional area in form of local pits or notches but also thinned out sections of the bar when high pitting corrosion occurs. These notches or reduced sections when elongated will cause the strains to concentrate where the general strain behavior of the corroded specimens will be minor than for uncorroded specimens at failure (U, 2001).

6.3 Engineering stress versus strain

In this section yielding strength, ultimate strength, and modulus of elasticity where obtained according to typical stress-strain curve from *Figure 2.3.*

Figure 6.11 and *Figure 6.12* displays the engineering stress-strain curves for the different type of naturally corroded rebars at various corrosion levels for average and critical cross-section with respect to the uncorroded steel bar. All the curves showed the similar trend for the different types of the specimen. With increasing average corrosion level, the combined results in *Figure 6.11* for type (A1, A2, and B1, B2) showed similar stress-strain curves as expected. Further for type (C1, C2) different behavior are observed. Also considered the increasing corrosion level at a critical cross-section in *Figure 6.12*, the stress value is much higher than for average corroded cross-section with increasing corrosion level, see *Figure 6.11*.

In the further sections 6.3.1, the effects of different corrosion levels for different types of bars are analyzed to obtain a correlation between the strengths and corrosion levels. Finally, the behavior of modulus of elasticity with increased corrosion levels is also discussed in section 6.3.2.

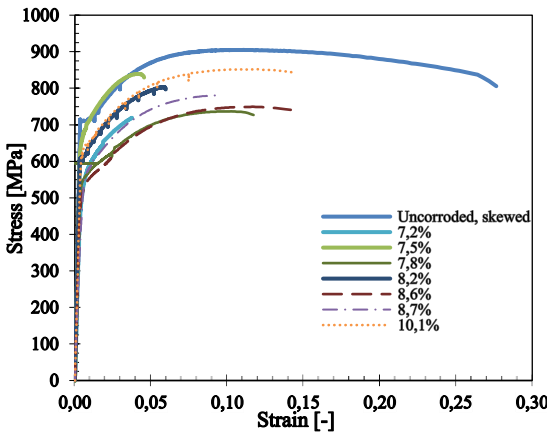

(a)

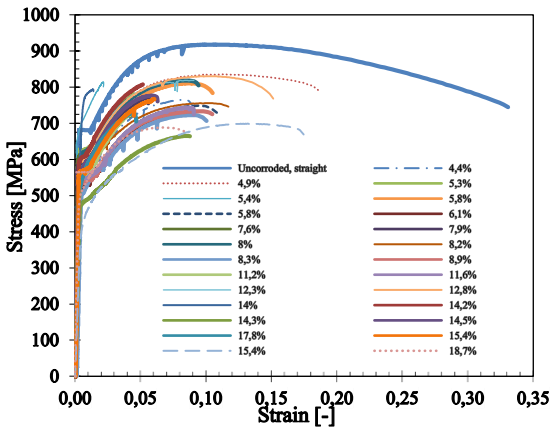

(b)

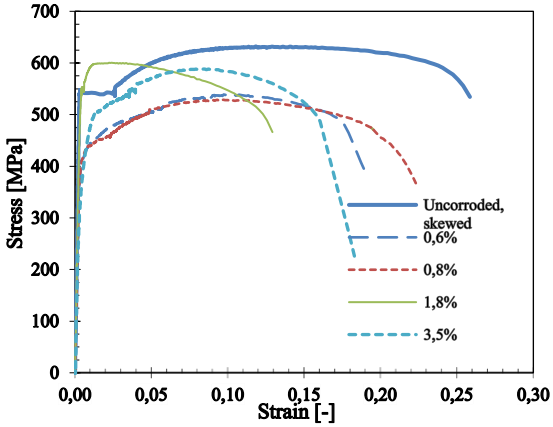

(c)

Figure 6.61: Engineering stress-strain curves for different type of naturally corroded rebars of various corrosion level at average cross-section. (a) A1 and A2, 16mm skewed bars, (b) B1 and B2, 16mm straight bars and (c) C1 and C2, 10mm skewed bars.

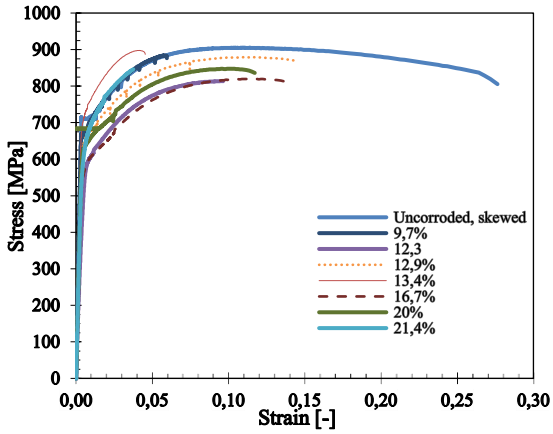

(a)

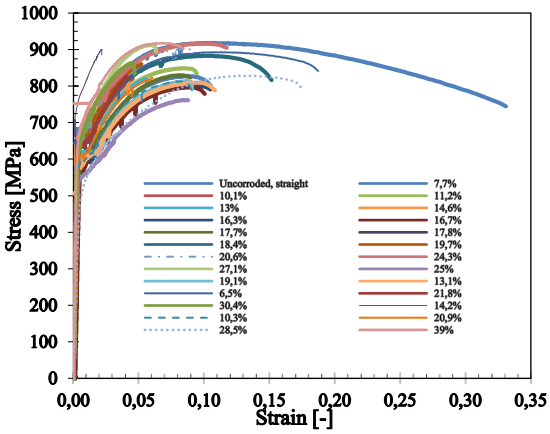

(b)

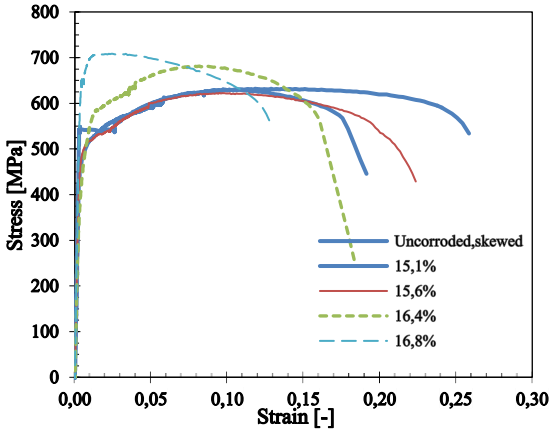

(c)

Figure 6.72: Engineering stress-strain curves for different type of naturally corroded rebars of various corrosion level at critical cross-section. (a) A1 and A2, 16mm skewed bars, (b) B1 and B2, 16mm straight bars and (c) C1 and C2, 10mm skewed bars.

6.3.1 Yield and ultimate strength

The change of yielding and ultimate strengths depended on increasing corrosion levels which are presented in *Figure 6.13* and *Figure 6.14*. The yielding and ultimate strengths produced a reduced trend for considered corrosion levels at the average corrosion level, and constant trend for the critical cross section. For both corrosion levels in *Figure 6.13* and *Figure 6.14*, the polynomic fit was used for type (B1, B2) to obtain a high coefficient of correlation, where the linear function was used for type (A1, A2). For type (C1, C2) specimens, the linear fit was also used which indicated the poor coefficient values, because of few tested specimens with high average corrosion levels. With this limitation, most of the curves showed that strengths are reducing with increased average corrosion levels. On the other hand, several researchers (Apostolopoulos, 2007; Zhang *et al.*, 2012; Fernandez, Bairán and Marí, 2015) also observed the similar decreasing behavior of yielding and ultimate strengths with increased corrosion levels.

From *Figure 6.13(a)* and *Figure 6.14(a)*, different interval-range of average corrosion levels are observed for several types of bars. The first range between 0-6% which is applied for all types of bars following the linear function. In next range between 7-13% with increased average corrosion levels, the strengths reduction remains unchanged for the type (B1, B2) instead of type (A1, A2) the strengths reduced linearly. For the final average corrosion level range between 14-19%, the yielding and ultimate strength reduction was observed. This can also be seen in coefficient of determination (R^2), which are slightly higher for *Figure 6.13(a)* and *Figure 6.14(a)* for type (A1, A2). But considered type (B1, B2) it is corresponding in opposite way. In *Figure 6.13(b) and Figure 6.14(b)*, the effect of corrosion level at the critical cross section on yielding and ultimate strength for the different type of rebars are considered. The total corrosion interval-range for the critical cross section was between 0-40%.

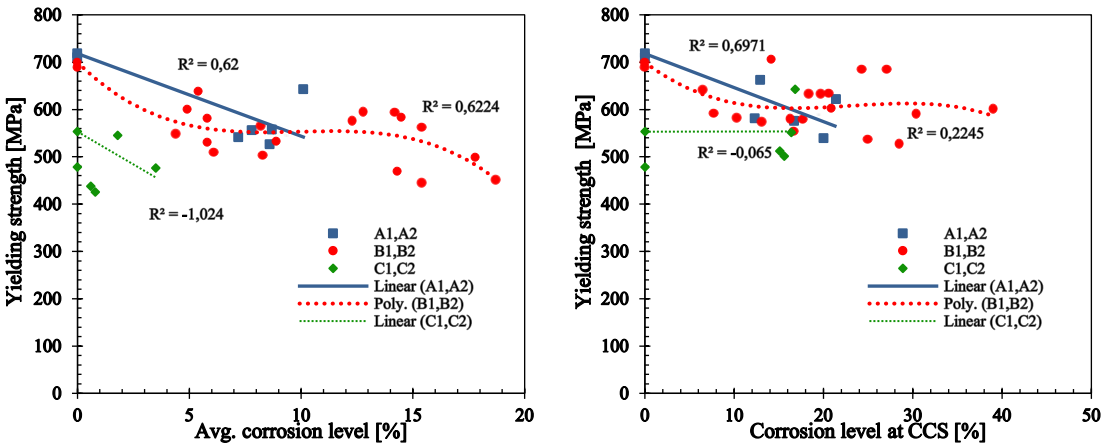

(a) *(b)*

Figure 6.13: The yielding strength effect on corrosion levels for different type of naturally corroded rebars. (a) corrosion level at average cross-section, (b) corrosion level at critical cross-section.

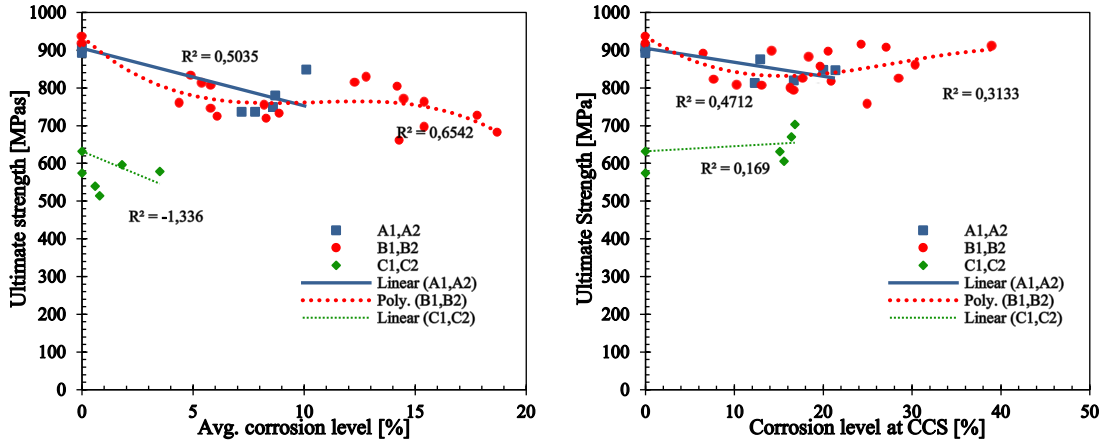

(a) *(b)*

Figure 6.14: The ultimate strength effect on corrosion levels for different type of naturally corroded rebars. (a) corrosion level at average cross-section, (b) corrosion level at critical cross-section.

As it was mention in the chapter 2.3.1.1 and in equation (2.1), stress is a relation between force/load and the area of the specimen. From the analyzed force section 6.1.2, the yield and ultimate force were reduced linearly with increased corrosion level. When comparing the reduction to the theoretical expectation, the corresponding result for the average corrosion level was reducing more, where the CCS value reduced more or less the same as expected (see *Figure 6.6*). As discussed earlier, the reduction of the area was concluded to reduce linearly with increased corrosion level. If the ratio of reduction is the same for both force and area, a constant strength value will be received disregard the corrosion level.

In the *Figure 6.13(a)* and *Figure 6.14(a)* the reducing yield and ultimate strength when considering average corrosion level can be explained by observing the *Figure 6.6(a).* The reduction of load is higher than the reduction of an area with the increase of corrosion. Due to this difference in reduction, the strength ratio will always be slightly reduced. This reducing behavior was also observed by Llano Trueba, 2015.

Further for the CCS section, a reduction was not noticed as for the average corrosion level, instead, the strength value stayed constant. This can be explained by the CCS method of measuring corrosion level is more realistic and more accurate than average corrosion level (see *Figure 6.6(b))*, creating a force reduction close to the expected one. The ratio between the force and the area is more or less of the same magnitude and by so resulting in a constant strength value as observed in the *Figure 6.13(b)* and *Figure 6.14(b)*

As concluded in section 6.1.2, loss of area at a critical cross section, a rapid change in the section significantly change the stress in failure point. The amount of stress concentration at critical cross section it is also depends on change on the section, i.e. depth of the pit.

6.3.2 Modulus of elasticity

The effect different corrosion levels on modulus of elasticity is presented in *Figure 6.15*. It can be seen that both average and critical corrosion level up to 7% does not have any effect on the modulus of elasticity (see *Figure 6.15)*.

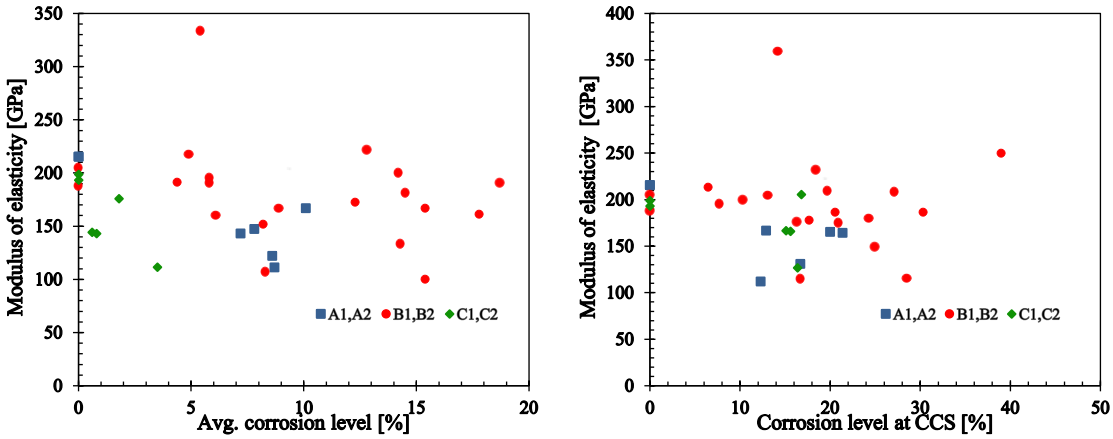

(a) *(b)*

Figure 6.15: The modulus of elasticity effect on corrosion levels for different type of naturally corroded rebars. (a) corrosion level at average cross-section, (b) corrosion level at critical cross-section.

The modulus of elasticity at average corrosion levels showed a higher scattered value see *Figure 6.15(a)*. Despite this, the measured modulus of elasticity seems to be reduced with the increasing corrosion levels. However, the scattered data did not allow to establish any trustworthy relationship with the average corrosion degree. These results are in line with the results of (Fernandez, Bairán and Marí, 2015).

Figure 6.15(b) displays the relationship between modulus of elasticity with corrosion level at the critical cross section. The modulus of elasticity slightly decreased with the increasing corrosion levels, but as in *Figure 6.14(a)*, the highly scatter data suppress the possibility to correlate between corrosion level and modulus of elasticity.

7 Conclusion

The aim of this thesis was to study the mechanical properties of uncorroded reinforcing bars and to describe apparent mechanical properties of corroded reinforcing bars and by so increase the level of knowledge in this field. An experimental program was set up to test a total of 57 uncorroded and naturally corroded reinforcement steel specimens gathered from different sources. A method of cutting, cleaning and preparing the test specimens is presented. It was concluded that sandblasting cleaning method was the most suited method to remove all the corrosion products from the test specimens and generate a respectable base for further measurements, moreover when coating and painting of the specimen is needed. The measurement of corrosion level was done following two different methods. First the gravimetric method measured the average corrosion level which represents more meaningful results for generalized corrosion. Second, 3D scanning of the bars, which allows the description of the corrosion distribution along the bar and consequently the attainment of the corrosion level at the critical cross-section where the bar failed which in turn is more related to pitting corrosion.

Furthermore, monotonic tests to failure measured by means of Digital Image Correlation (DIC) technique were conducted for earlier mentioned specimens. The DIC system uses a stochastic pattern imprinted on the specimen surface by means of what it is possible to follow the deformation of the specimen, provided the application of load by the tensioning machine. A sequence of images results from the use of the DIC which by comparison between the capture pattern between them allows the obtention of different type of results. The pattern as it was observed, had a significant role in providing trustworthy results, among others because if the pattern has not enough quality or it is damage during the tests no results can be captured.

The post processing of the results was carried out with the software GOM Correlate Professional 2017. A series of digital extensometers were used in combination with the measured force to obtain all the relevant results: strains, displacements and other important values needed to further acquire engineering and true stress-strain curves. It was observed that Digital Image Correlation (DIC) provided accurate strain results from 45mm down to 1mm length of extensometer at the critical region for this study.

From the analyzed results the following conclusion can be drawn:

- The mechanical properties of the reinforcing steel bars are strongly affected by corrosion due to loss of cross sectional area in global and local cases for naturally corroded specimens. Those factors cause degradation of the mechanical properties by increasing corrosion levels.
- In this study, the average and critical cross section (CCS) corrosion levels ranged from 0-20% and from 0-40% respectively. However, the observations made for the different parameters were not proportional to the measured corrosion level.

- An important reduction in the elongation was observed for all the specimens, even though the big scatter of the results. Moreover, this reduction was more acute in the interval-range 0-7% for the averaged corrosion level and 0-18% for the corrosion level at the critical cross section. This clearly indicates that the variable is very sensible to small corrosion levels.
- The yield and ultimate load capacity for the tested rebars presented a linear reduction for all types of specimens with the increase of corrosion level. The yield and ultimate load for average corrosion level showed the higher reduction respect to the theoretical value. Furthermore, the yield and ultimate load that utilize the corrosion level at CCS showed reduction that correspondent better to the theoretical fit. It was also established that decrease of load strongly related to loss of area, that was also reduced by increased of corrosion level.
- A reduced trend for the yield strain with increased of both average and CCS corrosion level was noticed. The highest reduction occurred in the corrosion interval range between 0-10%. The fracture strain for the result analysis showed that the influence of corrosion level reduced this mechanical parameter severely in the corrosion range of 0-7% for the averaged corrosion level and 0-18% for the corrosion level at the critical cross section.
- Considering the average corrosion level, the yielding and ultimate strengths provided reduced mechanical properties with increased corrosion level. For the averaged corrosion level with the interval of 0-6%, which was applied for all type of bars followed a reduced linear function for yielding and ultimate strength. The yielding strength reduced slightly higher than ultimate strength with the same increased average corrosion level. The yielding and ultimate strength at CCS corrosion level showed constant behavior. It was also concluded that the ratio between the force and area was of high importance for establishing the strength. The ratio between force and area resulted in a reduction of strength due to the force reduced faster than the area when using average cross section and for the CCS, the ratio between the force and the area was more or less of the same magnitude and by so resulting in a constant strength value. This can be explained by the method of a critical cross section which is closer to reality than the average corrosion level.
- The modulus of elasticity displayed the highly scatter data disregard of used corrosion type. Because of that, a trustworthy correlation could not be established.
- The findings presented in this study showed that both corrosion method i.e. average corrosion and critical corrosion, affected the considerate mechanical properties. It can be summarized that method of measuring corrosion in the critical cross was more realistic in its way of describing the behavior. This information will lead to better understanding of the behavior for the reinforced concrete structures and how much they are affected by corrosion. Furthermore, this study can be used as a base for future studies, but also directly applicable to the commercial engineering world.

8 Further research

In this study, a method of testing, postprocessing and finally obtaining true and engineering stress-strain graphs were established. For the “engineering part” several analyses were performed to obtain correlations between different relevant mechanical properties and corrosion levels. A recommendation for future study is to further develop “true strain-true stress part”. Also, it is suggested to increase the variety and number of tested specimens to increase the reliability of the study and for generalization of the findings.

9 References

Apostolopoulos, C. A. (2007) 'Mechanical behavior of corroded reinforcing steel bars S500s tempcore under low cycle fatigue', *Construction and Building Materials*, 21(7), pp. 1447–1456. doi: 10.1016/j.conbuildmat.2006.07.008.

Apostolopoulos, C. A., Demis, S. and Papadakis, V. G. (2013) 'Chloride-induced corrosion of steel reinforcement - Mechanical performance and pit depth analysis', *Construction and Building Materials*. Elsevier Ltd, 38, pp. 139–146. doi: 10.1016/j.conbuildmat.2012.07.087.

Angst, U. (2011) *Ueli Angst Chloride induced reinforcement corrosion in concrete*.

Burström P. (2007) *Byggnadsmaterial.*

Brinson, H. F. and Brinson, L. C. (2015) *Polymer engineering science and viscoelasticity: An introduction, Second edition, Polymer Engineering Science and Viscoelasticity: An Introduction*. doi: 10.1007/978-1-4899-7485-3.

Balestra, C. E. T. *et al.* (2016) 'Corrosion Degree Effect on Nominal and Effective Strengths of Naturally Corroded Reinforcement', *Journal of Materials in Civil Engineering*, 28(10), p. 4016103. doi: 10.1061/(ASCE)MT.1943-5533.0001599.

Berrocal, Carlos G. (2017). 'Corrosion of Steel Bars in Fibre Reinforced Concrete: Corrosion mechanisms and structural performance'. 10.13140/RG.2.2.18233.88166.

Du, Y. G., Clark, L. A. and Chan, A. H. C. (2005) 'Residual capacity of corroded reinforcing bars', *Magazine of Concrete Research*, 57(3), pp. 135–147. doi: 10.1680/macr.2005.57.3.135.

Division, C. E. (2002) *Prediction of Deterioration of Concrete Bridges in the Netherlands, Management*.

Das, P. (Unpublished) '3D Scanning of naturally corroded steel bars. An assessment of corrosion behavior and correlations to critical cross-sections', Unpublished.

El Maaddawy, T. a. and Soudki, K. a. (2003) 'Effectiveness of Impressed Current Technique to Simulate Corrosion of Steel Reinforcement in Concrete', *Journal of Materials in Civil Engineering*, 15(1), pp. 41–47. doi: 10.1061/(ASCE)0899-1561(2003)15:1(41).

Fernandez, I., Bairán, J. M. and Marí, A. R. (2015) 'Corrosion effects on the mechanical properties of reinforcing steel bars. Fatigue and σ-

ε behavior', *Construction and Building Materials*. Elsevier Ltd, 101, pp. 772–783. doi: 10.1016/j.conbuildmat.2015.10.139.

Fernandez, I., Bairán, J. M. and Marí, A. R. (2016) 'Mechanical model to evaluate steel reinforcement corrosion effects on σ-ε and fatigue curves. Experimental calibration and validation', *Engineering Structures*. Elsevier Ltd, 118, pp. 320–333. doi: 10.1016/j.engstruct.2016.03.055.

François, R., Khan, I. and Dang, V. H. (2013) 'Impact of corrosion on mechanical properties of steel embedded in 27-year-old corroded reinforced concrete beams', *Materials and Structures/Materiaux et Constructions*, 46(6), pp. 899–910. doi: 10.1617/s11527-012-9941-z.

Faridmehr, I. *et al.* (2014) 'Correlation between Engineering Stress-Strain and True Stress-Strain Curve', *American Journal of Civil Engineering and Architecture*, 2(1), pp. 53–59. doi: 10.12691/ajcea-2-1-6.

Gilat, A. and Seidt, J. D. (2014) 'Dynamic Material Characterization Using Digital Image Correlation ', *Applied Mechanics and Materials*, 566(January), pp. 3–9. doi: 10.4028/www.scientific.net/AMM.566.3.

Gestsdottir, E. and Gudmundsson, T. (2012) 'Bond Behaviour of Naturally Corroded Reinforcement in Concrete Structures', p. 88.

Llano Trueba, L. (2015) 'Patterns of corroded rebar surfaces and their impact on tensile mechanical properties.', (August). Available at: http://epubs.surrey.ac.uk/808602/.

Lau, K. and Lasa, I. (2016) 'Corrosion of Steel in Concrete Structures', *Corrosion of Steel in Concrete Structures*, pp. 37–57. doi: 10.1016/B978-1-78242-381-2.00003-1.

Morka, A. and Niezgoda, T. (2012) 'Evaluation of True Stress in Engineering Materials', *Journal of KONES*, 19(4), pp. 53–64.

Papadopoulos, M. P. *et al.* (2011) 'Corrosion of exposed rebars, associated mechanical degradation and correlation with accelerated corrosion tests', *Construction and Building Materials*. Elsevier Ltd, 25(8), pp. 3367–3374. doi: 10.1016/j.conbuildmat.2011.03.027.

Silva, N. (2013) *Chloride Induced Corrosion of Reinforcement Steel in Concrete: Threshold Values and Ion Distributions at the Concrete-Steel Interface Department of Civil and Environmental Engineering Chloride Induced Corrosion of Reinforcement Steel in Concrete*.

Svensk Betong (2018). *Svensk betong*. Retrieved 2018-03-30 from

https://www.svenskbetong.se/hallbarhet/karbonatisering.

Arnholm, B (2004). *Arnholm B.* Retrieved 2018-03-30 from http://kanaler.arnholm.nu/trollhattan/trollbros.html.

Gom.com (2018). *Gom.com*. Retrieved 2018-04-01 from https://www.gom.com/3d-software/gom-system-software/aramis professional.html.

Tahershamsi, M. (2016) *Structural Effects of Reinforcement Corrosion in Concrete Structures*.

Tahershamsi, M. *et al.* (2017) 'Investigating correlations between crack width, corrosion level and anchorage capacity', *Structure and Infrastructure Engineering*.

Taylor & Francis, 13(10), pp. 1294–1307. doi: 10.1080/15732479.2016.1263673.

Technology, B. and Structures, T. (2017) 'Material Characterization of Weld Toe Region Using Digital Image Correlation '.

U, A. A. A. (2001) 'Effect of degree of corrosion on the properties of reinforcing steel bars', pp. 361–368.

Wanat, S. F. (2016) 'Acquisition : Basic Issues', 25(2), pp. 142–147.

Zhang, W. *et al.* (2012) 'Tensile and fatigue behavior of corroded rebars', *Construction and Building Materials*. Elsevier Ltd, 34, pp. 409–417. doi: 10.1016/j.conbuildmat.2012.02.071.

Zhu, W. and François, R. (2014) 'Experimental investigation of the relationships between residual cross-section shapes and the ductility of corroded bars', *Construction and Building Materials*. Elsevier Ltd, 69, pp. 335–345. doi: 10.1016/j.conbuildmat.2014.07.059.

Zhu, W., François, R. and Liu, Y. (2017) 'Propagation of corrosion and corrosion patterns of bars embedded in RC beams stored in chloride environment for various periods', *Construction and Building Materials*. Elsevier Ltd, 145, pp. 147–156. doi: 10.1016/j.conbuildmat.2017.03.210.

Zhu, W. *et al.* (2017) 'Influences of corrosion degree and corrosion morphology on the ductility of steel reinforcement', *Construction and Building Materials*. Elsevier Ltd, 148, pp. 297–306. doi: 10.1016/j.conbuildmat.2017.05.079.

Zhu, W., François, R. and Liu, Y. (2017)
'Propagation of corrosion and corrosion patterns of bars embedded in

RC beams stored in chloride environment for various periods', *Construction and Building Materials*. Elsevier Ltd, 145, pp. 147–156. doi: 10.1016/j.conbuildmat.2017.03.210.

Appendix

Appendix A.1: All corroded rebars (Type A1, skewed)

Force versus displacement

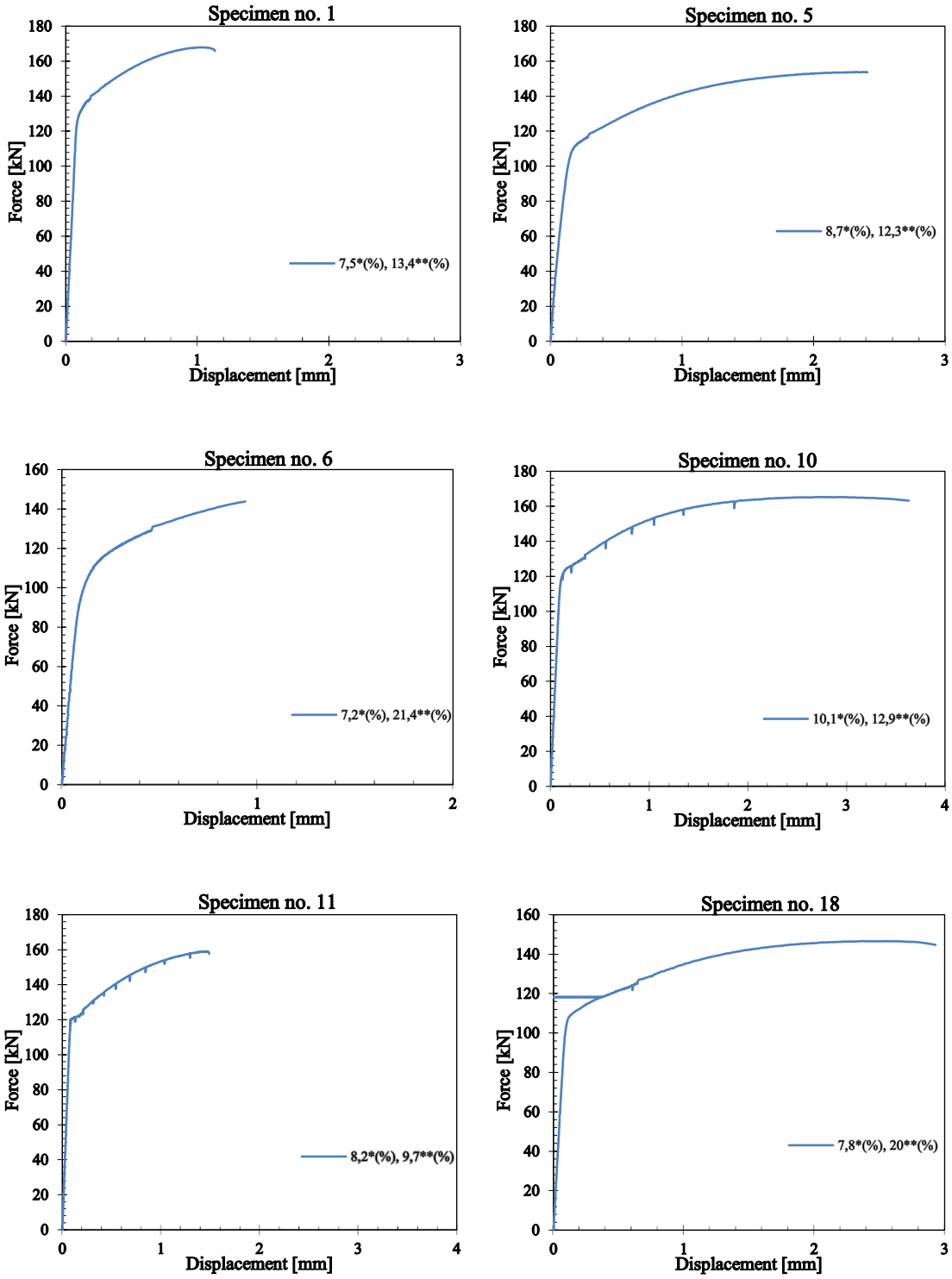

* Average corrosion level.

** Corrosion level at critical cross section (CCS).

Force versus engineering strain

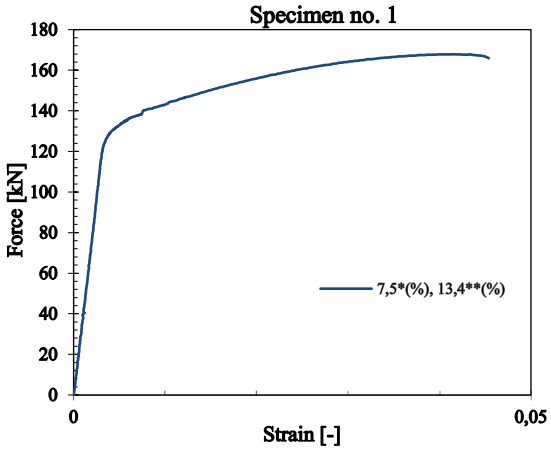

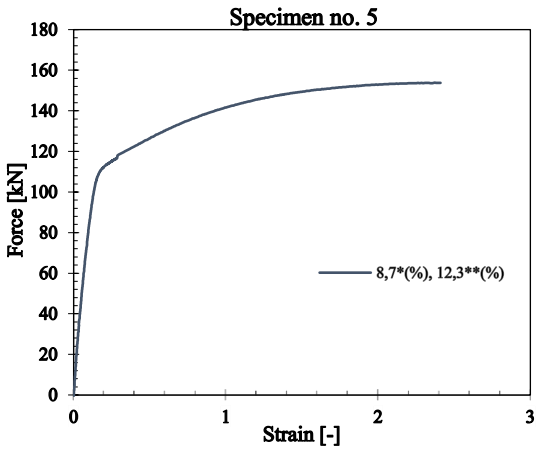

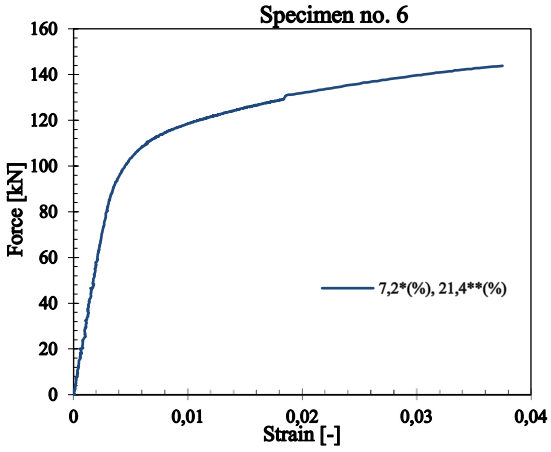

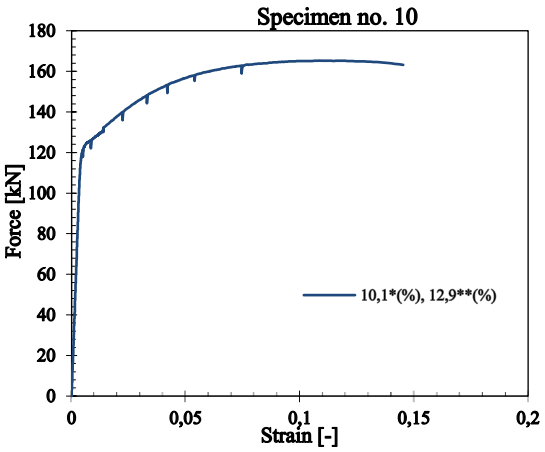

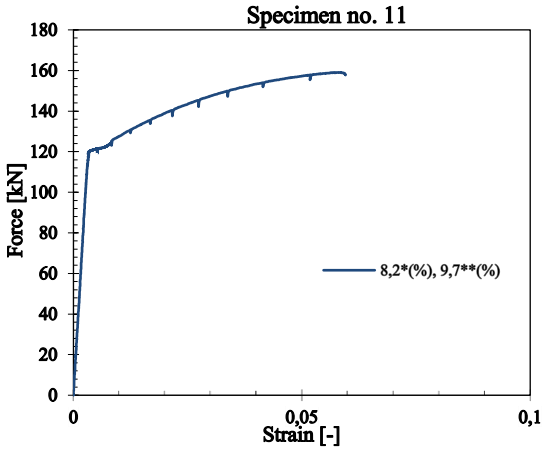

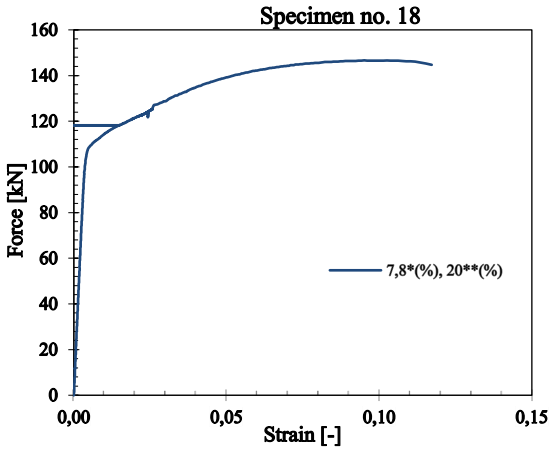

* Average corrosion level.

** Corrosion level at critical cross section (CCS).

Engineering stress-strain curve

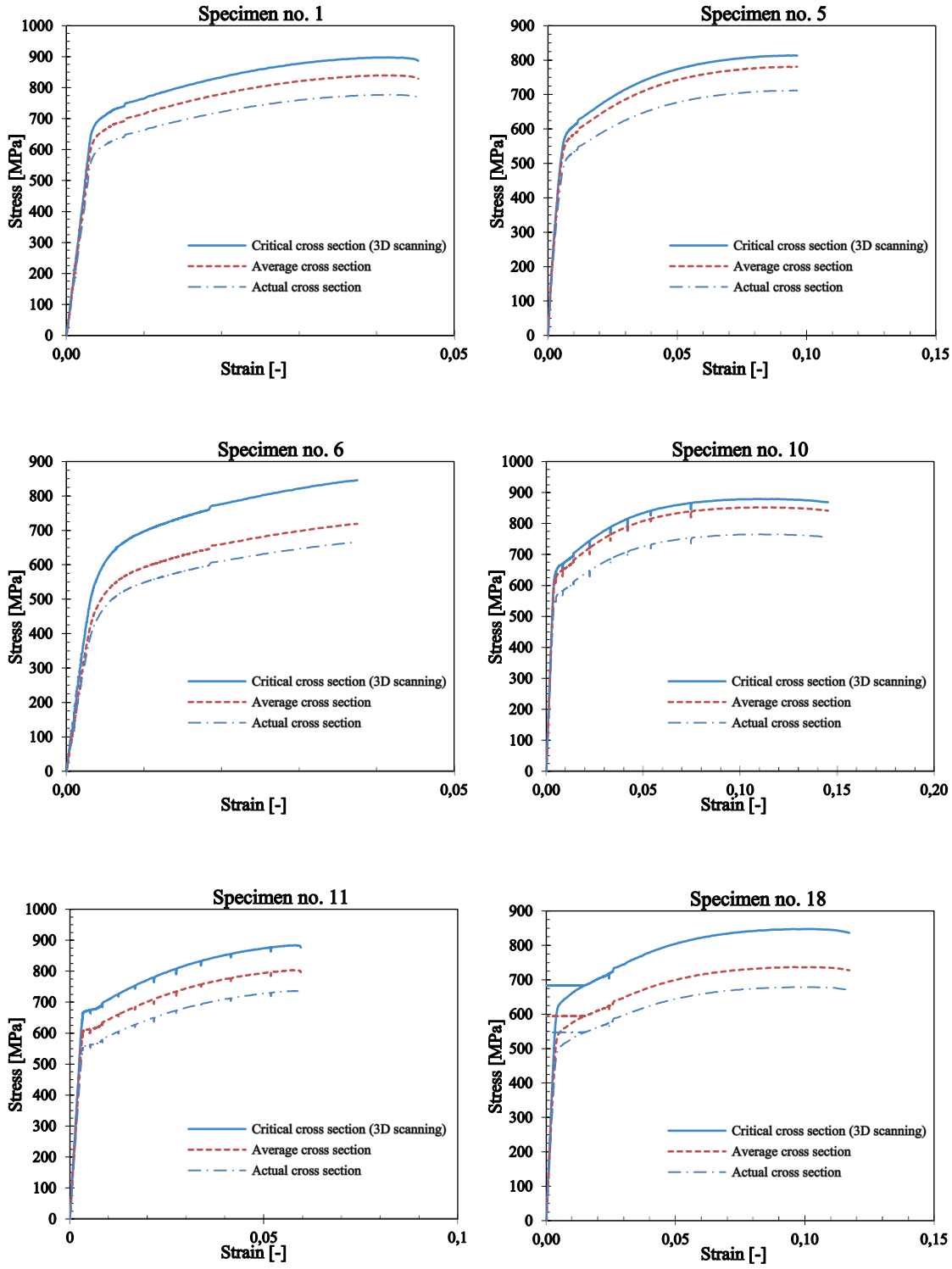

Appendix A.2: Uncorroded rebar (Type A2, skewed)

Force versus displacement

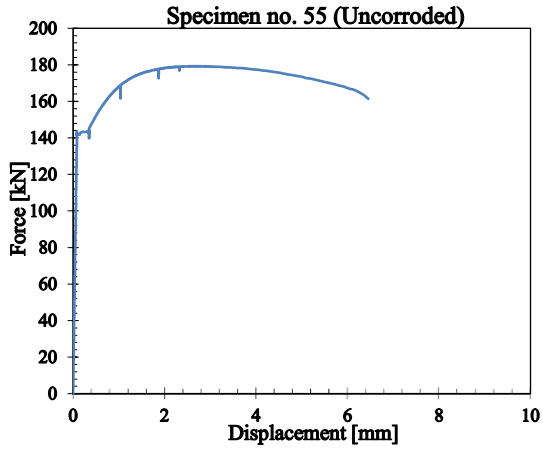

Force versus engineering strain

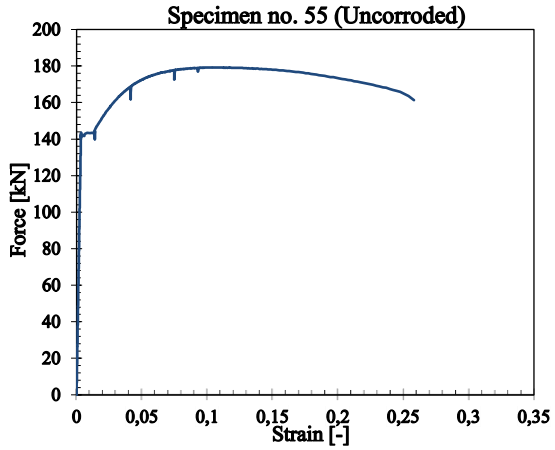

Engineering stress-strain curve

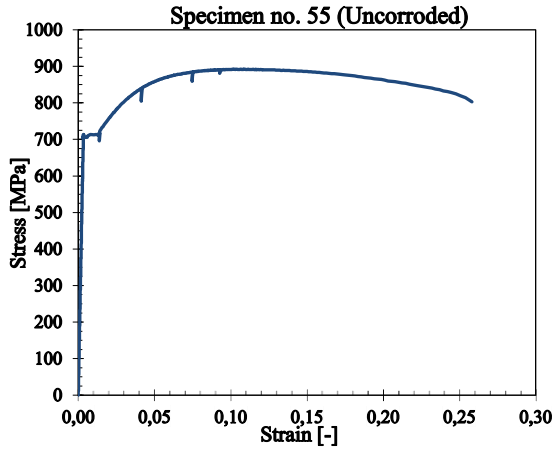

Appendix B.1: All corroded rebars (Type B1, straight)

Force versus displacement

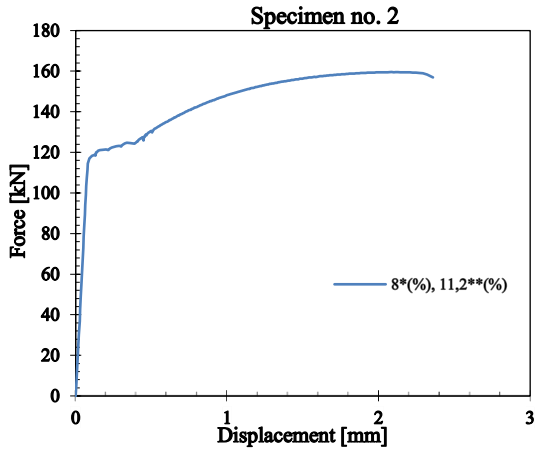

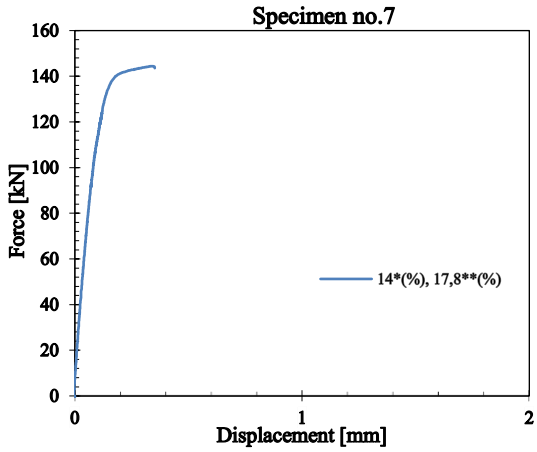

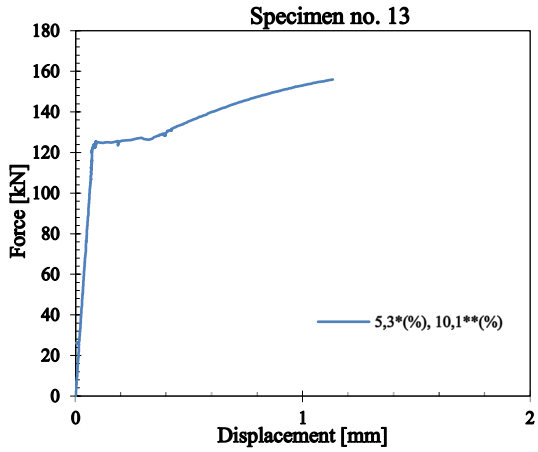

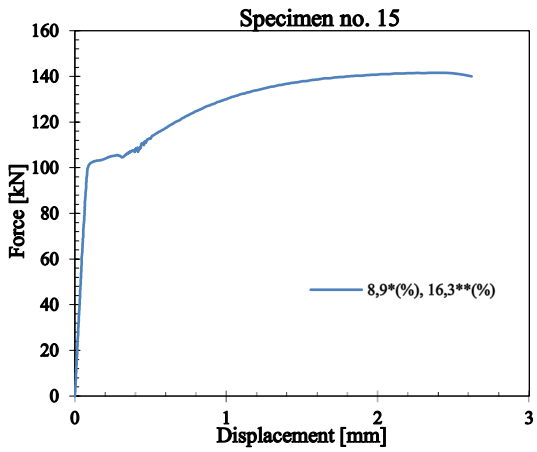

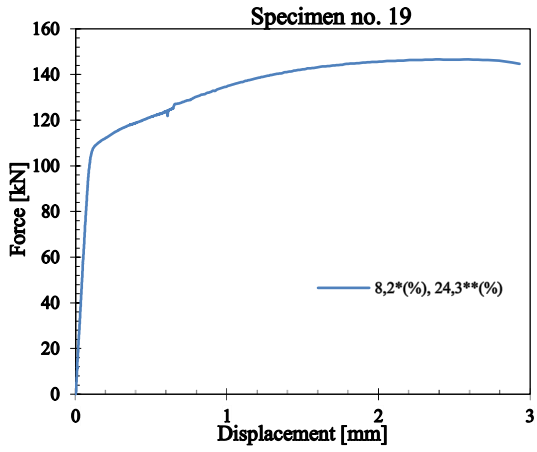

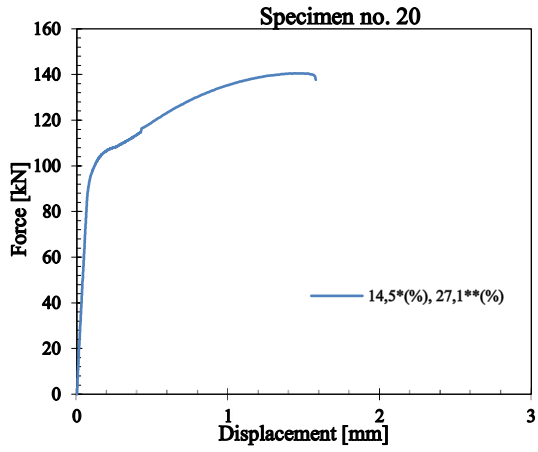

* Average corrosion level.

** Corrosion level at critical cross section (CCS).

Force versus displacement

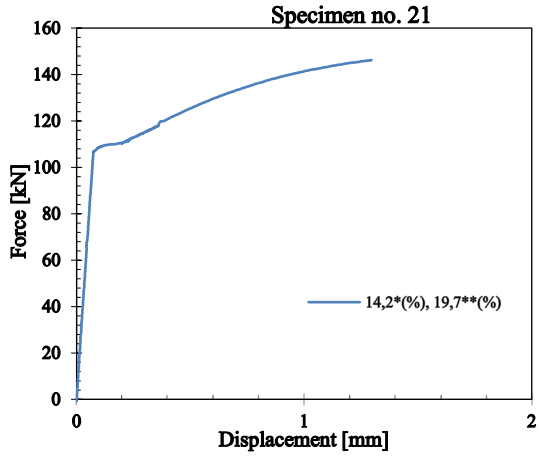

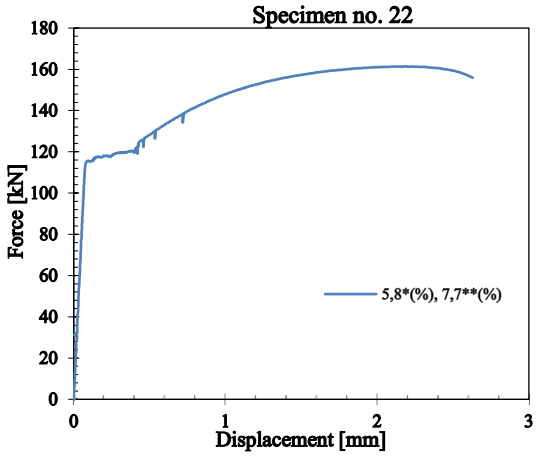

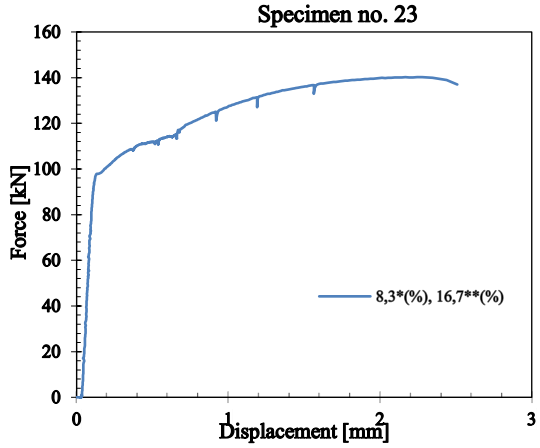

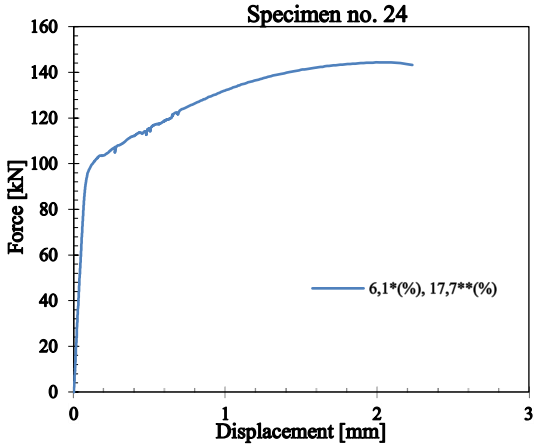

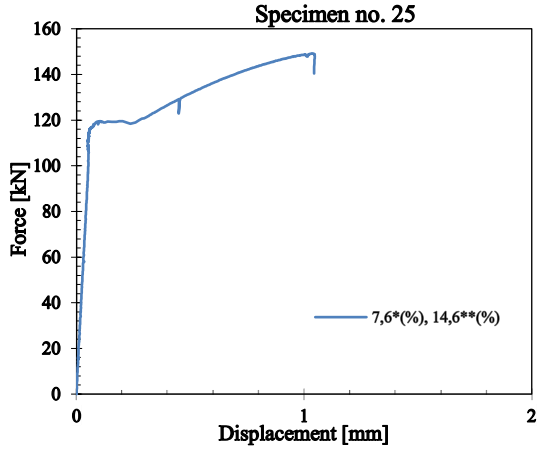

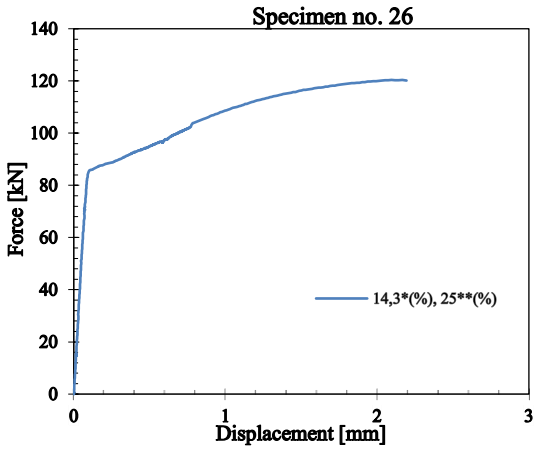

* Average corrosion level.

** Corrosion level at critical cross section (CCS).

Force versus displacement

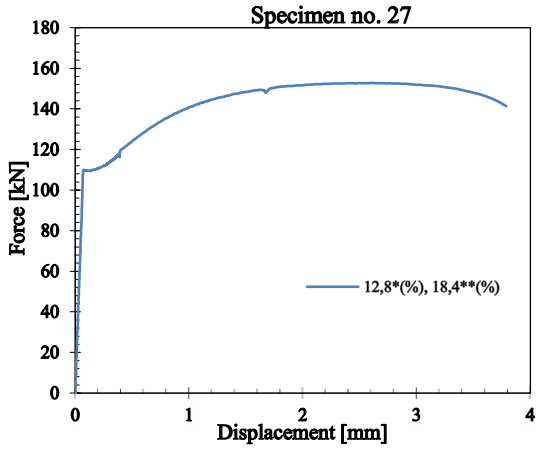

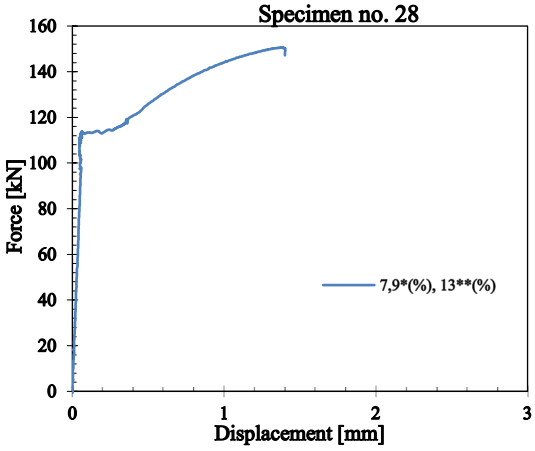

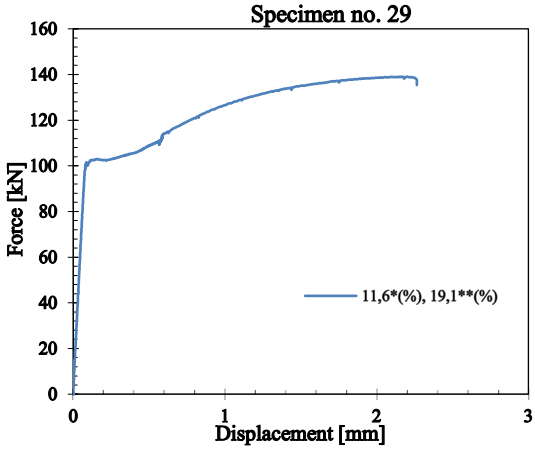

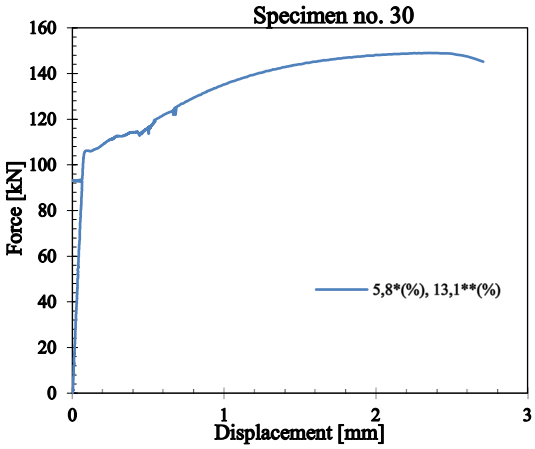

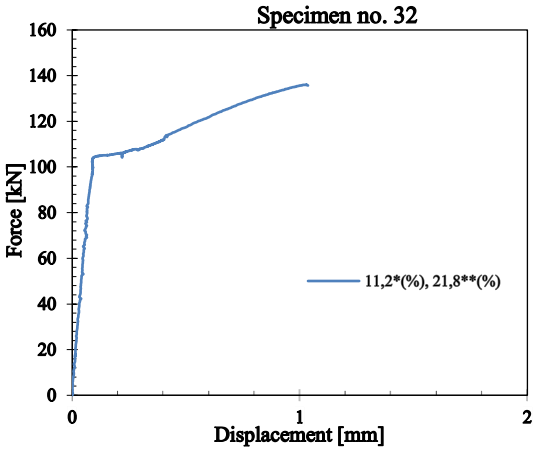

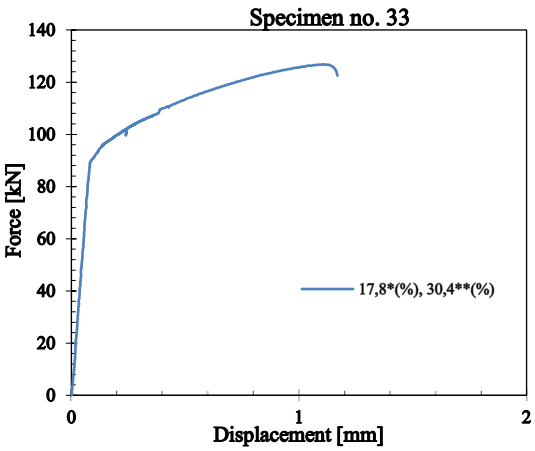

* Average corrosion level.

** Corrosion level at critical cross section (CCS).

Force versus displacement

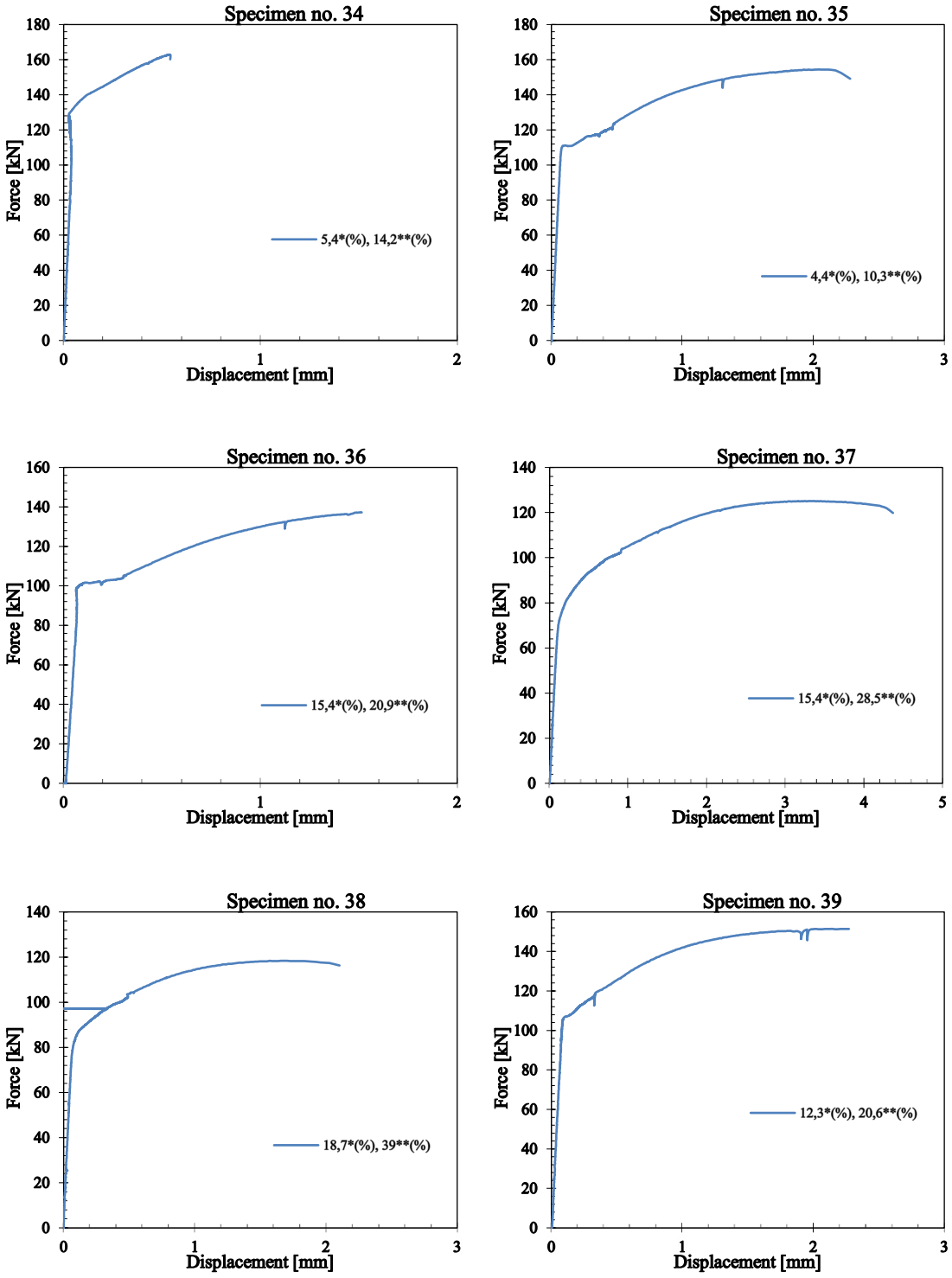

* Average corrosion level.

** Corrosion level at critical cross section (CCS).

Force versus engineering strain

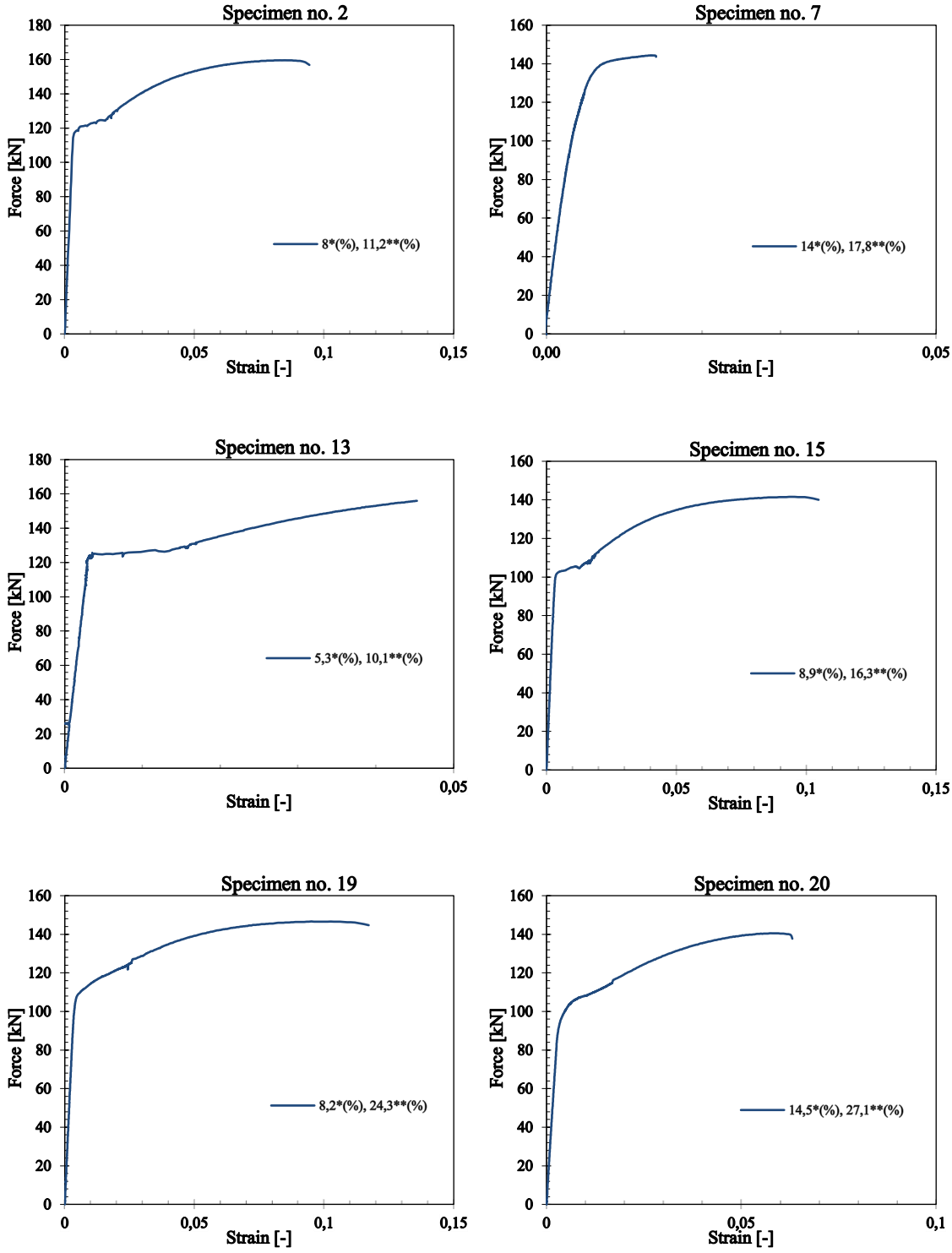

* Average corrosion level.

** Corrosion level at critical cross section (CCS).

Force versus engineering strain

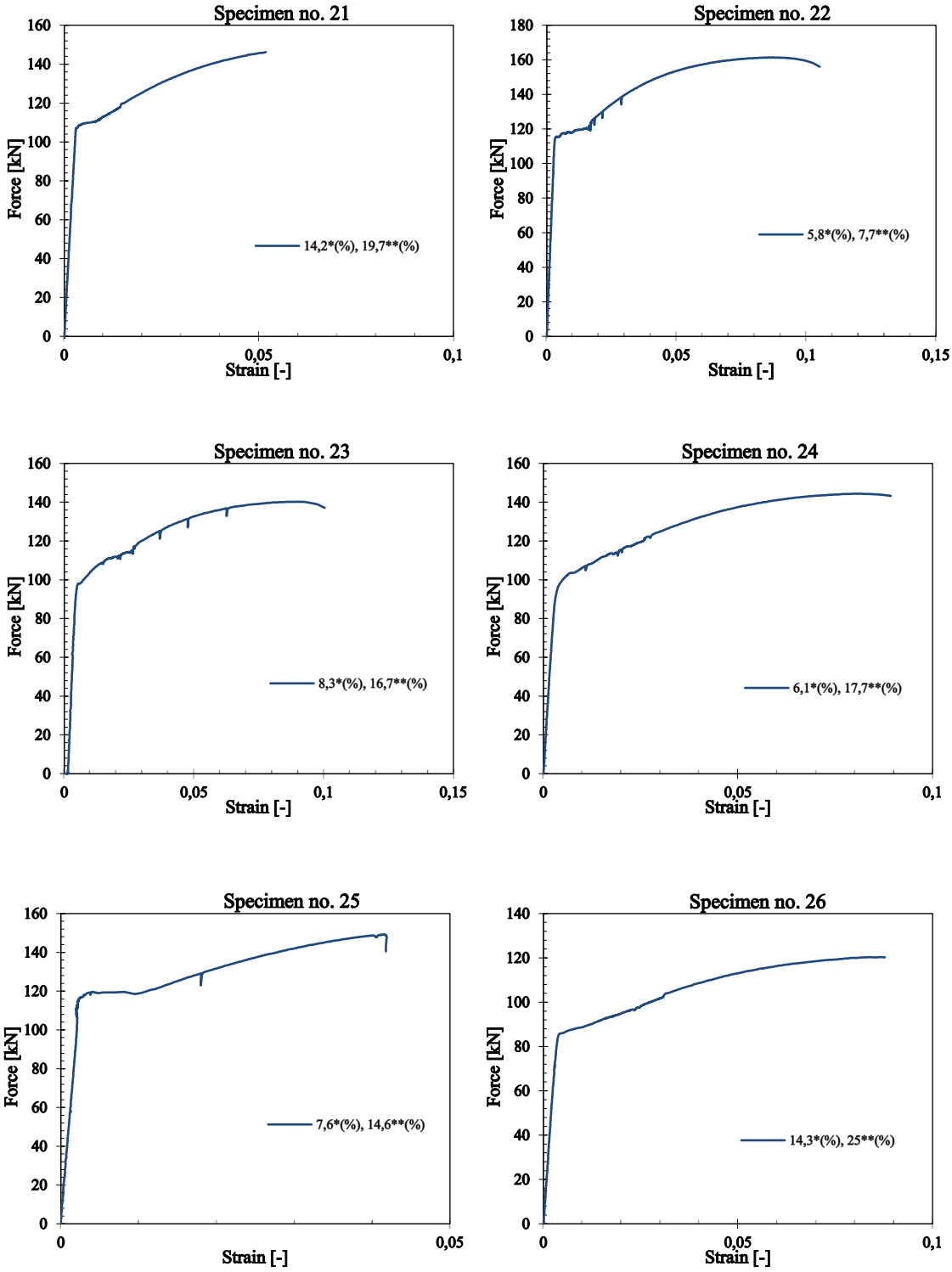

* Average corrosion level.

** Corrosion level at critical cross section (CCS).

Force versus engineering strain

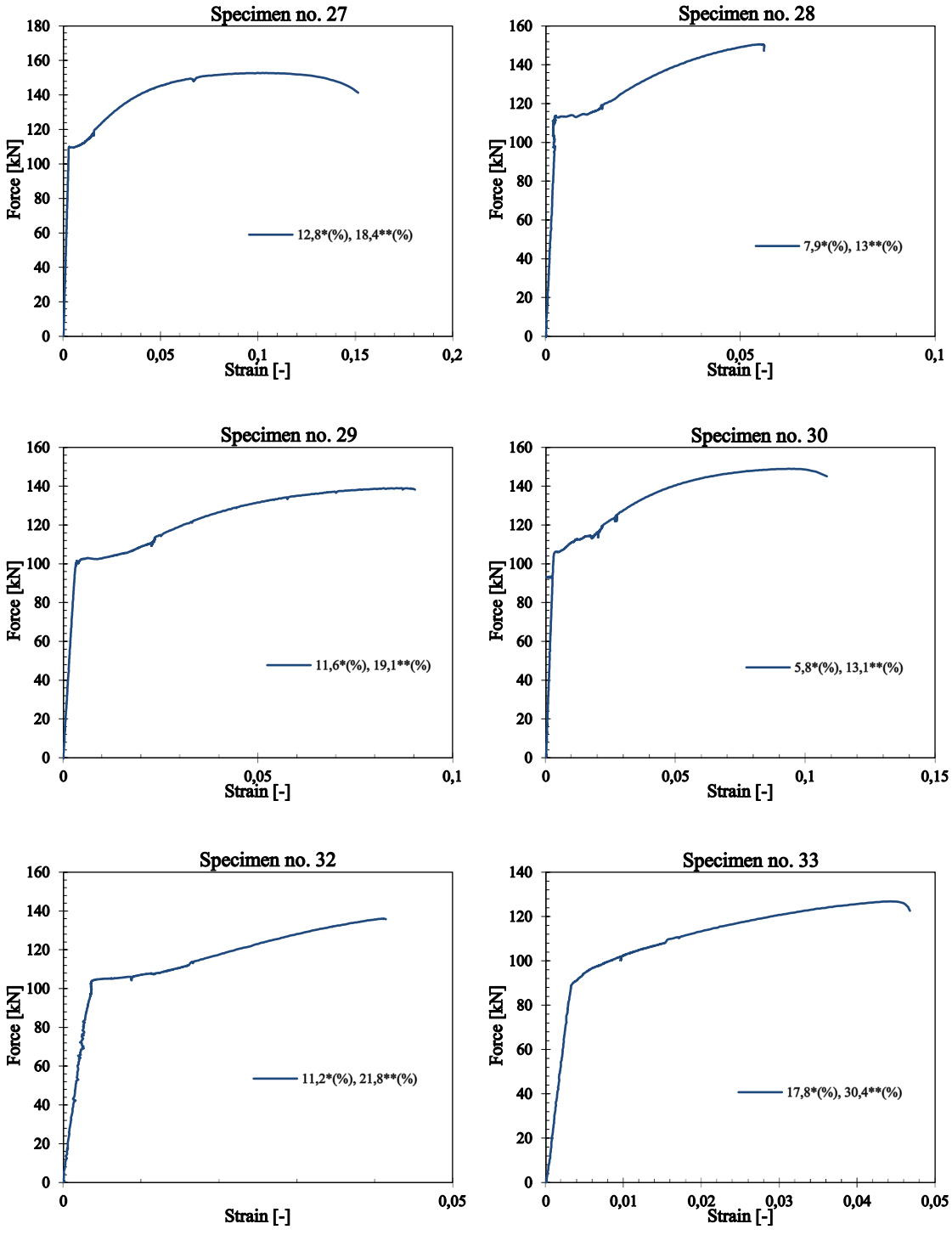

* Average corrosion level.

** Corrosion level at critical cross section (CCS).

Force versus engineering strain

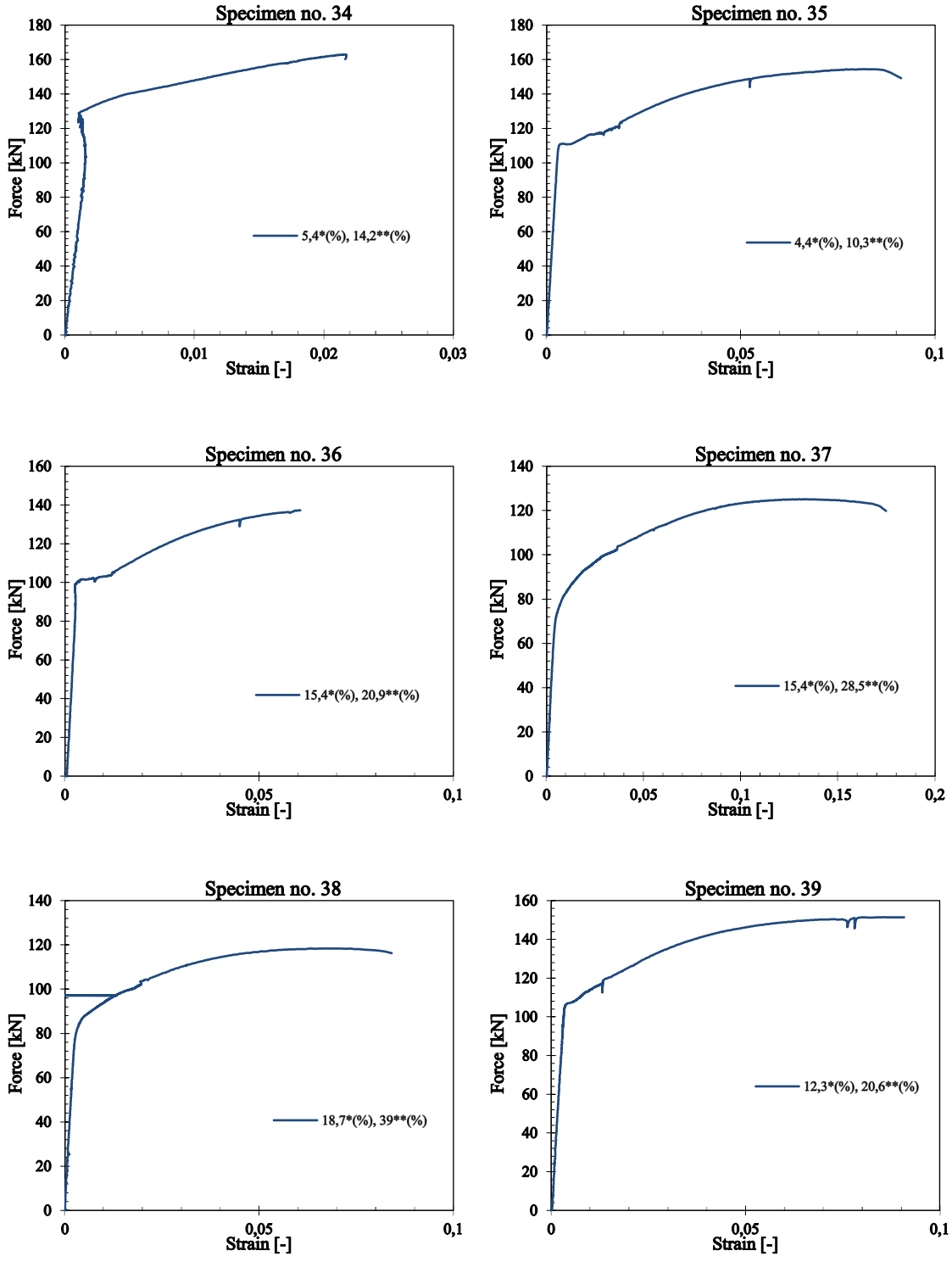

* Average corrosion level.

** Corrosion level at critical cross section (CCS).

Engineering stress-strain curve

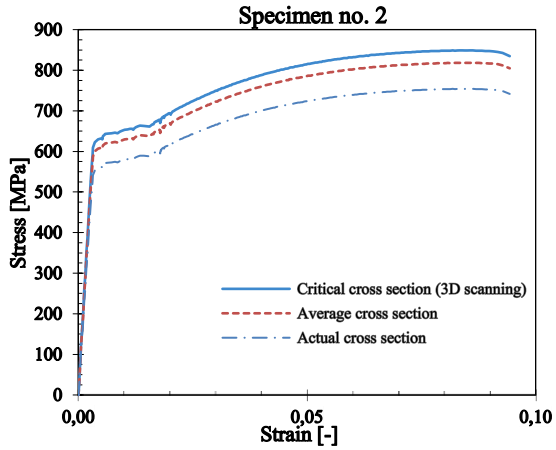

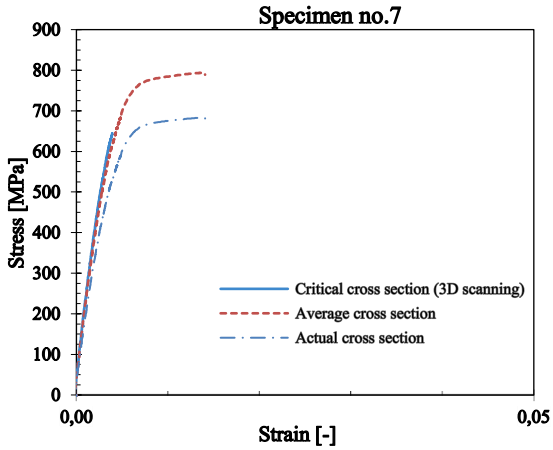

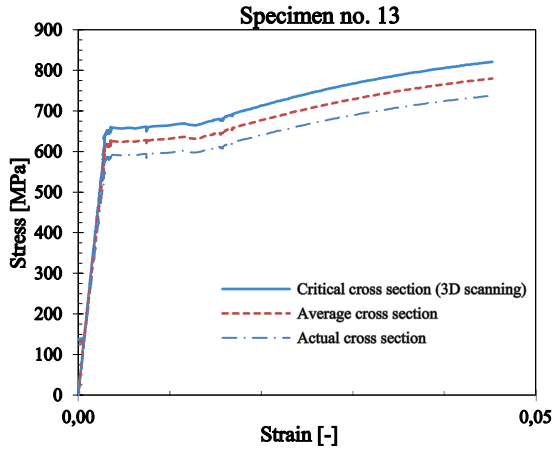

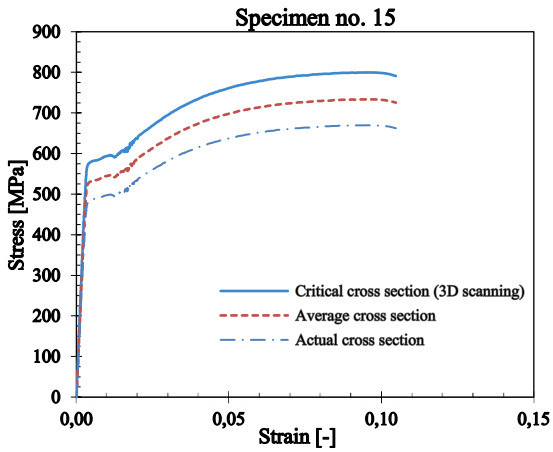

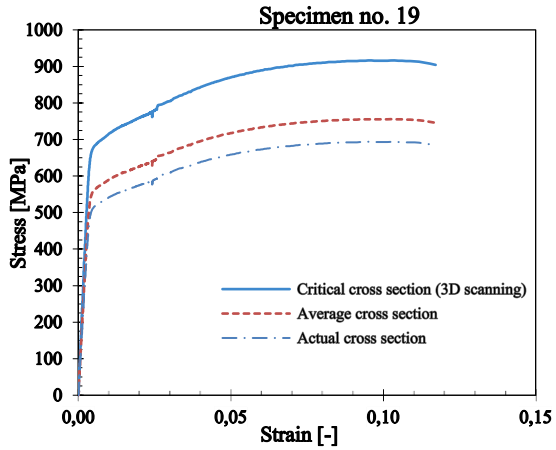

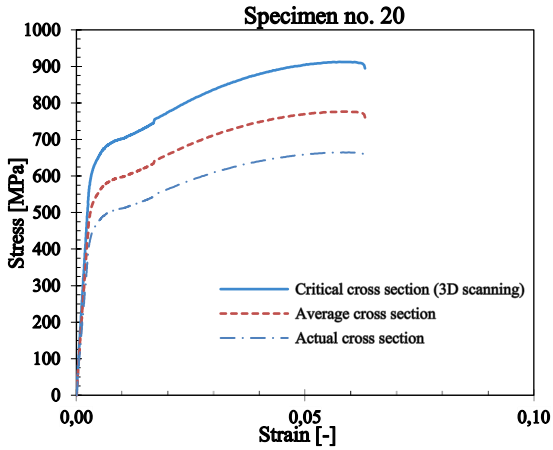

Engineering stress-strain curve

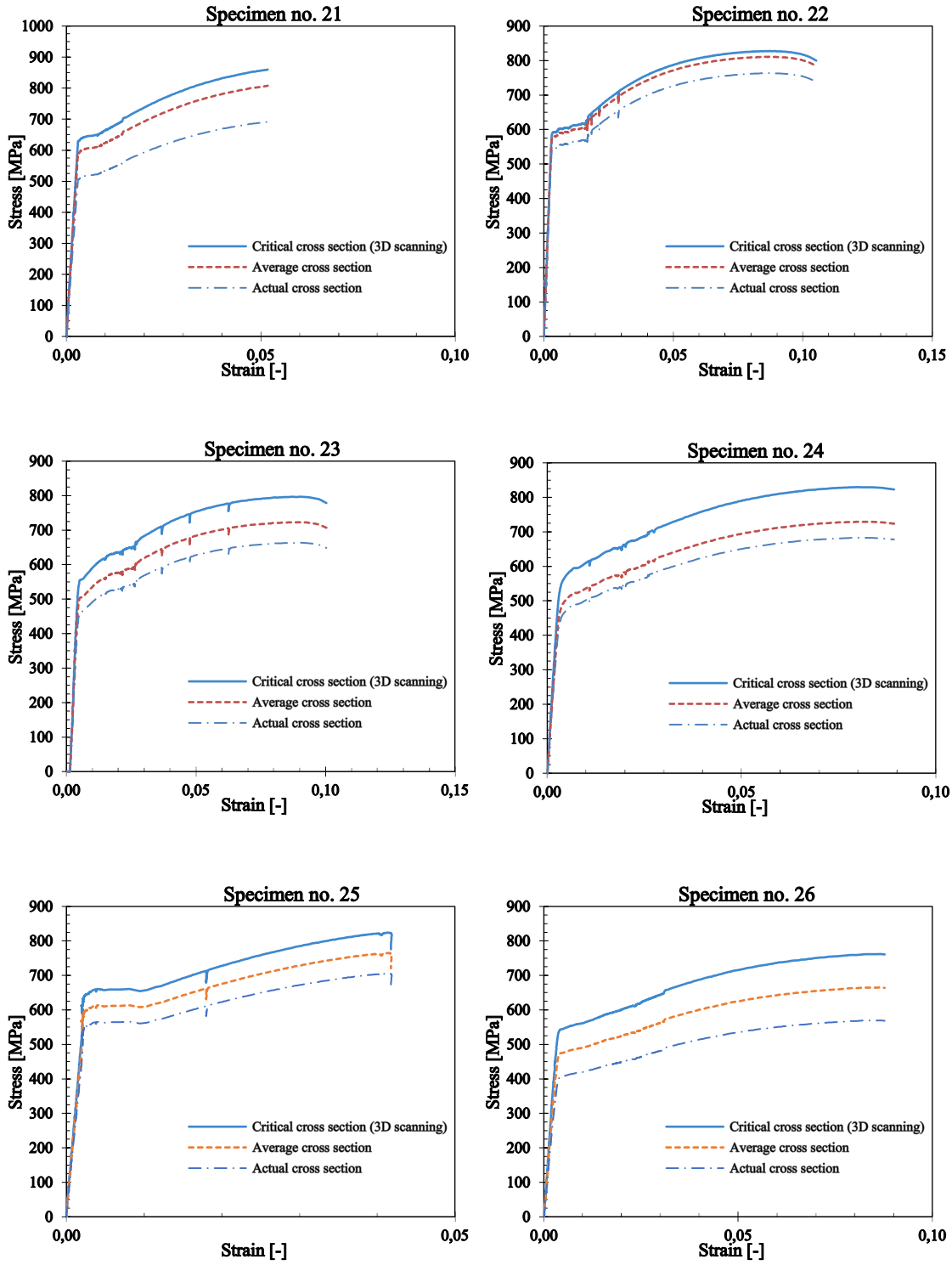

Engineering stress-strain curve

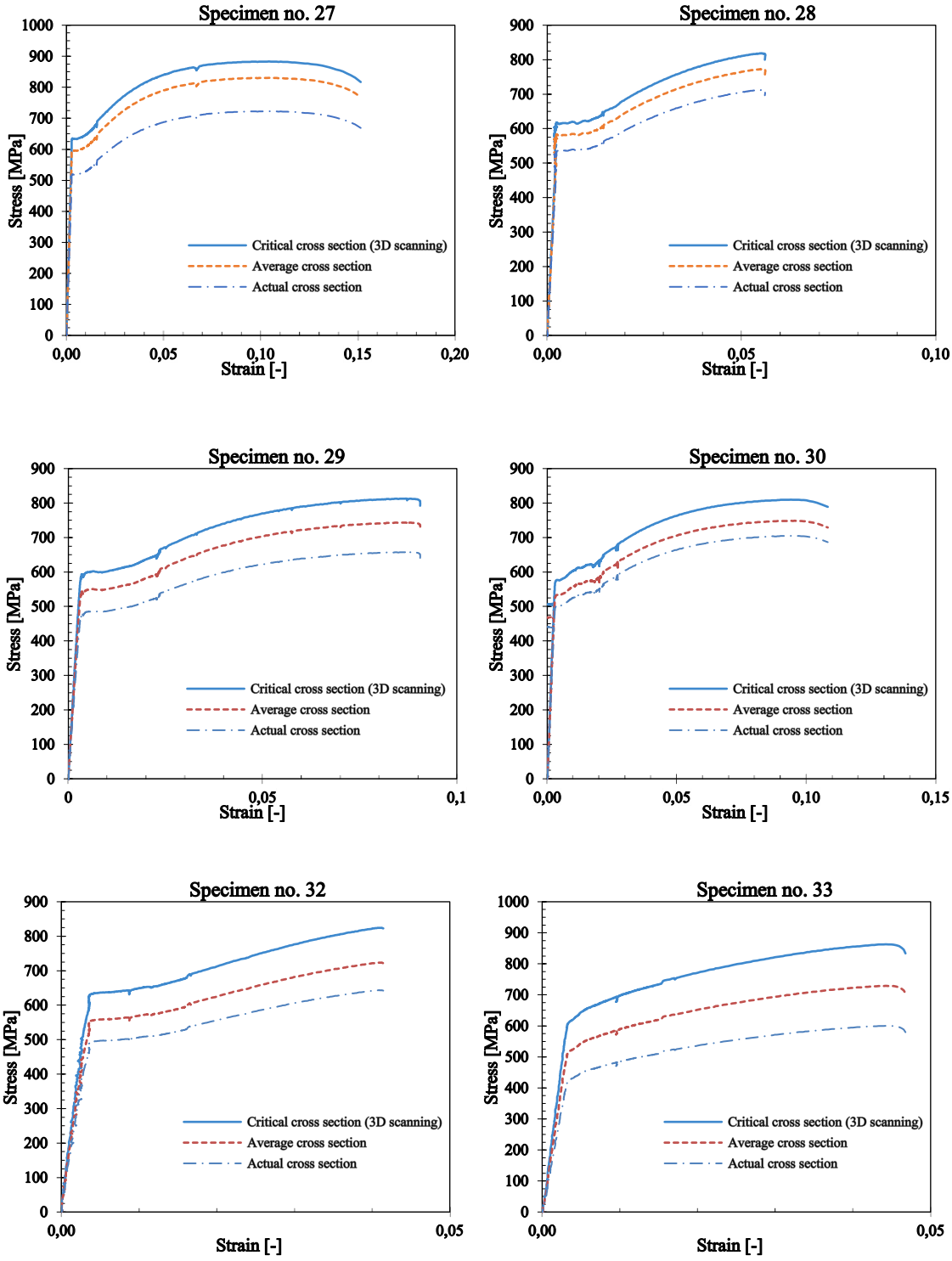

Engineering stress-strain curve

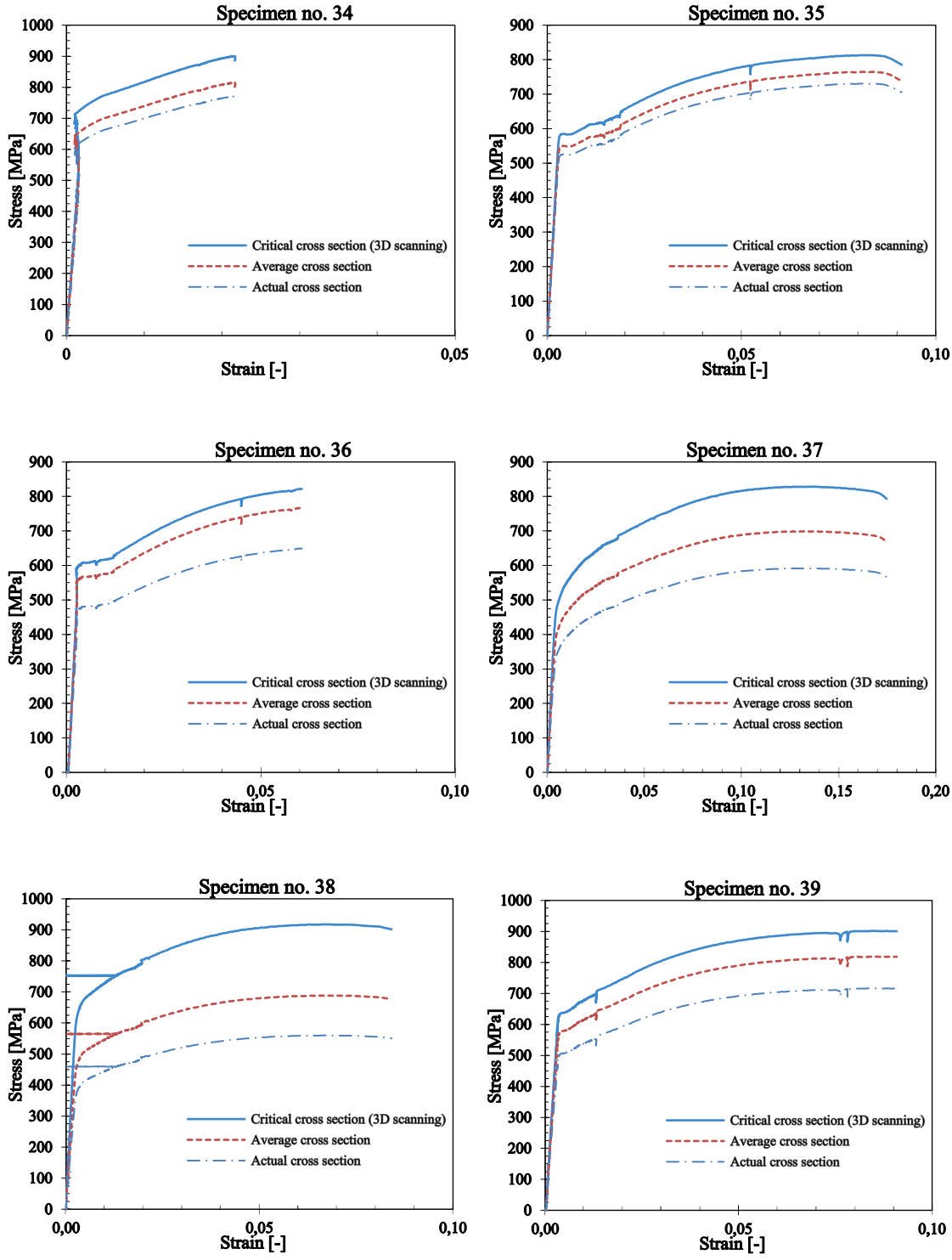

Appendix B.2: Uncorroded rebar (Type B2, straight)

Force versus displacement

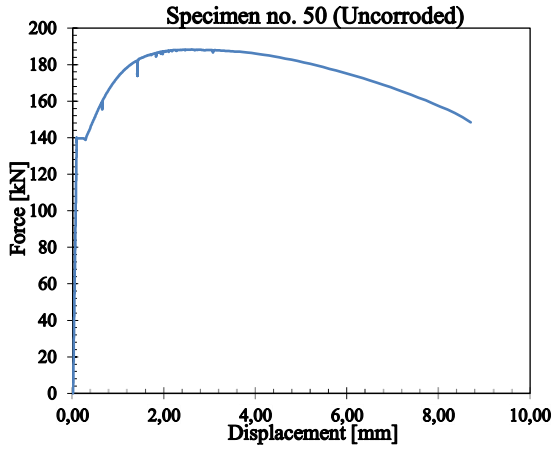

Force versus engineering strain

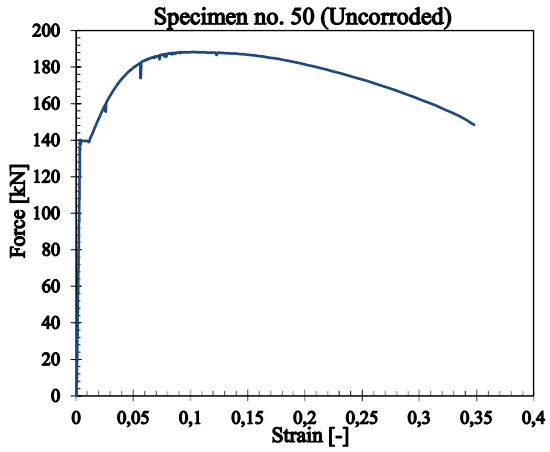

Engineering stress-strain curve

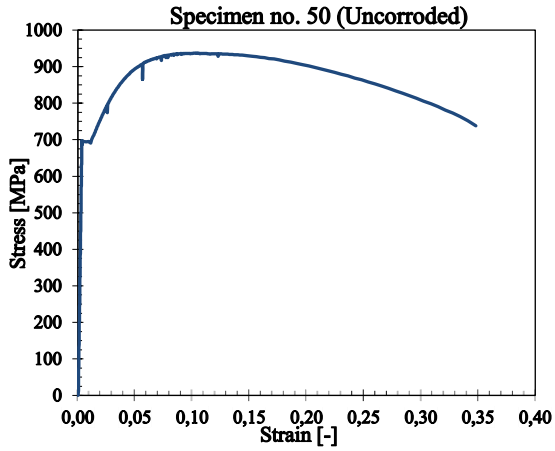

Appendix C.1: All corroded rebars (Type C1, skewed)

Force versus displacement

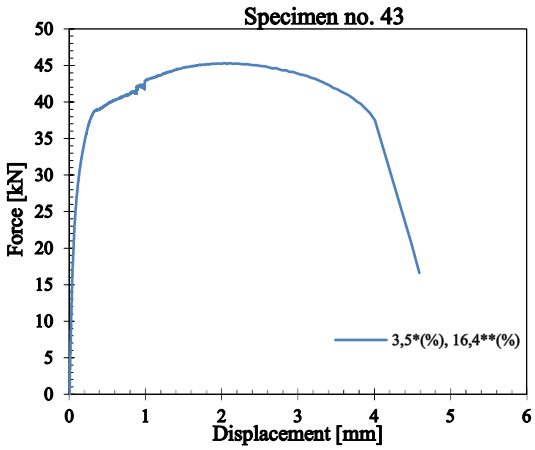

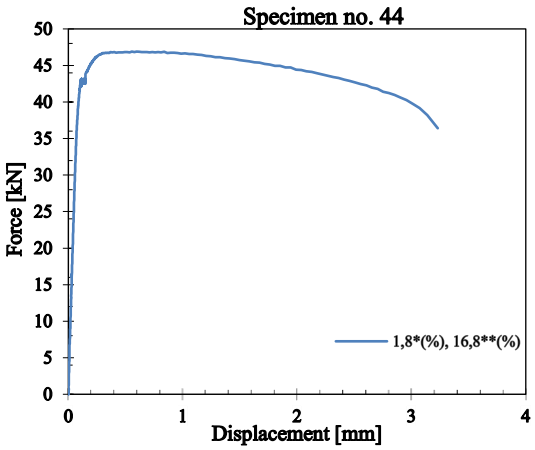

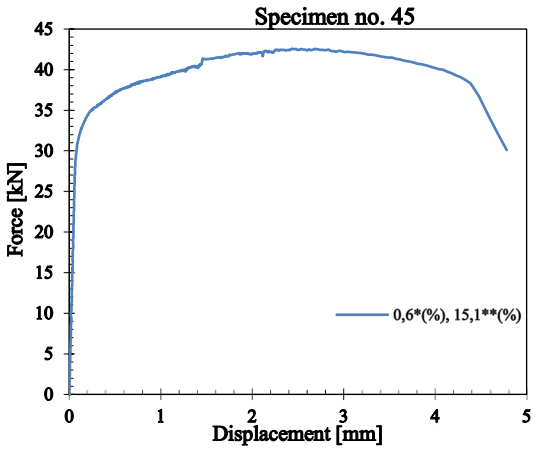

* Average corrosion level.

** Corrosion level at critical cross section (CCS).

Force versus engineering strain

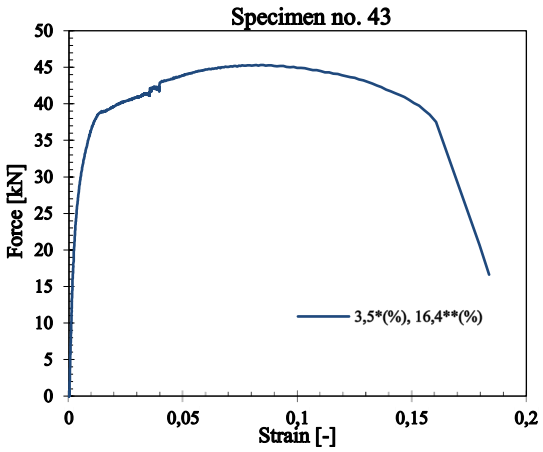

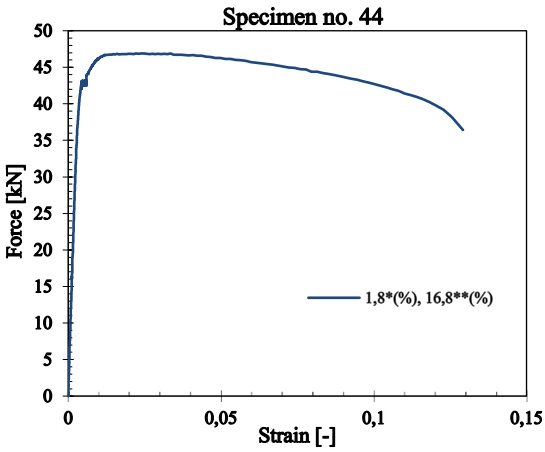

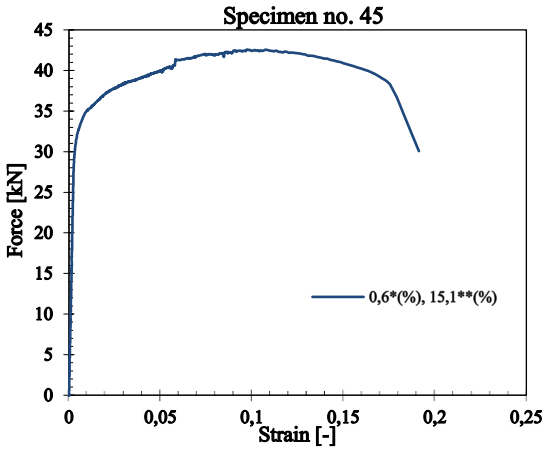

* Average corrosion level.

** Corrosion level at critical cross section (CCS).

Engineering stress-strain curve

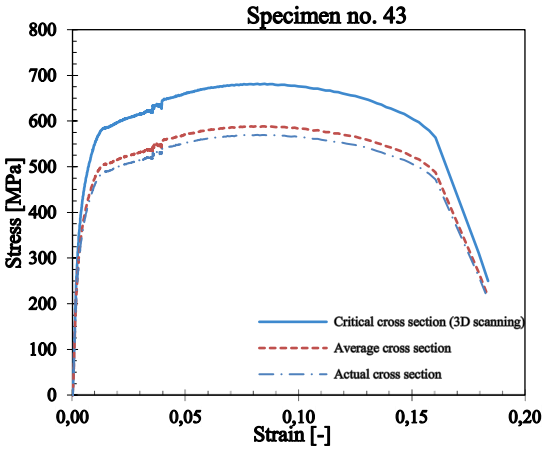

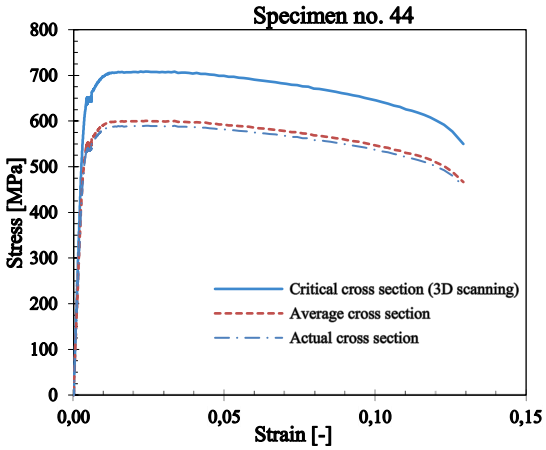

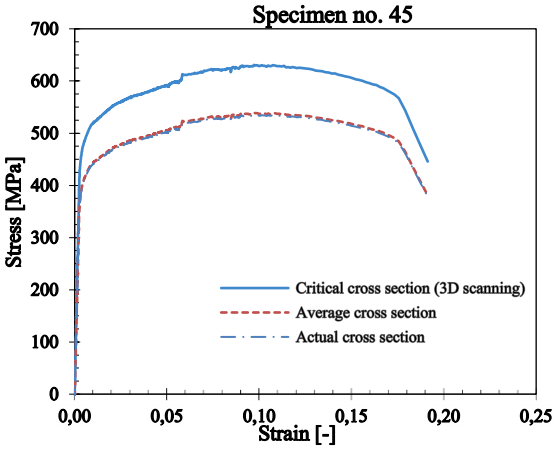

Appendix C.2: Uncorroded rebar (Type C2, skewed)

Force versus displacement

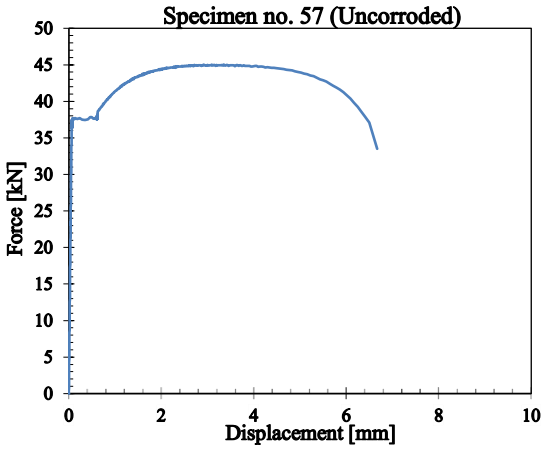

Force versus engineering strain

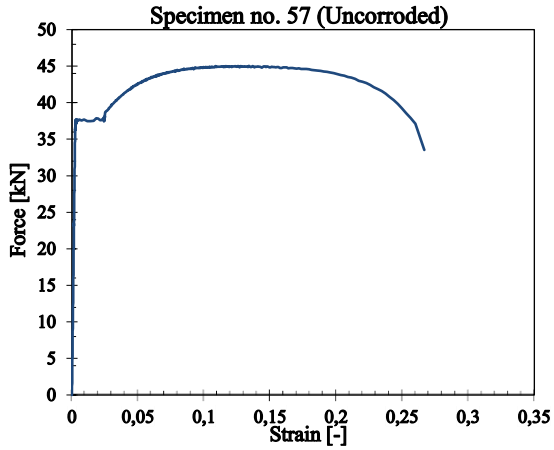

Engineering stress-strain curve

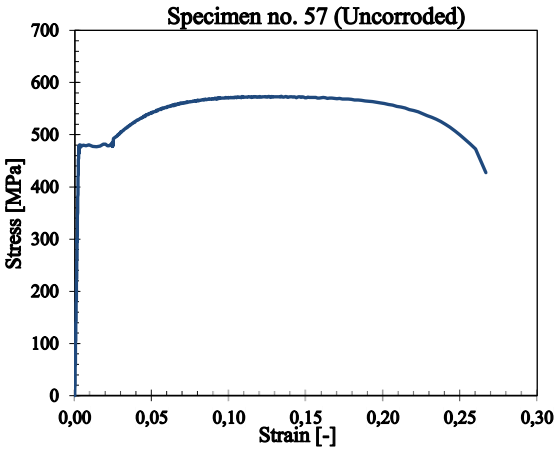

Appendix D: Table 1

Table 1: Summarized mechanical parameters for tested specimens.

Type of specimen	Specimen number	Actual diameter [mm]	Average corrosion level (wt. loss) [%]	Corrosion level at critical cross-section (3D scan) [%]	Yielding load [kN]	Ultimate load [kN]	Yield strain	Fracture strain	Modulus of elasticity [GPa] (Avg. cl.)	Modulus of elasticity [GPa] (Cl. at CCS)	Yielding strength [MPa] (Avg. cl.)	Yielding strength [MPa] (Cl. at CCS)	Ultimate strength [MPa] (Avg. cl.)	Ultimate strength [MPa] (Cl. at CCS)	Elongation [%]	Type of rib	Failure point captured
Type A1	1**	16,59	7,5	13,4	128	-	0,004	-	200	208	638	682	-	-	-	Skewed	No
	3	-		-	-	-	-	-	-	-	-	-	-	-	-	-	*N/A
	5	16,59	8,7	12,3	110	154	0,007	0,10	111	112	557	581	779	812	10	Skewed	Yes
	6	16,59	7,2	21,4	106	144	0,006	0,04	143	164	541	621	736	846	4	Skewed	Yes
	8	-		-	-	-	-	-	-	-	-	-	-	-	-	-	*N/A
	9	-		-	-	-	-	-	-	-	-	-	-	-	-	-	*N/A
	10	16,59	10,1	12,9	125	165	0,008	0,15	167	167	642	662	848	875	15	Skewed	Yes
	11**	16,59	8,2	9,7	121,0	-	0,005	-	200,0	198,4	609,0	670,0	-	-	-	Skewed	No
	16	16,59	8,6	16,7	104	148	0,006	0,14	122	131	526	575	749	819	14	Skewed	Yes
	17	-		-	-	-	-	-	-	-	-	-	-	-	-	-	*N/A
	18	16,59	7,8	20,0	111	147	0,007	0,12	147	165	556	539	736	847	12	Skewed	Yes
Type A2	U49	-	-	-	-	-	-	-	-	-	-	-	-	-	-	-	*N/A
	U51	16,59	-	-	-	-	-	-	-	-	-	-	-	-	-	-	*N/A
	U53	16,59	-	-	-	-	-	-	-	-	-	-	-	-	-	-	*N/A
	U54	16,59	0,0	0,0	144	182	0,012	0,28	215	215	718	718	905	905	28	Skewed	Yes
	U55	16,59	0,0	0,0	143	179	0,012	0,26	215	215	710	710	892	892	26	Skewed	Yes
Type B1	2**	16,4	8,0	11,2	117,0	-	0,014	-	198,8	200,4	600,0	623,0	-	-	-	Straight	No
	4	-	-	-	-	-	-	-	-	-	-	-	-	-	-	-	*N/A
	7**	16,4	14,0	17,8	138,0	-	0,006	-	185,2	189,6	757,0	791,0	-	-	-	Straight	No
	12	-	-	-	-	-	-	-	-	-	-	-	-	-	-	-	*N/A

* Technical failure/ further research.

** Extensometer not provided between the failure point (only yielding properties are obtained).

*** All the mechanical properties for the nominal diameter.

Table 1: Summarized mechanical parameters for tested specimens (continued).

Type of specimen	Specimen number	Actual diameter [mm]	Average corrosion level (wt. loss) [%]	Corrosion level at critical cross-section (3D scan) [%]	Yielding load [kN]	Ultimate load [kN]	Yield strain	Fracture strain	Modulus of elasticity [GPa] (Avg. cl.)	Modulus of elasticity [GPa] (Cl. at CCS)	Yielding strength [MPa] (Avg. cl.)	Yielding strength [MPa] (Cl. at CCS)	Ultimate strength [MPa] (Avg. cl.)	Ultimate strength [MPa] (Cl. at CCS)	Elongation [%]	Type of rib	Failure point captured
Type B1	13**	16,4	5,3	10,1	125,0	-	0,005	-	208,3	214,2	623,0	656,0	-	-	-	Straight	No
	14	-	-	-	-	-	-	-	-	-	-	-	-	-	-	-	*N/A
	15	16,41	8,9	16,3	103	142	0,007	0,10	167	176	532	580	733	800	10	Straight	Yes
	19	16,41	8,2	24,3	110	147	0,006	0,12	152	180	565	685	755	916	12	Straight	Yes
	20	16,41	14,5	27,1	106	140	0,007	0,06	182	208	583	685	771	907	6	Straight	Yes
	21	16,41	14,2	19,7	108	146	0,004	0,05	200	209	594	633	804	857	5	Straight	Yes
	22	16,41	5,8	7,7	116	161	0,005	0,11	195	195	581	592	807	823	11	Straight	Yes
	23	16,41	8,3	16,7	98	140	0,007	0,10	107	115	503	554	719	793	10	Straight	Yes
	24	16,41	6,1	17,7	101	144	0,006	0,09	160	178	509	579	725	825	9	Straight	Yes
	25**	16,4	7,6	14,6	117,0	-	0,003	-	250,0	264,4	598,0	644,0	-	-	-	Straight	No
	26	16,41	14,3	25,0	85	120	0,004	0,09	133	149	469	537	661	757	9	Straight	Yes
	27	16,41	12,8	18,4	110	153	0,006	0,15	222	232	595	633	829	882	15	Straight	Yes
	28**	16,4	7,9	13,0	114,0	-	0,009	-	250,5	258,5	582,0	617,0	-	-	-	Straight	No
	29**	16,4	11,6	19,1	102,0	-	0,005	-	182,3	194,1	543,0	594,0	-	-	-	Straight	No
	30	16,41	5,8	13,1	106	149	0,005	0,11	190	204	531	574	746	807	11	Straight	Yes
	31	16,41	4,9	6,5	121	168	0,009	0,19	217	213	600	641	833	891	19	Straight	Yes
	32**	16,4	11,2	21,8	105,0	-	0,006	-	167,1	196,3	556,0	633,0	-	-	-	Straight	No
	33	16,41	17,8	30,4	87	127	0,003	0,05	161	186	498	590	727	861	5	Straight	Yes
	34	16,41	5,4	14,2	128	163	0,001	0,02	333	359	638	705	813	898	2	Straight	Yes
	35	16,41	4,4	10,3	111	154	0,007	0,09	191	200	548	582	760	808	9	Straight	Yes

* Technical failure/ further research.

** Extensometer not provided between the failure point (only yielding properties are obtained).

*** All the mechanical properties for the nominal diameter.

Table 1: Summarized mechanical parameters for tested specimens.

Type of specimen	Specimen number	Actual diameter [mm]	Average corrosion level (wt. loss) [%]	Corrosion level at critical cross-section (3D scan) [%]	Yielding load [kN]	Ultimate load [kN]	Yield strain	Fracture strain	Modulus of elasticity [GPa] (Avg. cl.)	Modulus of elasticity [GPa] (Cl. at CCS)	Yielding strength [MPa] (Avg. cl.)	Yielding strength [MPa] (Cl. at CCS)	Ultimate strength [MPa] (Avg. cl.)	Ultimate strength [MPa] (Cl. at CCS)	Elongation [%]	Type of rib	Failure point captured
Type B1	36	16,41	15,4	20,9	101	137	0,004	0,06	167	175	562	602	763	817	6	Straight	Yes
	37	16,41	15,4	28,5	80	125	0,008	0,17	100	115	445	527	696	825	17	Straight	Yes
	38	16,41	18,7	39,0	78	118	0,003	0,08	190	250	451	601	683	911	8	Straight	Yes
	39	16,41	12,3	20,6	107	151	0,004	0,09	172	186	576	634	814	896	9	Straight	Yes
Type B2	U48***	16,41	0,0	0,0	142	189	0,013	0,33	205	205	689	689	918	918	33	Straight	Yes
	U50***	16,41	0,0	0,0	141	188	0,012	0,35	188	188	700	700	937	937	35	Straight	Yes
	U52***	-	-	-	-	-	-	-	-	-	-	-	-	-	-	-	*N/A
Type C1	40	10,1	0,8	15,6	34,0	41,0	0,006	0,22	143	166	425,0	501,0	514,0	605,0	22,4	Skewed	Yes
	41	-	-	-	-	-	-	-	-	-	-	-	-	-	-	-	*N/A
	42	-	-	-	-	-	-	-	-	-	-	-	-	-	-	-	*N/A
	43	10,1	3,5	16,4	37,0	45,0	0,01	0,18	111	127	476,0	551,0	578,0	670,0	18,4	Skewed	Yes
	44	10,1	1,8	16,8	43,0	47,0	0,004	0,13	176	205	545,0	642,0	596,0	703,0	12,9	Skewed	Yes
	45	10,1	0,6	15,1	35,0	43,0	0,01	0,19	144	167	437,0	512,0	539,0	631,0	19,1	Skewed	Yes
	46	10,1	4,6	-	-	-	-	-	-	-	-	-	-	-	-	-	*N/A
	47	10,1	2,9	-	-	-	-	-	-	-	-	-	-	-	-	-	*N/A
Type C2	U56***	10,1	0,0	0,0	43	50	0,026	0,26	193	193	553	553	632	632	26	Skewed	Yes
	U57***	10,1	0,0	0,0	38	45	0,024	0,27	199	199	478	478	574	574	25	Skewed	Yes

* Technical failure/ further research.

** Extensometer not provided between the failure point (only yielding properties are obtained).

*** All the mechanical properties for the nominal diameter.